Fall 1968

MEASUREMENT OF IONOSPHERIC ABSORPTION BY THE COSMIC RADIO NOISE METHOD

J RONALD EARHART

69-7027

EARHART, J. Ronald, 1941-
MEASUREMENT OF IONOSPHERIC ABSORPTION BY THE COSMIC RADIO NOISE METHOD.

University of New Hampshire, Ph.D., 1968
Physics, general

University Microfilms, Inc., Ann Arbor, Michigan

MEASUREMENT OF IONOSPHERIC ABSORPTION BY THE COSMIC RADIO NOISE METHOD

by

J. RONALD EARHART

B.S. Lebanon Valley College, 1963

M.S. University of New Hampshire, 1966

A THESIS

Submitted to the University of New Hampshire

In Partial Fulfillment of

The Requirements for the Degree of

Doctor of Philosophy

Graduate School

Department of Physics

September, 1968

This thesis has been examined and approved.

Harry K. Hall

Lyman Mower

Roger S. Arnold

John E. Mulhern Jr.

Robert E. Houston Jr.

August 16, 1968
Date

ACKNOWLEDGMENTS

The author sincerely thanks Dr. Robert E. Houston, Jr., adviser and friend, who guided this study through its duration.

Thanks are due to Dr. C. O. Bostrom of the Johns Hopkins Applied Physics Laboratory for generously supplying proton data from the satellite 1963 38C.

Appreciation is extended to Mrs. Judy Huntley and Mr. Peter Dewdney for data reduction and Mr. Archer Buck for programming assistance. Thanks are extended to Mr. Herbert Scheibel for the drawings and Mrs. Joan Wallingford for the typing.

The author sincerly acknowledges the support and encouragement of his wife, Marianne Earhart, during the course of this study.

This work was supported by the National Aeronautics and Space Administration under Grant NsG-614.

TABLE OF CONTENTS

LIST OF TABLES

LIST OF FIGURES

Number Page

Number Page

Number Page

Number | Page

ABSTRACT

MEASUREMENT OF IONOSPHERIC ABSORPTION BY THE COSMIC RADIO NOISE METHOD

by

J. RONALD EARHART

This study may be divided into two parts. Both portions utilize the technique of cosmic radio noise absorption on 22 MHz. The instrument used is a riometer which records signal intensity obtained from a wide beam antenna.

The first portion of the study is concerned with the contribution of the quiet sun to ionospheric absorption. The study was carried out over the two-year period 1966 and 1967. The reference curve is determined from the hourly values over a year's period of time that occur at least three hours after sunset and three hours before sunrise. The data is organized into 24 hourly averages for each month. The trends evident are: (1) a single maximum in absorption occurring very close to local noon; (2) a larger magnitude of absorption in the summer months than winter months; and (3) an asymmetry around local noon with the decay to zero absorption extending well into the night-time. The first two results indicate close solar control while the latter conclusion indicates lack of solar control.

By choosing a reference curve for sunrise and sunset at 150 km, one may set upper and lower limits on the solar

ionospheric absorption occurring in the lower ionosphere (below 150 km) and the upper ionosphere (above 150 km). The trends evident are: (1) the upper ionospheric solar absorption rises to a plateau value in the morning, remains essentially at this value during the day, and commences to decay by late afternoon; (2) the plateau value is greater in the summer than the winter; (3) the lower ionospheric solar absorption is symmetric about local noon; and (4) 50 to 65% of the solar ionospheric absorption is occurring in the lower ionosphere at local noon with lesser amounts before and after local noon. The conclusion to be drawn is that while the upper ionospheric solar absorption is somewhat dependent on the sun, the effect is not nearly so great as the lower ionospheric solar absorption.

The second portion of the study is concerned with the contribution of the disturbed sun to the ionospheric absorption. The period of interest is late August and early September, 1966 when two Polar Cap Absorption Events occurred. The satellite 1963 38C, at an altitude of 1100 km, measured protons at the latitude of Durham on three separate occasions: 2342UT and 2353UT on September 3, 1966 and 0406UT on September 4, 1966. This corresponded to a very disturbed magnetic period ($D_{st} > 100\ \gamma$). At the same time the Durham 22 MHz riometer was showing absorption.

Calculating the absorption expected from the ionization caused by the protons interacting in the atmosphere for the three satellite passes and comparing this calculated absorption to the measured absorption results in good agreement if one neglects the electron precipitation absorption component. The enhanced absorption when protons reach the latitude of Durham under disturbed magnetic conditions and the lack of absorption when the protons do not reach Durham suggest that the geomagnetic field condition is the determining factor in whether PCA riometer absorption occurs at Durham.

CHAPTER I

INTRODUCTION

The discovery of extraterrestrial radio waves impinging upon the earth is a concept that is less than four decades old. Jansky [1932] discovered these radio waves on a wavelength of 14.6 meters, while studying the direction of arrival of the atmospheric disturbances which interfer with Trans-Atlantic short-wave radio communications. He found that in addition to the familiar atmospheric static of thunderstorms, his receiver was picking up persistent strange static noise. He concluded that this static noise was coming from the general direction of the Milky Way and suggested it might be originating in the stars or in interstellar space. The name cosmic radio noise or cosmic static evolved from the steady audible crackling hiss from the speaker of the receiver recording these cosmic radio waves.

There was little advance in the knowledge of this phenomenon until after World War II. In Australia, Bolton and Stanley [1947] discovered a new type of radio source in the radio sky in addition to the radio radiation widely distributed along the Milky Way. These discrete sources had a well defined boundary as measured on narrow beam antennas and were called radio stars.

The above discovery again aroused interest in looking for other sources of radio waves and there soon developed a vigorous endeavor to map the radio sky in a manner analogous to that which had been done for the optical sky [Shain, 1951; Brown and Hazard, 1953; Shain and Higgins, 1954]. These groups were looking for both the general background radiation and discrete sources by using high frequency receivers and directional antennas.

After much conjecture, the mechanisms which cause the extraterrestrial radio waves seem to be fairly well established [Oort, 1959]. It is found that the radio domain is mostly continuous with line emission being observed in only one case, that being the hyperfine structure line of atomic hydrogen at 21.1 cm. The continuous radiation is believed caused by two different mechanisms. One is the so-called free-free transitions in ionized gases giving thermal radiation, and the other is the non-thermal radiation caused by the deceleration of high-energy electrons in large-scale magnetic fields commonly called synchrotron radiation. The continuous radiation is observed to come from other galaxies, from intergalactic space, from a nearly homogeneous atmosphere surrounding the Galactic System, and from the thin galactic layer approximately 3° wide lying along the galactic equator. Part of the radiation from the galactic layer comes from clouds of ionized hydrogen emitting thermal radiation which are discrete and are referred to as radio sources. The intense galactic sources have been identified with certain luminous sources called nebulosities. The radio frequency radiation from these nebulosities is due to the synchrotron process. It is believed that most of the non-thermal galactic radiation is due to relativistic electrons in interstellar magnetic fields.

The first suggestion that the cosmic radio noise was modulated by the ionosphere was made by Jansky [1937], who found that during the day the intensity of the cosmic noise was lower than expected and attributed this to ionospheric absorption. This idea again lay dormat until Mitra and Shain [1953] revived it and attempted to measure the total absorption suffered by a 18.3 MHz signal completely traversing the ionosphere. They found that there were several decibels of absorption on occasion.

Little [1954] instrumented a system to measure the cosmic radio noise and its absorption by the ionosphere in which he used a stable high gain receiver, directional antenna, and a pen recording device to continually measure the output of the receiver. The advantages of the cosmic noise method of monitoring the ionosphere are quite evident. With echo sounding techniques the radio transmitters required are expensive and are completely unreadable during intense absorption events since they operate at low frequencies. However, the cosmic noise method requires no transmitter and can be operated at much higher frequencies than a sounder, giving information even during severe ionospheric absorption events.

Although, the cosmic noise method had advantages over the sounding method, it had the serious drawback of not being stable over a long period of time due to change of gain in the receiver. This led to the development of the self-balancing or servo-type receiver for the recording of cosmic radio noise. This instrument was independent of receiver gain [Little and Leinbach, 1958; Little and Leinbach, 1959] and was called a riometer, an acronym for relative ionospheric opacity meter. The development of this stable receiver, made possible inexpensive, routine, and continuous monitoring of ionospheric absorption. In this dissertation the experimental data is obtained by the riometer method.

The purpose of this study is twofold. One segment is concerned with the determination of the ionospheric absorption caused by the sun under quiet solar conditions. In addition a method is presented to separate the absorption into a component occurring in the upper ionosphere, here defined to be greater than 150 km and a component occurring in the lower ionosphere defined to be less than 150 km. This study is made for the two years 1966 and 1967.

The second segment deals with polar cap absorption, particularly with the event of September 1966. The proton energy spectrum at three separate times of this event corresponding to unusual and quite disturbed conditions on the 22 MHz riometer are analyzed. From the energy spectrums, the theoretical absorption to be expected may be calculated and compared to the absorption actually measured. The purpose of this is to make a definitive statement about the primary source of the absorption and the effect of the geomagnetic cutoff.

Chapter II discusses the formation of the ionosphere and its effect on electromagnetic waves. Chapter III deals with experimental techniques while Chapters IV and V are devoted to the discussion of the experimental results. Chapter VI is concerned with the conclusions of the study.

CHAPTER II

THEORY OF THE IONOSPHERE

1. Formation

a. General Properties

The existence of the ionosphere was postulated in 1882 by Balfour Stewart to explain the daily variation of the earth's magnetic field. In 1925 Breit and Tuve experimentally verified the existence of an ionospheric layer by measuring the time delay of reflected radio signals. That one or more layers should exist is quite reasonable. When an ionizing radiation impinges upon the earth's atmosphere, it encounters an increasing concentration of ionizable atmospheric particles as it penetrates. However, as the ionizing radiation penetrates deeper into the atmosphere, there will be an increased absorption of its initial intensity. Therefore, with an increase in atmospheric concentration and a decrease in intensity, a maximum level of ionization will occur, forming an ionospheric layer. With more than one radiation present and with more than one atmospheric constituent involved, the existence of several layers is not difficult to understand.

b. Electron Production

Chapman [1931] gave the first analysis of the effect of ionizing radiation interacting with the earth's atmosphere. More recently Davies [1965] has obtained a similar result by assuming a parallel beam of monochromatic ionizing radiation from the sun impinging on the top of a plane atmosphere. In addition the atmosphere is assumed to have only one type of gas present which obeys the perfect gas law.

Let S_∞ be the incident ionizing radiation energy flux on the top of the atmosphere at a zenith angle X. The intensity of this radiation is diminished as it penetrates into the atmosphere. If one assumes that the absorption of the ionizing radiation takes place in a cylinder of unit cross section and axis parallel to the direction of the incident beam one obtains

$$dS = \sigma_a N_a S \, dh \sec X \tag{1}$$

where dS is the energy absorbed in going from a height h+dh to a height h, S is the energy flux at a height h, σ_a is the absorption cross section of the molecules of the gas and N_a the number density of the molecules of the gas causing the absorption. If equation 1 is written in the integral form one obtains

$$\int_{S_\infty}^{S} \frac{dS}{S} = \sec X \int_{\infty}^{h} N_a \sigma_a \, dh = - \tau \sec X \tag{2}$$

where

$$\tau = - \int_{\infty}^{h} N_a \sigma_a \, dh$$

is the optical depth of the atmosphere down to the height h. Integration of the above equation yields

$$S = S_\infty \exp(-\tau \sec X) \tag{3}$$

which gives the energy flux at a height h if the energy flux at the top of the atmosphere is known.

The energy absorbed per unit volume is given by

$$\frac{dS}{dh\sec X} = \sigma_i N_i S \tag{4}$$

and utilizing equation 3 yields

$$\frac{dS}{dh\sec X} = \sigma_i N_i S_\infty \exp(-\tau \sec X) \tag{5}$$

in terms of the incident energy flux. Let η be defined as the ionization efficiency which is the number of ion pairs produced per unit of energy absorbed. The number of ion pairs produced per unit volume per second is then

$$q(X,h) = \sigma_i N_i S_\infty \eta \exp(-\tau \sec X) \tag{6}$$

It should be noted here that although only one type of gas is being considered, equation 6 is written in the most general form using σ_i, the ionization cross section for the atmospheric constituent of number density, N_i, being ionized at height h independent of the absorption of the ionizing radiation. This will be elaborated upon when equation 6 is generalized to an atmosphere containing more than one gas.

The pressure difference between height h and h+dh may be written as

$$dp = -\rho g dh \tag{7}$$

or

$$dp = -Nmgdh \tag{8}$$

where m is the mass of a molecule and g is the acceleration of gravity. Rewriting equation 8 in the form

$$\int_0^p \frac{dp}{mg} = -\int_\infty^h N dh = \frac{\tau}{\sigma_a} \tag{9}$$

It is apparent that if g is independent of height in the lower ionosphere, then

$$\tau = \frac{\sigma_a p}{mg} \tag{10}$$

Assuming the perfect gas law, the pressure can be written as

$$p = NkT \tag{11}$$

where k is Boltzmann's constant (= 1.372×10^{-16} erg/deg) and T is the Kelvin temperature. Equation 10 then takes the form

$$\tau = \frac{\sigma_a NkT}{mg} \tag{12}$$

or

$$\tau = \sigma_a NH \tag{13}$$

where

$$H = \frac{kT}{mg}$$

is the scale height.

To generalize equation 6 for more than one atmospheric constituent it is necessary to let

$$q(\chi,h) = \sum_j q_{pj}(\chi,h) = \sum_j \sigma_{ij}\, N_{ij}\, S_\infty\, \eta_j \exp(-\tau_1) \quad (14)$$

where

$$\tau_1 = -\sum_k \sigma_{ak} \int_\infty^h N_{ak} \sec\chi dh$$

σ_{ij} is the ionization cross section of the j^{th} constituent, N_{ij} the number density of the j^{th} constituent, and η_j the ionization efficiency of the ionizing radiation on the j^{th} constituent. τ_1 is the sum of the separate products of the absorption cross section, σ_{ak}, and the total number of the k^{th} absorbing constituent in a unit cross section from h to the top of the atmosphere.

It should be noted that for near grazing incidence, when χ is greater than 85^o, the assumption of plane stratification of the atmosphere is no longer valid and it is necessary to replace $\sec\chi$ by a special function called the Chapman function. In this dissertation, there will be no need to use the Chapman function, and it will not be used.

c. Electron Losses

The region of the ionosphere below approximately 100 km is characterized by the formation of negative molecular ions. The solar ionizing radiation that causes molecular dissociation is strongly absorbed above 90 km [Nicolet and Aikin, 1960]. Therefore the free electrons formed below 90 km are surrounded by an atmosphere composed almost exclusively of the molecular species of its constituent elements. The mean temperature in this region is about 250 degrees Kelvin with little variation. The collision frequency between electrons and neutrals is quite high ranging from about 10^{10} sec^{-1} at 30 km to 10^{5} sec^{-1} at 90 km.

Mitra [1952] describes the general equations dealing with electron loss. The equation of continuity for the electron distribution in the lower ionosphere is given by

$$\frac{dN_e}{dt} = q - L \qquad (15)$$

This equation says that the time rate of change of the electron density is given by the production of electrons, q, described in the previous section and by the loss of electrons, L, to be discussed in this section.

The specific equation for the rate of change of electron density is given as

$$\frac{dN_e}{dt} = q - \alpha_D N_e N^+ - \eta\, n(O_2) N_e + k\, n\, N^- + \rho S N^- \qquad (16)$$

where

q = rate of electron production $\left(\frac{\text{electrons}}{\text{cm}^3\text{sec}}\right)$

N_e = electron number density (#/cm3)

N^+ = positive ion number density (#/cm3)

N^- = negative ion number density (#/cm3)

n = number density of all neutral particles which may detach electrons from negative ions by collisions (#/cm3)

$n(O_2)$ = number density of O_2 molecules to which electrons may become attached (#/cm3)

α_D = dissociative recombination coefficient for collisions between electrons and positive ions ($cm^3\ sec^{-1}$)

η = attachment coefficient of electrons to O_2 molecules ($cm^6\ sec^{-1}$)

k = collisional detachment coefficient of electrons from O_2^- ions ($cm^3\ sec^{-1}$)

ρS = photodetachment rate of electrons from O_2^- ions (sec^{-1})

In addition to describing the rate of change of the electron density similar equations may be written for the rate of change of positive and negative ion densities

$$\frac{dN^+}{dt} = q - \alpha_D N_e N^+ - \alpha_i N^+ N^- \tag{17}$$

and

$$\frac{dN^-}{dt} = \eta\, n(O_2) N_e - k\, n\, N^- - \alpha_i N^+ N^- - \rho S N^- \tag{18}$$

where all terms are as defined previously and the additional term α_i is the mutual neutralization coefficient of positive and negative ions in units of $cm^3\ sec^{-1}$.

The reactions corresponding to the rate coefficients listed above will be briefly described. The dissociative recombination coefficient, α_D, corresponds to the reaction

$$(XY)^+ + \text{electron} \rightarrow X^* + Y^* \tag{19}$$

where the asteriks indicate the products to be in excited states.

The attachment coefficient, η, describes the reaction

$$O_2 + \text{electron} + (XY) \rightarrow O_2^- + XY \tag{20}$$

where a third body, XY, is needed to conserve momentum in the reaction.

The collisional detachment coefficient, k, describes the reaction

$$(XY) + O_2^- \rightarrow O_2 + XY + \text{electron} \tag{21}$$

while the photodetachment coefficient ρS describes the reaction

$$O_2^- + h\nu \rightarrow O_2 + \text{electron} \tag{22}$$

indicating a photon detaching the electron from O_2^-.

The mutual neutralization coefficient, α_i, describes the reaction

$$O_2^- + (XY)^+ \rightarrow O_2 + XY \tag{23}$$

again showing O_2^- to be the principal negative ion.

By definition

$$\lambda = N^-/N_e \tag{24}$$

which is the negative ion to electron ratio. Since the ionospheric regions are neutral

$$N^+ = N_e + N^- \tag{25}$$

which also implies that equation 17 is not an independent equation and therefore will no longer be utilized.

In order to solve the rate equations listed above it is necessary to assume the condition of quasi-equilibrium [Houston, 1967]. This condition states that

$$\frac{dN_e}{dt} = \frac{dN^-}{dt} = \frac{dN^+}{dt} = 0 \tag{26}$$

This condition is valid at all times of the day with the possible exception of sunrise and sunsets [Mitra, 1952]. Applying quasi-equilibrium conditions to equations 16 and 18 and using equations 24 and 25 which define

$$N^+ = N_e(1+\lambda) \tag{27}$$

resulting in

$$q - \alpha_D N_e^2(1+\lambda) - \eta\, n(O_2)N_e + kn\lambda N_e + \rho S\lambda N_e = 0 \tag{28}$$

and

$$- \alpha_i \lambda(1+\lambda)N_e^2 + \eta\, n(O_2)N_e - kn\lambda N_e - \rho S\lambda N_e = 0 \quad (29)$$

Adding equations 28 and 29 gives the result

$$q - \alpha_D N_e^2(1+\lambda) - \alpha_i (1+\lambda)N_e^2 = 0 \qquad (30)$$

Solving for N_e yields

$$N_e = \left[\frac{q}{(1+\lambda)(\alpha_D+\lambda\alpha_i)}\right]^{1/2} \qquad (31)$$

and defining

$$\alpha_{eff} = (1+\lambda)\,(\alpha_D+\lambda\alpha_i) \qquad (32)$$

gives

$$N_e = \left[\frac{q}{\alpha_{eff}}\right]^{1/2} \qquad (33)$$

Considering equation 18 under quasi-equilibrium conditions, one obtains

$$\lambda = \frac{N^-}{N_e} = \frac{\eta n(O_2)}{kn+\rho S+\alpha_i N^+} \qquad (34)$$

which holds as long as $kn+\rho S > \alpha_i N^+$. From this equation it is seen that at night when $\rho S = 0$ λ will be larger than in the daytime. The value of λ in the daytime becomes quite small at altitudes above 80 km [Whitten and Poppoff, 1965].

Webber [1962] calculates a value of λ at 80 km for daytime conditions of roughly 10^{-2} while the nighttime value at 80 km is about 3, reaching a value of 1 at about 90 km for quiet ionospheric conditions.

If one allows λ to approach zero in equation 31 the electron density is then given by

$$N_e = \left[\frac{q}{\alpha_D}\right]^{1/2} \tag{35}$$

This is the condition that applies at altitudes greater than 90 km [Weir, 1962]. In the ionosphere at altitudes greater than 300 km the equation of continuity must include a term for the effect of mass motion [Aikin and Bauer, 1965]. The equation of continuity will appear as

$$\frac{dN_e}{dt} = q - L - \frac{\delta F}{\delta Z}$$

where F is a flux caused by gravity diffusion. Since this dissertation will not be concerned with any mathematical calculations concerning the upper ionosphere, the complicated solutions of this equation will not be discussed.

d. Chapman Layer

In Section b equation 4 for the production function, q, was derived. In the derivation no assumption was made concerning the temperature distribution. To obtain Chapman's formula [1931] the assumption of an isothermal atmosphere is made. This says that H, the scale height, is independent of height. Rewriting equation 6 one obtains

$$q(\chi,h) = \frac{\tau S_\infty}{H\ \varepsilon}\ \eta\ \exp(1-\tau\sec\chi) \tag{37}$$

where ε is the base of the natural logarithms and equals 2.718.

Define a quantity Z by the relation

$$Z = -\ \ell n\ \tau \tag{38}$$

$$\tau = \exp(-Z). \tag{39}$$

Substituting into equation 37 results in

$$q(\chi,Z) = \frac{S_\infty \eta}{H\ \varepsilon} \exp\ [1-Z-\sec\chi\exp(-Z)] \tag{40}$$

or

$$q(\chi,Z) = q_o\ \exp\ [1-Z-\sec\chi\exp(-Z)] \tag{41}$$

where

$$q_o = \frac{S_\infty \eta}{H\ \varepsilon}$$

and is the rate of production of ion pairs at the level Z = 0 when the sun is overhead.

If $\chi = 0$ then:

$$q(0,Z) = q_o\exp[1-Z-\exp(-Z)] \tag{42}$$

Let $Z = Z' - \ell n\ \sec\chi$

$$q(0,Z' - \ell n\sec\chi) = q_o\ \exp[1-Z'+\ell n\sec\chi-\exp(-Z'+\ell n\sec\chi)] \tag{43}$$

$$q(0,Z) = q_o \sec\chi \exp[1-Z' - \sec\chi \exp(-Z)] \tag{44}$$

$$q(0,Z) = \sec\chi \; q(\chi,Z') \tag{45}$$

This equation says that $q(\chi,Z')$ has the same shape as $q(0,Z)$; it is moved up in altitude by an amount $\ln\sec\chi$ and is smaller by an amount $\cos\chi$. The height of maximum production occurs when

$$Z' - \ln\sec\chi = 0 \tag{46}$$

$$Z_m = \ln\sec\chi \tag{47}$$

The maximum rate of production is found by putting this value into the equation for $q(\chi,Z)$

$$q_m(\chi,Z) = q_o \exp[1-\ln\sec\chi - \sec\chi \exp(-\ln\sec\chi)] \tag{48}$$

$$q_m = q_o \cos\chi \tag{49}$$

Changing the flux does not alter the height at which maximum production occurs. If equation 41 is substituted into equation 35 the resulting equation is

$$N = \left[\frac{q_o}{\alpha}\right]^{1/2} \exp 1/2[1-Z-\sec\chi \exp(-Z)] \tag{50}$$

Similarly the maximum electron density is given by

$$N_{max} = \left[\frac{q_o}{\alpha}\right]^{1/2} \cos^{1/2}\chi \tag{51}$$

e. D-Region

The D-region is the portion of the ionosphere that exists between 50 km and 85 km. Physical processes occurring under both quiet and disturbed solar conditions are important. Particular emphasis will be placed on the processes occurring in this region since this dissertation encompasses many calculations related to the physical phenomena occurring at these altitudes.

Under quiet solar conditions, meaning the absence of any large solar flares, the dominant source of ionization in the lower D-region is galactic cosmic rays [Nicolet and Aikin, 1960]. The production rate of ion pairs from galactic cosmic rays is proportional to the neutral particle density. For 2.5×10^{19} molecules cm^{-3}, 100 to 300 ion pairs cm^{-3} sec^{-1} may be produced between the geomagnetic latitudes of 40° and 60°. The latitude effect will cause a decrease, by a factor of 3, in the electron concentration from 60° to the magnetic equator. At solar minimum galactic cosmic rays may be the dominant ionization source to altitudes of 75 km, while at solar maximum they are not important about 65 km [Whitten and Poppoff, 1965].

The origin of the upper D-region under quiet solar conditions is caused by ionization produced by solar electromagnetic radiation. For wavelengths greater than 1900 A, there is little interest in the D-region since the maximum energy corresponds to 6.5 ev, a number which is less than the ionization potentials of all atmospheric constituents except sodium, potassium, and lithium [Reid, 1964]. It is unlikely that ionization of these metals can contribute appreciably to the D-region. Aikin and Bauer [1965] state that the sodium concentration at 80 km is of the order of only a few atoms per cm^3.

The ionization of the principal constituents, such as molecular nitrogen and oxygen, cannot contribute since the ionization cross sections for ultraviolet radiation are not less than 10^{-18} cm^2. This precludes the penetration of such ionizing radiation below 100 km [Nicolet and Aikin, 1960]. At wavelengths less than 1900 A the Schumann-Runge continuum, beginning at 1750 A and extending to 1300 A, is encountered. Also, since the absorption cross section of O_2 between 1700 A and 1220 A is more than 10^{-19} cm^2, the penetration of solar radiation to sufficiently low altitudes occurs only in atmospheric windows near 1216, 1187, 1167, 1157, 1143, and 1108 A. For these wavelengths unit optical depth is reached at about 10^{20} molecules cm^{-2} of vertical column which corresponds to about 75 km for an overhead sun. The deepest window is almost exactly at the wavelength of Lyman α, 1215.7 A, one of the strongest emission lines of the solar spectrum [Reid, 1964]. This wavelength corresponds to an energy of 10.2 ev and is sufficient to ionize nitric oxide, a minor constituent in the D-region, which has an ionization potential of 9.25 ev. However, the nitric oxide hypothesis has not been verified because its concentration in the

D-region is not known. Barth [1964] measured a value of 5.8×10^7 molecules cm^{-3} at 85 km. Barth [1966] reduced this value to 3.9×10^7 molecules cm^{-3} at 85 km. However, the values are two orders of magnitude greater than the theoretically predicted densities. This discrepancy has not been resolved to the present time.

The importance of x-rays in the formation of the upper portion of the D-region is also subject to debate. Nicolet and Aikin [1960] state that since the absorption cross section of x-rays shorter than 10 A decreases rapidly from 10^{-19} cm^2 at 10 A to about 10^{-22} cm^2 at 1 A, the entire atmospheric region between 90 and 60 km is capable of being penetrated. The principal atmospheric constituents ionized by x-rays of wavelength less than 10 A are N_2, O_2, and Argon. The authors cited above concluded that x-ray ionization is unimportant below 85 to 90 km due to the small flux under quiet conditions. Reid [1964] agrees with this conclusion. However, Whitten and Poppoff [1965] conclude that under quiet conditions x-ray ionization is important in the D-region.

Under disturbed solar conditions the physical processes occurring in the D-region change. Whereas, under quiet conditions, the energy flux of Lyman α radiation is about 5 ergs cm^{-2} sec^{-1}, and the energy flux of x-rays between 0 and 20 A about 10^{-3} erg cm^{-2} sec^{-1}, under disturbed conditions the former changes little if any and the latter significantly [Reid, 1964]. Kreplin et al. [1962] have shown by satellite data a one-to-one correlation between solar x-ray bursts in this spectral range and ionospheric disturbances. During these bursts the enhancement of Lyman α radiation was either slight or absent indicating that Lyman α does not play a part in the disturbed D-region. During a solar flare the x-ray flux between 2 and 8 A may rise by as much as a factor of 10^5 [Aikin and Bauer, 1965].

Under disturbed conditions at high latitudes the enhanced x-ray ionization occurs but is usually masked by other effects [Reid, 1964]. Reid and Collins [1959] have described the unusual absorption events occurring at high latitudes and divided them into two major categories. One division is called a polar cap absorption event (PCA) and occurs almost uniformly over the polar caps. The term absorption is defined to mean a decrease in signal strength of HF and VHF radio waves. This type of event is caused by intense flares on the sun which throw out protons and alpha particles with energies in the range of 1 to 100 Mev. Because of the earth's magnetic field these particles cannot under normal circumstances reach latitudes lower than the auroral zone. Owing to storage properties in the interplanetary magnetic field, the absorption may continue for several days. The absorption is caused by the increased electron density created by the interaction of the bombarding particles with the atmosphere.

The second division is called auroral absorption and occurs with greatest intensity between 65° and 75° geomagnetic latitude. The effect is again described in terms of the absorption suffered by HF and VHF radio waves. It is associated with aurora and magnetic disturbances and is believed caused by the precipitation of energetic electrons into the atmosphere. It is not clear where these electrons come from, although it is known that the absorption takes place higher in the atmosphere than in PCA events, most likely in the lower E-region.

The rate coefficients for the various physical processes described in Section c and occurring in the lower ionosphere are best approximated by the following: Nicolet and Aikin [1960] list $\alpha_D(N_2^+) \sim 5 \times 10^{-7}$ cm^3 sec^{-1}, $\alpha_D(O_2^+) \sim 3 \times 10^{-8}$ cm^3 sec^{-1}, and $\alpha_D(NO^+) \sim 3 \times 10^{-9}$ cm^3 sec^{-1}. Webber [1962] defines an average electron-positive ion recombination coefficient from the relative abundance of positive ions. This value ranges from 3×10^{-7} cm^3 sec^{-1} below 65 km to 7×10^{-8} cm^3 sec^{-1} at 80 km.

Below 80 km O_2 is the dominant ion to which electrons become attached. This rate coefficient is 2.0×10^{-30} $[n(O_2)]^2$ sec^{-1} with values ranging from 1.1×10^4 sec^{-1} at 30 km to 1.5×10^{-2} sec^{-1} at 80 km.

The collisional detachment as determined by Phelps and Pack [1961] from laboratory measurements at 230°K resulted in a value of 4×10^{-20} cm^3 sec^{-1}. Ionospheric observations by Bailey and Branscomb [1960] gave a value of 2×10^{-17} cm^3 sec^{-1}. Webber [1962], taking account of the number density of molecular oxygen, arrives at a value ranging from 6.0 sec^{-1} at 30 km to 1.5×10^{-2} sec^{-1} at 80 km.

The photodetachment coefficient, ρS, has an average value of .4 sec^{-1} between 30 and 80 km and is taken by Webber [1962] to be .35 sec^{-1} at 30 km and .48 sec^{-1} at 80 km.

The mutual neutralization coefficient, α_i, changes from a three-body process at less than 50 km to a two-body process between molecular oxygen ions with a coefficient of 1.8×10^{-7} cm^3 sec^{-1}.

Following the approach of Webber [1962], this dissertation will use his α_{eff} as defined by equation 32 and determined by the parameters listed above. Also, the effect of λ varying as the production function varies will be taken into account using the appropriate α_{eff}.

f. E-Region

The altitude regime between 85 km and 150 km is designated the E-region of the ionosphere. Under quiet solar conditions the E-region is formed through the ionization of molecular oxygen and molecular nitrogen by x-rays of wavelengths between 30 A and 100 A; through the ionization of molecular oxygen by the extreme ultraviolet radiation of Lyman β at 1025.7 A as well as the Lyman continium at 865 to 912 A, and finally through the ionization of atomic oxygen by the extreme ultraviolet radiation in the Lyman continium plus x-rays [Nicolet, 1962].

It is not clear whether the dominant mechanism is ionization of atmospheric constituents by the x-ray component of solar radiation or ionization of the constituents by selective extreme ultraviolet bands or lines [Whitten and Poppoff, 1965]. Watanabe and Hinteregger [1962] concluded from rocket measurements of extreme ultraviolet and X radiation that Lyman β is very important in the determination of the E layer ionization. Aikin and Bauer [1965] further state that the effect of the Lyman β is to produce a Chapman-like layer centered around 105 km with a noontime electron density of the order of 10^5 cm^{-3}. However, Norton et al. [1963] show that x-ray radiation is more important in forming the E layer peak due to a larger atomic oxygen concentration than previously thought. The answer to this puzzle will not be found until there are careful measurements of photoionization cross sections, solar radiation fluxes, concentration of atmospheric species, and recombination coefficients.

The principal photons found in the E-region are N_2^+ and O_2^+ below 140 km and O^+ above 140 km [Aikin and Bauer, 1965]. It is found that although N_2^+ is produced in large quantities in the E-region it is not found in large concentrations. This is believed due to the following ion-molecule reactions

$$N_2^+ + O_2 \rightarrow NO^+ + NO \qquad (52)$$

$$N_2^+ + O_2 \rightarrow O_2^+ + N_2 \tag{53}$$

$$N_2^+ + O \rightarrow N_2 + O^+ \tag{54}$$

$$N_2^+ + O \rightarrow NO^+ + N \tag{55}$$

A recent study by Bourdeau et al. [1966] at the time of solar minimum showed that the region 88 km to 93 km is formed by 33.7 A x-rays with NO^+ as the principal ionic species. The region 93-115 km is ionized principally by extreme ultraviolet radiation producing O_2^+ and 40 A to 75 A x-ray radiation producing N_2^+. The N_2^+ disappears by the above listed reactions.

Under disturbed solar conditions, the ultraviolet radiations change little, if any, from quiet conditions. Aikin and Bauer [1965] state that while x-ray radiation may increase by a factor of 10^5 in the 2 A to 8 A range during disturbed conditions the x-ray radiation at wavelengths of 100 A and greater varies by less than a factor of two during solar flares. Thus while some modification of electron density distribution occurs above 100 km the major effect of solar flare radiation is in the D-region. The dissociative recombination coefficient varies from 7×10^{-8} cm^3 sec^{-1} at 80 km to 3×10^{-8} cm^3 sec^{-1} at 100 km. The attachment coefficient refers to a two-body attachment to O_2 above 80 km and must also include two-body attachment to atomic oxygen [Webber, 1962]. The value used in this dissertation ranges from 1.5×10^{-2} sec^{-1} at 80 km to 2.4×10^{-4} sec^{-1} at 100 km. The collisional detachment varies from 8.0×10^{-3} sec^{-1} at 80 km to 1.2×10^{-4} sec^{-1} at 100 km.

At altitudes greater than 80 km photodetachment from the oxygen ion becomes important. This causes the photodetachment coefficient to increase slightly at altitudes greater than 80 km. This at 80 km ρS is .48 sec^{-1} increasing to .80 sec^{-1} at 100 km. The positive ion-negative ion neutralization coefficient retains the same value as in the D-region.

g. F-Region

The F-region of the ionosphere refers to that region above 150 km. While the D- and E-regions of the ionosphere show behavior closely linked to the position of the sun, the F-region is a much more complex phenomena. The F-region is described by two peaks of electron density, one at roughly 170 km with a value of 3.5×10^5 electrons cm^{-3} called F1, and a second at roughly 250 km to 300 km with a value of 6.5×10^5 electrons cm^{-3} called F2 [Ratcliffe and Weeks, 1960]. At night the F1 ledge disappears and the maximum electron density occurs about 50 km higher than the daytime with a value of electron density about an order of magnitude less than the daytime value.

Aikin and Bauer [1965] state that at altitudes above 160 km the atmosphere is composed principally of atomic oxygen formed by photoionization. Although the oxygen ion disappears by recombination with electrons the slow rate of recombination ($\sim 10^{-9}$ cm^3 sec^{-1}) allows ion-atom interchange processes to predominate. <u>Yonezawa</u> [1962] lists the following two-step processes, consisting of ion-atom interchange followed by dissociative recombination, for the removal of atomic oxygen ions.

$$O^+ + O_2 \rightarrow O_2^+ + O \tag{56}$$

$$O_2^+ + e \rightarrow O + O \tag{57}$$

and

$$O^+ + N_2 \rightarrow NO^+ + N \tag{58}$$

$$NO^+ + e \rightarrow N + O \tag{59}$$

The rate coefficient for the first O^+ reaction is given as 2×10^{-11} cm^3 sec^{-1} and the second O^+ reaction is given as 1×10^{-12} cm^3 sec^{-1}. The O_2^+ reaction has a rate coefficient of 2×10^{-8} cm^3 sec^{-1} while the NO^+ has a rate coefficient given by 5×10^{-9} cm^3 sec^{-1}.

The mechanism for the formation of the F1 and F2 layers is somewhat different. At lower levels, including the F1 region, chemical reactions leading to the removal of electrons and ions take place rapidly enough so that there is not enough time for electrons and ions to be redistributed by the action of electron-ion diffusion in the gravitational field. At high altitudes diffusion predominates over chemical reactions due to the much lower density of the atmospheric constituents. At intermediate altitudes the two effects balance each other and result in the formation of the F2 peak.

Under disturbed solar conditions there are fluctuations of the geomagnetic field as well as changes in the total electron content in the F-region. During the main phase of a geomagnetic storm, there is a general increase of the total electron content of the equatorial F-region. This increase is accompanied by an enhancement of the electron density at the peak of the F_2 layer and by an altitude increase of the layer. In contrast, the total electron content and maximum electron density of the F_2 layer decreases at geomagnetic latitudes greater than 47°.

The F-region shows unusual character. The diurnal variation of the electron density is not symmetric about local noon. The maximum electron density is found late in the afternoon. The anomalous behavior of the F-region includes the equatorial anomaly which is a minimum in electron density at the geomagnetic equator and a maxima at roughly 20° on either side of the equator. The December anomaly occurs for the months of November, December, and January, appearing as higher daytime electron densities for 50° North geomagnetic to 35° S geomagnetic. The winter anomaly indicates that the electron densities are larger in local winter than summer, especially at solar maximum.

2. Electro-Magnetic Wave Propagation

a. Sen-Wyller Formulation

The theory of ionospheric absorption measured through the cosmic radio noise method is based on the magneto-ionic theory of radio wave propagation. For many years the Appleton-Hartree derivation was used to explain the propagation of an electromagnetic wave through a weak uniform plasma with a static magnetic field, taking into account the effect of collisions between electrons and neutral particles. This theory shows that a wave propagating through such a plasma will be attenuated. The loss of energy suffered by the wave can be thought of in terms of conversion of the ordered motion imparted to the electrons by the E field of the radio wave, to disordered motion through collisions of the electrons with neutral particles. Thus, some of the energy which would have been reradiated by the electrons to continue the forward propagation of the wave is lost and the total field strength of the electromagnetic wave is decreased.

Quantitatively, the field strength of the wave after penetration through the medium is given by

$$E = E_o e^{-\int_s k\,ds} \tag{60}$$

where

E_o = the field strength of the incident plane wave

E = the field strength after traversing a distance s through the ionized medium

and k = the absorption coefficient of the wave which varies from altitude to altitude

Rewriting, one obtains

$$E/E_o = e^{-\int_s k ds} \tag{61}$$

and taking the logarithm of both sides gives

$$\log E/E_o = -\frac{1}{2.30} \int_s k ds \tag{62}$$

By definition

$$A(\text{decibels}) = -20 \log E/E_o \tag{63}$$

which results in

$$A(\text{decibels}) = -8.69 \int_s k ds \tag{64}$$

In order to measure the theoretical absorption it is necessary to determine the absorption coefficient as the wave propagates through the ionosphere.

Sen and Wyller [1960] modified the solution of the magneto-ionic equations by taking account of the fact that the collision frequency between electrons and neutral particles is dependent on the energy of the electrons. Previously, Appleton-Hartree theory assumed that the electron-collision frequency was constant, independent of energy. The Sen-Wyller change was based on the laboratory measurement of Phelps and Pack [1959] who showed that the collision frequency is proportional to the electron energy. A brief outline of the derivation of the absorption coefficient, k, by the newer theory is given below.

The derivation assumes that the gas is lightly ionized, the neutral molecules are very heavy, there are only elastic collisions, collisions between charged particles can be ignored, the medium is homogeneous, the motion of the positive ions due to fields is negligible, the neutral particles have a Maxwellian velocity distribution, and the electrons need not have a Maxwellian velocity distribution. Using these assumptions, one derives the complex refractive index from which one obtains the absorption coefficient.

Start with two of Maxwell's equations

$$\nabla \times \vec{E} = -\frac{1}{c}\frac{\delta \vec{H}}{\delta t} \tag{65}$$

and

$$\nabla \times \vec{H} = \frac{4\Pi}{c}\vec{J} + \frac{1}{c}\frac{\delta \vec{D}}{\delta t} \tag{66}$$

Taking the conduction current to equal zero, and expressing the electron motion as a displacement current, one obtains

$$\vec{\nabla} \times (\vec{\nabla} \times \vec{E}) = -\frac{1}{c}\frac{\delta}{\delta t}\vec{\nabla} \times \vec{H} \tag{67}$$

which yields

$$\vec{\nabla}(\vec{\nabla}\cdot\vec{E}) - \nabla^2\vec{E} = 1/c^2 \frac{\delta^2}{\delta t^2}\vec{D} \tag{68}$$

Assume the electric intensity may be given by

$$\vec{E} = \vec{E}_o\, e^{i(\omega t - \vec{k}\cdot\vec{r})} \tag{69}$$

Substituting this into equation 68 gives

$$-k^2\,\vec{n}\,(\vec{n}\cdot\vec{E}) + k^2\,\vec{E} = \frac{\omega^2}{c^2}\vec{D} \tag{70}$$

with $\vec{n}$ being the unit vector in the wave propagation direction. Writing the displacement vector in terms of the electric field

$$\vec{D} = ||\varepsilon||\,\vec{E} \tag{71}$$

where $||\varepsilon||$ is the dielectric tensor for the medium, one obtains

$$-k^2\,\vec{n}\,(\vec{n}\cdot\vec{E}) + k^2\,\vec{E} = \frac{\omega^2}{c^2}||\varepsilon||\,\vec{E} \tag{72}$$

Since $k = \omega/u$, where u is the phase velocity of the wave, the following relation results

$$\frac{c^2}{u^2} [\vec{E} - \vec{n} (\vec{n} \cdot \vec{E})] = \|\varepsilon\| \vec{E} \tag{73}$$

The displacement current density is

$$\frac{\delta \vec{D}}{\delta t} = \frac{\delta \vec{E}}{\delta t} + 4\pi \frac{\delta \vec{P}}{\delta t} \tag{74}$$

and the polarization current density is

$$\frac{\delta \vec{P}}{\delta t} = \vec{j} = \|\sigma\| \vec{E} = n_2 e \vec{v}_2 \tag{75}$$

with $\|\sigma\|$ the conductivity tensor, n_2 the electron number density, and v_2 the electron velocity. Putting this into equation 74 yields

$$i \omega \vec{D} = i \omega \vec{E} + 4 \|\sigma\| \vec{E} \tag{76}$$

or

$$\|\varepsilon\| = 1 - i \frac{4\pi\|\sigma\|}{\omega} \tag{77}$$

The method used is to find the velocity distribution function for the electrons and use it to calculate j in equation 75. Then $\|\varepsilon\|$ can be found from equation 77, and this result used to calculate c^2/u^2 in equation 73.

The Boltzmann equation for electrons is written as

$$\frac{\delta f_2}{\delta t} + [\Gamma_2 \cos\omega t + \frac{e}{m_2 c} (\vec{v}_2 x \vec{H}_o)]\nabla v_2 f_2 =$$

$$(f_1{'}f_2{'} - f_1f_2)gbdbd\varepsilon dv_1 \qquad (78)$$

where

$$\vec{\Gamma}_2 = \frac{e}{m_2}\vec{E}_o$$

and

$$g = \vec{v}_2 - \vec{v}_1 = \vec{v}_2{'} - \vec{v}_1{'}$$

and b and ε are impact parameters defined by Chapman and Cowling [1960]. The primed terms represent quantities after the collisions and unprimed terms represent quantities before the collisions. The subscript 2 stands for electrons and 1 for molecules. Using Phelps and Pack velocity dependence for collision frequency, namely

$$\nu = \nu_m \frac{m_2 v_2^2}{2kT} \qquad (79)$$

where ν_m is the collision frequency for an electron of energy kT, the polarization current is found.

After a very complicated and involved algebraic process the result obtained is the complex refractive index given by

$$\left[n - \frac{ikc}{\omega}\right]^2 = L - iM = \frac{A+B\sin^2\phi \pm \sqrt{B^2\sin^4\phi - C^2\cos^2\phi}}{D+E\sin^2\phi}$$

where

$$A = 2\varepsilon_1(\varepsilon_1+\varepsilon_{111})$$

$$B = \varepsilon_{111}(\varepsilon_1+\varepsilon_{111}) + \varepsilon_{11}^2$$

$$C = 2\varepsilon_1\varepsilon_{11}$$

$$D = 2\varepsilon_1$$

$$E = 2\varepsilon_{111}$$

$$\varepsilon_1 = (1-a) - ib$$

$$\varepsilon_{11} = 1/2(f-d) + i/2(c-e)$$

$$\varepsilon_{111} = [a-1/2(c-e)] + i[b-1/2(f+d)],$$

$$a = \frac{\omega_o^2}{v_m^2} C_{3/2}[\omega/v_m]$$

$$b = \frac{5\ \omega_o^2}{2\omega v_m} C_{5/2}\ [\omega/v_m]$$

$$c = \frac{\omega_o^2(\omega-s)}{\omega v_m^2} C_{3/2}\ [\frac{\omega-s}{v_m}]$$

$$d = \frac{5\ \omega_o^2}{2\omega v_m} C_{5/2}\ [\frac{\omega-s}{v_m}]$$

$$e = \frac{\omega_o^2(\omega+s)}{\omega v_m^2} C_{3/2}\ [\frac{\omega+s}{v_m}]$$

$$f = \frac{5\,\omega_o^2}{2\omega v_m} C_{5/2}\left[\frac{\omega+s}{v_m}\right]$$

and where

$$\omega_o^2 = \frac{4\Pi n_2 e^2}{m_2}$$

is the plasma frequency,

$$S = e_2 H_o / m_2$$

is the gyrofrequency and ϕ is the angle between the propagation direction and the earth's field lines. The quantities $C_p(\chi)$ are known as Dingle integrals and are given as

$$C_p(\chi) = \frac{1}{p!}\int_o^{\infty} \frac{\varepsilon^p}{\varepsilon^2+\chi^2 e^{\varepsilon}}\, d\varepsilon \tag{81}$$

which are tabulated by Dingle et al. [1957]. Hara [1963] has written series approximations for these integrals. The final result may be written simply as

$$k = \omega/c \sqrt{\frac{-L+L^2+m^2}{2}} \tag{82}$$

2. Simplified Derivation of Ionospheric Birefringence

If two circularly polarized waves rotate in opposite directions, the index of refraction of the ionosphere for each of the two circular waves is different.

Following Jackson [1962] one may show that if a plane electromagnetic wave of frequency ω in a collisionless weak uniform plasma propagates in the direction of a uniform magnetic field B_o, the equation of motion of an electron is given by

$$m \frac{d\vec{v}}{dt} = e \vec{E} e^{-i\omega t} + e/c\ \vec{v} \times \hat{k} B_o \tag{83}$$

Magnetic induction is small and is neglected and the ions are considered stationary.

The linearly polarized wave is written as a pair of circularly polarized waves

$$\vec{E} = E (\hat{i} + i\hat{j}) \tag{84}$$

and

$$\vec{E} = \vec{E} (\hat{i} - i\hat{j}) \tag{85}$$

Assume

$$\vec{v}(t) = v(\hat{i} \pm i\hat{j})e^{-i\omega t} \tag{86}$$

which results in

$$\omega m v = i e E \mp \frac{eB_o v}{c} \tag{87}$$

giving

$$v = \frac{i\, e}{m(\omega \pm s)} E \tag{88}$$

where s was defined previously.

The polarization current density is given as

$$\frac{\delta \vec{P}}{\delta t} \equiv \vec{j} = N_e\, e\vec{v} \tag{89}$$

or

$$\vec{j} = \frac{i\, N_e e^2}{m(\omega \pm s)} \vec{E} \tag{90}$$

Assuming the conduction current is zero and using Maxwell's third equation there results

$$\vec{\nabla} \times \vec{H} = 4\Pi/c\, \frac{\delta P}{\delta t} + \frac{1}{c}\frac{\delta E}{\delta t} \tag{91}$$

$$\vec{\nabla} \times \vec{H} = \left[\frac{i\omega/c \dfrac{4\Pi N\, e^2}{m}}{\omega(\omega \pm s)} - i\,\omega/c\right] \vec{E} \tag{92}$$

$$\nabla \times \vec{H} = -i\,\omega/c\,\left[1 - \frac{\omega_o^{\,2}}{\omega(\omega \pm s)}\right. \vec{E} \tag{93}$$

where $\omega_o^{\,2}$, the plasma frequency, has been defined previously. The bracket is interpreted as ε and since $n = \sqrt{\varepsilon}$

$$n = \left[1 - \frac{\omega_o^{\,2}}{(\omega \pm s)}\right]^{1/2} \tag{94}$$

Thus n has a value which depends upon the direction of rotation of the circular wave. The birefringence results only because of the earth's magnetic field.

CHAPTER III

THE EXPERIMENTAL TECHNIQUE OF MEASURING COSMIC NOISE ABSORPTION

1. Introduction

Having briefly mentioned the riometer in the Introduction, it is now necessary to go into detail with respect to the experimental technique for measurement of cosmic noise absorption. The advantages of the cosmic noise technique are particularly evident at high geomagnetic latitudes, where the absorption is often so intense that ionospheric vertical and oblique incidence sounders are completely "blacked out". The cosmic noise method also avoids the necessity of constructing and maintaining an expensive transmitter.

The cosmic radio noise technique involves little more than recording the signal intensity of the extra terrestrial noise, usually with a wide beam antenna. After a suitable period of time (not less than a month), one can construct a "quiet day curve" which gives the expected cosmic noise level under undisturbed ionospheric conditions. This quiet day curve shows a diurnal variation which is caused by the daily rotation of the non-uniformly bright radio sky through the antenna pattern.

The absorption at any specified time is estimated by comparing the strength of the cosmic noise signal with the expected quiet day value at the same sidereal time. Therefore, a relative absorption is really determined, i.e., the signal loss over and above the absorption occurring in the quiet ionosphere. One readily sees that the absorption measured is the attenuation of the signal over its entire path from the top of the ionosphere to the receiver. However, during disturbances the actual absorbing region is confined to regions of the ionosphere below 100 km. This is due to the relatively high electron collision frequencies at these heights and the increased ionization which results [Holt et al., 1961].

The cosmic radio noise method is used at frequencies in excess of the ionospheric critical frequency, since at frequencies less than the critical frequency the cosmic radio signal would be partially or totally reflected back into space. Generally the maximum critical frequencies seldom rise above 12 to 15 MHz and then only at midday hours during the peak of the sunspot cycle. Investigators have used frequencies as low as 18 MHz with success. With a riometer one must choose a frequency sufficiently low to obtain measurable absorption effects but also high enough to avoid an excessive amount of absorption during major disturbances which would exceed the dynamical limit of the receiver.

Here at Durham, an initial attempt was made to use a frequency of 20 MHz. However, man-made interference, especially during the late morning and afternoon hours necessitated the switching to 22 MHz. This frequency has proven to be subject to less interference than the 20 MHz, but does suffer terrestrial interference during the equinox and winter months.

2. Riometer

Early cosmic radio absorption work carried out mainly at the Geophysical Institute, College, Alaska, used total power cosmic noise receivers [Little and Leinbach, 1958]. This type of receiver has the twin disadvantages of poor gain stability and highly non-linear output. Because of these disadvantages a self-calibrating receiver called a riometer was developed.

The circuitry of the riometer has been explained by Little and Leinbach [1959]. The 22 MHz Durham riometer is an Aerospace Research Inc., Mark II Model ARI-100C. The basic operating principles follow. The riometer is a self-balancing receiving system in which a local noise source is continuously made equal to the noise power from the antenna. The block diagram in Figure 1 shows how the instrument operates.

The input of the receiver is switched alternately between the antenna and the local noise diode by means of a 340 Hz switching unit. If there is an inequality in amplitude between the antenna signal and the local noise diode a square wave output will appear at the output of the receiver, oscillating at the switching frequency. The amplified signal is then fed into a phase sensitive detector which produces a dc signal proportional to the difference

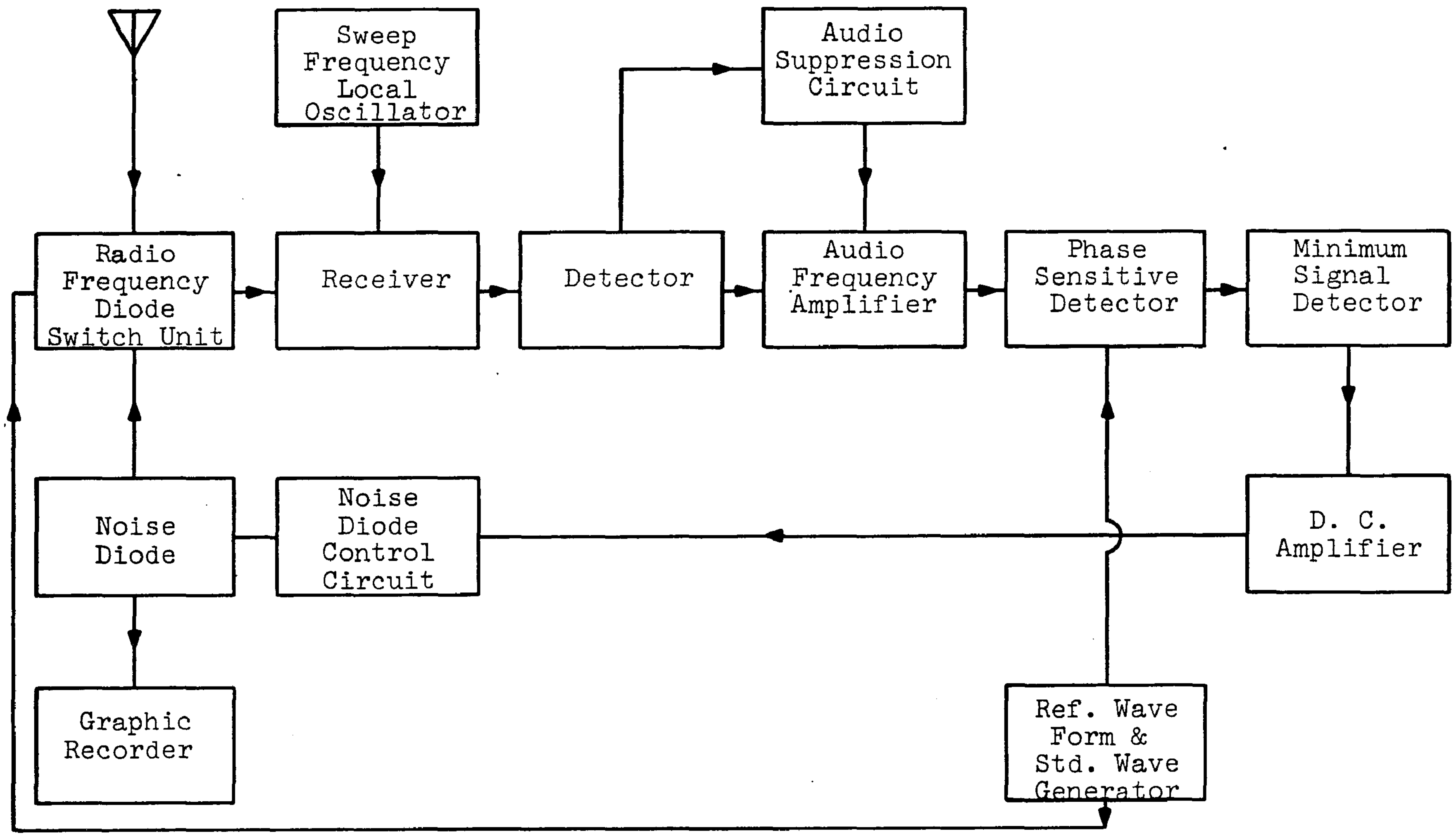

BLOCK DIAGRAM OF A RIOMETER

Figure 1

of the two noise signals and whose polarity depends on which signal is greater. This dc voltage signal is used to change the filament temperature, and, therefore, the output noise power of the temperature limited noise diode, in such a manner as to reduce the difference of antenna and noise diode signal power to zero. The noise power from the noise diode is continuously made equal to the noise power from the antenna. Since the noise power from the noise diode is accurately proportional to the dc current flowing through it [Pawsey and Bracewell, 1955], the antenna noise power can be measured by recording the noise diode current.

The riometer incorporates specialized circuits to minimize the effect of propagated radio-frequency interference and any other transient interference which rises far above the expected cosmic noise level. One of these is the audio suppression circuit or differential time constant circuit. This circuit presents a long time constant (up to 30 seconds or more) to signals rising rapidly above the mean noise level but presents a short time constant (approximately 1 second) to signals of decreasing strength. Another is the servo-diode limiter circuit which places a limit on the positive going signal which is to be matched by the noise diode. This causes the signal intensity to rise to a resting value and prevents the riometer from going off scale.

3. The Antenna

The Durham field station is equipped with a vertically directed, two-element Yagi antenna. The Yagi antenna is characterized by a single driven element, with one or more parasitic elements in front and in back of the driven element, all in the same plane. The basic design for the antenna used in this experiment is a driven dipole, a single parasitic director, and an artificial ground screen of tough wire mesh. This type of antenna is chosen because it is easy to construct, simple to install and relatively easy to adjust electrically. It is also used on most other riometers around the world and makes comparisons more valid. For this antenna the driven element length is $.58\ \lambda$, the director length is $.44\ \lambda$, the driven element to ground separation is $.20\ \lambda$, and the driven element to director separation is $.15\ \lambda$.

The ground screen has dimensions of 40 feet wide by 50 feet long with the plane of the antenna parallel to the length of the screen. The ground screen is used in place of a parasitic reflecting element. Being of finite size it only partially performs the function of a true ground plane; however, it does supply a highly conductive reflecting layer for the structure mounted above it, and the finite conductivity of the local ground is increased in the region of the antenna. The presence of the ground screen reinforces reception normal to the screen and suppresses broadside effects which lead to side lobes in the radiation pattern. This will necessarily decrease the antenna response to man-made interfering signals. The ground screen is constructed of ten four foot sections each fifty feet long. Each length is joined to its neighboring length at one foot increments both mechanically and electrically (with rosin-core solder).

An 80 foot length of 50 ohm RG-8/U coaxial cable was used for the antenna feed line. Since the input impedance of the riometer is 50 ohms resistive and since the cable impedance is 50 ohms, maximum transfer of power to the riometer requires the antenna to show 50 ohms impedance. Impedance matching between the Yagi antenna and the cable is accomplished with a 4:1 half-wave balun with a single capacitor matching system. The capacitor is mounted in a protective plastic box and all exposed connections are protected against the weather by a plastic spray. The antenna was tuned with an RX meter to 50 ohms plus .7μf which is well within the requirements of 50 ohms plus or minus 15μf needed to obtain a voltage standing wave ratio of 1.05:1. The radiation pattern of this antenna is broader in the H-plane than in the E-plane. The beamwidth to the half-power points for E is about 60° while it is roughly 110° for H.

4. Reduction of the Riometer Data to Absorption Values

The chart recording obtained from the riometer measures the current flowing in the noise diode tube. This noise power output is continuously and automatically brought into equality with the input signal of the antenna. The noise current is directly proportional to the noise power developed across the load resistor which makes the recording obtained linearly proportional to the antenna input power. Calibration is carried out automatically once every 24 hours by replacing the noise diode by a second matched noise diode source called a test diode. For a fifteen minute period the test diode cycles through six different current readings, each of 2 1/2 minutes duration. The reproducibility of these readings from day to day checks the stability of the riometer.

Before absorption values can be obtained by the cosmic radio noise technique, it is necessary to determine the reference curve or quiet day curve corresponding to the absence of ionospheric absorption. This is an estimate of the sidereal time variation of the cosmic noise power which would be recorded by the riometer under normal ionospheric conditions. The cosmic radio noise technique is sensitive to the reference curve chosen. In all cases in this dissertation the reference curve is computed from the average reading of the first minute of each hour. This corresponds to twenty-four values per day. However, the reference curve may use only selected hourly values of a day depending on what effect is being studied in the ionosphere. In all cases the reference curve is represented as a scatter plot of Esterline August (EA) units, which are proportional to noise power, versus sidereal time. A typical scatter plot of a month's data is shown in Figure 2. This plot includes all day and night EA values. From the envelope curve which encloses the scatter plot, an average absorption-free day is defined for the month. The envelope curve or reference curve is drawn through the top of the scatter plot of noise power points because the top of the dense distribution of points corresponds to the maximum signal strength received by the antenna under normal ionospheric conditions. Another way to look at the envelope curve enclosing the top of the scatter plot is that the maximum in noise power or signal strength corresponds to a minimum of ionospheric attenuation under normal conditions. It is readily seen that from the large amount of data to be handled a computer data reduction program is desirable. This program is discussed in Appendix A. Furthermore, it should be pointed out that any unusual data, either greatly enhanced or greatly depressed, if restricted to periods of days and not including the whole month, will have no effect on the determination of the envelope curve but will stand out distinctly from the envelope values.

Having obtained an envelope curve, a value from the curve for each sidereal hour is transcribed. The twenty four values obtained are then used in a Fourier series computer

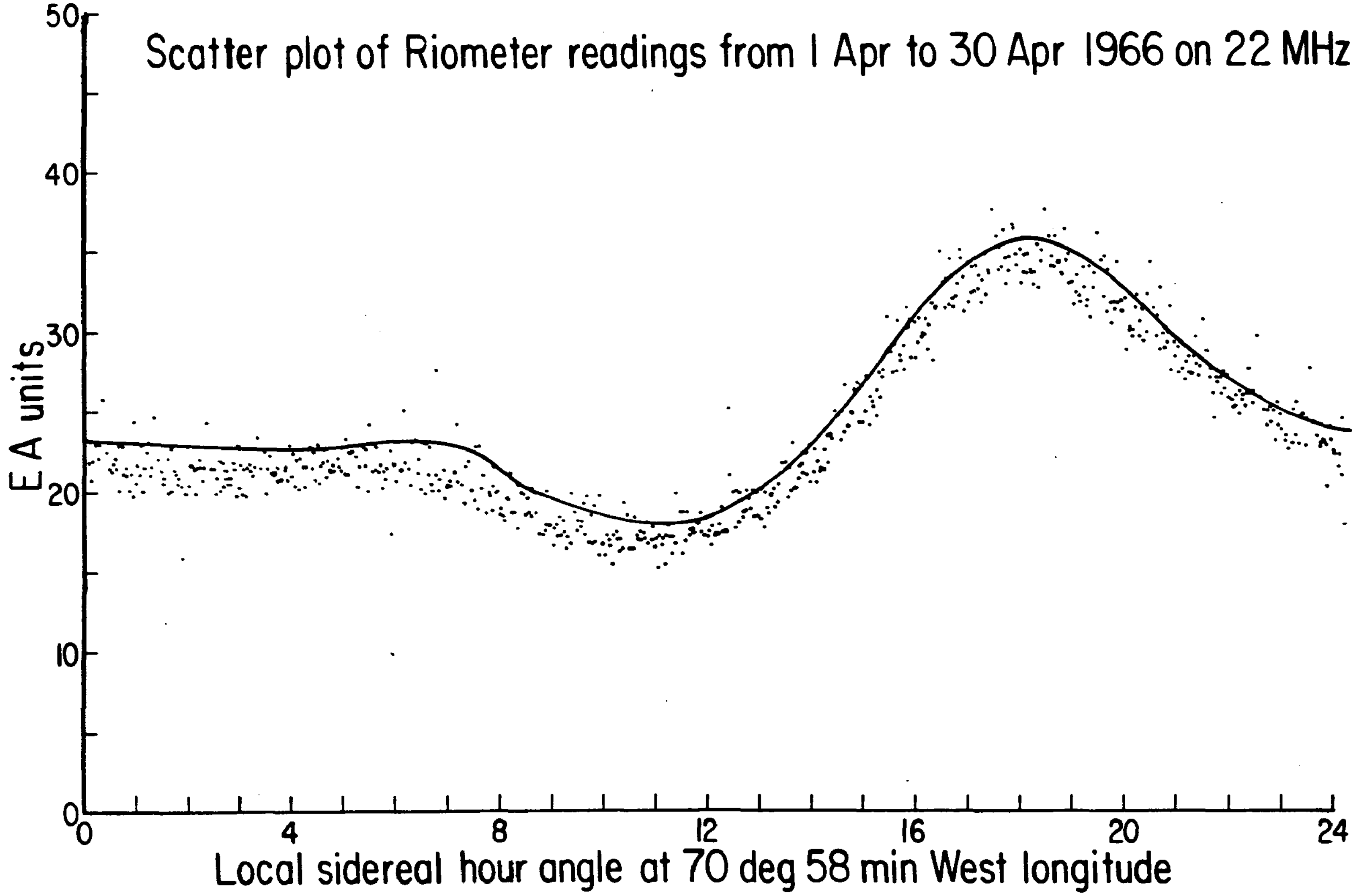
Scatter plot of Riometer readings from 1 Apr to 30 Apr 1966 on 22 MHz
E A units
50
40
30
20
10
0
0
4
8
12
16
20
24
Local sidereal hour angle at 70 deg 58 min West longitude

Figure 2

program to determine the Fourier coefficients. This makes it possible to determine analytically the value of the reference curve at any non-integral hour. This program is discussed in Appendix B.

The absorption in decibels is defined by the relation

$$A(dB) = 10 \log \frac{I_q}{I_d} \tag{95}$$

when I_q is the equivalent noise diode current for the reference curve, here described in EA units. It is measured at the same sidereal time as the disturbed day equivalent noise diode current, I_d, which is also measured in EA units. The absorption is calculated by computer methods from the above equation. Generally the absorption is computed on the hour, any smaller designation of time being too small and time consuming for a long term study. For selected, short duration, unusually disturbed periods, however, the program will calculate absorption at three-minute intervals if the disturbed data is read into the computer in these increments of time. This program is discussed in Appendix C. The absorption data may also be plotted by means of the program discussed in Appendix D.

CHAPTER IV

EXPERIMENTAL RESULTS FROM SOLAR INDUCED IONOSPHERIC ABSORPTION STUDY

1. Introduction

The first measurement of ionospheric absorption by the cosmic radio noise technique was made by Mitra and Shain [1953]. Using a frequency of 18 MHz, they studied the absorption for the months of July, September, November, and December of 1950. The reference curve used was computed over the period of one year but it has not been made clear in what manner the values were selected. However, the authors do state that hourly values were chosen for which ionospheric attenuation is negligible.

Mitra and Shain made use of a total power receiver with a beamwidth to the half power points of 17°. The total integrated hourly absorption values determined by the cosmic noise method were plotted against the hourly values of the critical F_2 frequency, f_oF_2, determined by the sounder method. The frequency, f_oF_2, is the maximum frequency of reflection from the F_2 layer for vertical incidence. A clear dependence of the integrated absorption on f_oF_2 was evident by averaging the observed total absorption for intervals of one MHz for each hour of the day for one month. The resulting curve extrapolated to zero f_oF_2 did not intercept the absorption axis at zero as supposed but at some finite value. The resulting intercept value of absorption for each hour of the day was the average for that hour for the month. The intercept value of absorption proved to be independent of f_oF_2 while the f_oF_2 absorption was the difference between the intercept value and the total average monthly value for the hour. The results showed there were a few tenths of a dB absorption in the F2 region although it was not clear whether there was more absorption in one month than another. The absorption not occurring in the F2 region was assumed to be occurring in the D-region. The D-region absorption showed a maximum around local noon with values of one dB in November and December and 0.6 dB in July. Since the site was at Hornsby (34°S, 151°E) the D-region was showing maximum absorption values in local summer and minimum values in local winter.

Warwick and Zirin [1957] made a study at a site in Boulder, Colorado (40°N, 105°W) for a period of a week in June, 1956 on a 18 MHz receiver with a beamwidth of 90° to the half-power points. Their receiver recorded a local noon maximum of .35 dB all of which they assumed to occur in the D-region. This assumption was based on the earlier work of Mitra and Shain [1953], who found little F2-region absorption compared to that in the D-region.

Bhonsle and Ramanathan [1958] reported results from the continuous recording of cosmic radio noise on 25 MHz at Ahmedabad, India (23°N, 72°E) for the period March, 1957 to February, 1958. The reference curve was based on a year of data restricted to the hours between 0300 and 0600 local time. The D-region and F2-region absorption were separated by the method of Mitra and Shain [1953]. The conclusions reached by this study were that a daytime maximum in the absorption occurs near local noon with a second maximum occurring after sunset and before midnight, usually between 2000 and 2200 hours local time, in the winter and equinoctial months. The D-region showed maximum absorption symmetric about local noon of roughly 3 dB in June and roughly 1 dB in December. The F2-region absorption was maximum in the winter with the first maximum of 3 dB at 1300 local time and the second maximum reaching 4.5 dB in January. This second maximum in absorption was present from September until April. In the summer months the second maximum did not occur and the F2-region absorption maximum at about 1300 local time was less than 2 dB in June. The nighttime values of F2-region absorption went to zero except at the equinoxes. The D-region did not reach zero absorption in the summer months but reached zero for a few hours in winter. Ramamathan and Bhonsle [1959] credited F scatter with the increased absorption in the F-region after sunset at Ahmedabad.

Lusignan [1960] carried out a cosmic noise absorption experiment with two 27.5 MHz riometers, one located at Stanford, California (37° N, 122° W) and the other located at Pullman, Washington (47°N, 117°W) for the year 1958. His reference curve was determined by using a year's data and selecting the local time hours from 0400 to 0700. His analysis separated D-region absorption from F2 region absorption by the Mitra and Shain [1953] method. However, where it was previously assumed that the absorption not taking place in the F2-region was in the D-region, this author made a further separation of absorption components.

The minimum frequency reflected by the F layer, called f_{min}, is a measure of the absorption below the F layer most of which occurs in the D-layer. By using f_{min} in the analogous fashion to f_oF_2 in Mitra and Shain's method, D-region absorption may be separated. Then by subtracting both D-region and F2-region absorption from the total absorption, the remaining absorption was called extra absorption.

The results showed that for the total absorption the maximum occurs at 1200 to 1300 hours local time with the summer months showing 2.5 dB of absorption at maximum. The total absorption did not go to zero at night but also did not show the second maximum after sunset. The D-region absorption showed a maximum symmetric about local noon with a value at maximum of about 1 dB in the summer months and a maximum of roughly 0.6 dB in the winter months. The nighttime values of D-region absorption did not go to zero. The F2-region absorption was not symmetric about noon and exhibited a maximum occurring at roughly 1400 local time. This maximum value was 0.6 dB in winter and 0.2 dB in summer. The F2-region absorption went to zero at nighttime. The extra absorption was very irregular, ordinarily less than 1 dB, and believed caused by the F-region but independent of f_oF_2.

Abdu et al. [1957] report on a cosmic noise absorption study made on 25 MHz at Ahmedabad from 1957 to 1964. Their results showed that the cosmic radio noise absorption at 25 MHz decreased with decrease of solar activity from 1958 to 1964 with the second maximum in absorption found in equinoctial and winter months occurring only in high sunspot years. In high sunspot years the local noontime maximum reached 6 dB in the equinoxes decaying to less than 3 dB at sunspot minimum. The noontime maximum absorption reached its lowest value in the summer both for high and low sunspot years.

An error that could change the absolute magnitude of the solar ionospheric absorption measured is the ionospheric iris or window effect [Fredriksen and Dyce, 1960; Steiger and Warwick, 1961]. Basler [1963] describes this effect as absorption not occurring because of attenuation in the ionosphere but due to the reflection back into space of a part of the incoming cosmic radio noise. This energy is reflected for cosmic radio noise incident at angles larger than the critical angle, θ_c, defined as

$$\cos\theta_c = f_oF_2/f \tag{96}$$

where f_oF_2 is the critical frequency of the F2-region and f is the operating frequency of the riometer. This equation implies that the ionospheric window grows smaller as f_oF_2 increases.

For a 22 MHz riometer, an f_oF_2 of 6.8 MHz corresponds to an absorption by the window effect of less than 0.1 dB.

For f_oF_2 less than 6.8 MHz, the error is proportionally less. Table 1 lists the monthly average value of f_oF_2 for the Billerica, Massachusetts (43°N, 71°W) sounder for each of the 24 hours of a typical month. The hours of the days used to compute the average value of f_oF_2 were the same hours used to calculate the average monthly solar ionospheric absorption. The values shown for a typical month demonstrate that neglecting this effect will not introduce any appreciable error in the absolute magnitude of the solar ionospheric absorption calculated at Durham.

2. Solar Induced Absorption for 1966 and 1967

The preceding section described several ionospheric absorption measurements made under undisturbed conditions during the past 15 years by the cosmic radio noise method. None of these experiments attempted to determine the magnitude of the ionospheric absorption caused by the sun or in what region of the ionosphere the solar absorption occurs. This Section will attempt to answer the first of these questions.

A fundamental key to this study involves selecting a reference curve which is independent of the solar ionospheric absorption. To determine the reference curve called a "quiet night" or "total night" curve, a scatter plot was made of EA units versus sidereal time for the whole year. This was accomplished by selecting daily EA hourly values that fell at least three hours after ground sunset or at least three hours before ground sunrise. This

TABLE 1

MAY 1967

HOUR (U.T.)	0	1	2	3	4	5	6	7	8	9	10	11
Average f_oF_z(MHz)	5.6	6.0	5.7	5.6	5.0	4.9	4.7	4.3	3.8	3.6	4.6	5.2
HOUR (U.T.)	12	13	14	15	16	17	18	19	20	21	22	23
Average f_oF_z(MHz)	5.6	6.2	5.8	5.6	5.3	5.7	5.7	6.0	6.0	6.3	6.1	6.4

insures that at all times of the year the upper ionosphere has been in darkness at least one and one half hours [Hellweg, 1945]. This is reasonable since the time constant of the upper ionosphere is given as one hour [Ratcliffe and Weeks]. Figure 3 shows the scatter plot and envelope curve for the year 1967. A similar curve has been obtained for 1966. The computer programs to calculate the scatter plot and determine the Fourier coefficients have been mentioned previously and are discussed in Appendices A and B.

Having obtained a reference curve free of solar ionospheric absorption, it is necessary to establish the criteria with which to select the daily hourly values to be used in determining the solar ionospheric absorption for each month. Because this study is concerned with the average undisturbed ionosphere the criteria chosen must reflect this average condition. Although there are many geophysical phenomena recorded, none have been demonstrated to have a one-to-one effect on the ionosphere under quiet conditions. In this study the hourly values of absorption determined from the quiet day reference curve for each month have been chosen as the basic criteria. The quiet day curve, determined for each month, represents the normal undisturbed ionosphere for that month, and includes day and night values. Ideally the EA values which fall directly on the envelope curve of the quiet day curve for each month are the EA values to be selected. However, with this stringent criteria it would be impossible to obtain sufficient data for valid results. Hence only hourly EA values which exhibit less than

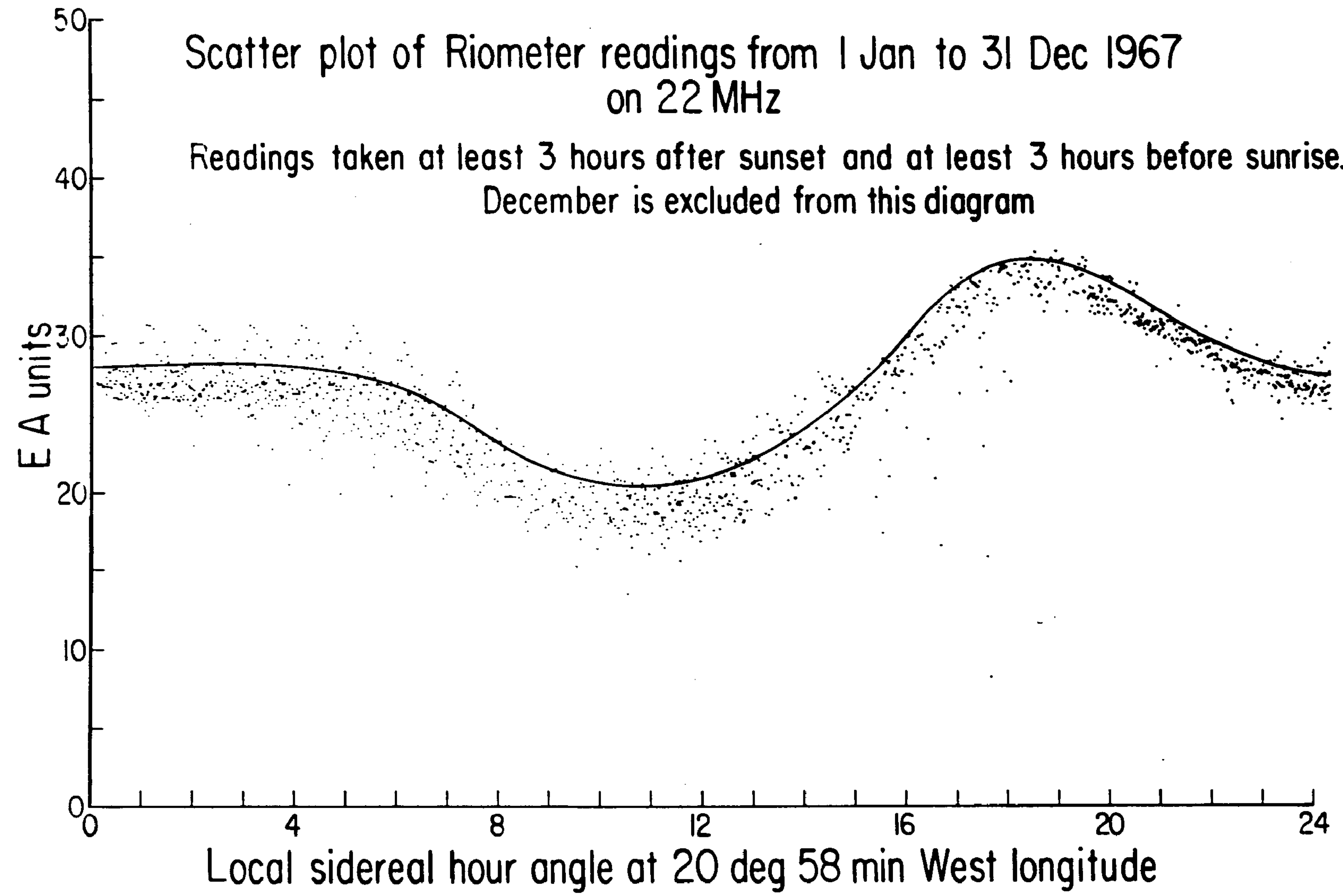
Scatter plot of Riometer readings from 1 Jan to 31 Dec 1967
on 22 MHz
Readings taken at least 3 hours after sunset and at least 3 hours before sunrise.
December is excluded from this diagram
E A units
0
10
20
30
40
50
0
4
8
12
16
20
24
Local sidereal hour angle at 20 deg 58 min West longitude

Figure 3

$|0.10|$ dB absorption when compared to the monthly quiet day curve are utilized. The value of $|0.10|$ dB was chosen because it represents a small absorption but still of significance. The technique developed takes one month of hourly EA values and, using the envelope curve for that month, determines the absorption by equation 95. Hence any hourly absorption value determined from the quiet day curve that shows less than $|0.10|$ dB variation becomes data. The solar time [EST or LMT] for this EA value is converted to sidereal time. The EA value from the reference quiet night curve at the same sidereal time is used with the EA value meeting the $|0.10|$ dB requirement in equation 95 to find the solar ionospheric absorption for the solar time hour. This same criteria was then applied to each hour for each day of the month. The mean value of each of the twenty four solar time hours was then determined month by month. The error analysis is shown in Appendix E. The choice of monthly hourly averages of absorption is dictated by the fact that over a month period the solar zenith angle for a particular EST hour does not change by more than 5° at the time of maximum change which occurs during the equinoxes. At other times of the year the change is considerably less than 5° and is only a few degrees. The month is then a natural division to study seasonal effects with negligible change in the sun's position [Lerfald, 1967].

As an example of how the solar ionospheric absorption is determined, consider the value that occurs at hour 1700UT on April 19, 1966. The EA value, which is proportional to the noise power of the signal at the receiver, is read for the first minute of hour 1700UT and is given as 21.8 EA units. The hour 1700UT corresponds to a sidereal time of 0204 at Durham.

Initially, a scatter plot for April 1966 is obtained. This plot includes all hourly EA values for each day of the month. The EA values are read in solar time units and converted to sidereal time before being plotted. The resulting plot and envelope curve, shown in Figure 2, represents the normal and undisturbed ionosphere for a sidereal day in April 1966. At the sidereal time 0204 the envelope curve has a value of 22.2 EA units. Using equation 95 with I_d equal to 21.8 EA units and I_q equal to 22.2 EA units results in .08 dB absorption. This value of absorption falls within the criteria of 0.10 dB and is taken as data in all subsequent calculations.

To determine the solar ionospheric absorption the quiet night scatter plot and envelope curve are used for 1966. The scatter plot and envelope curve for 1966 are similar to 1967 as shown in Figure 3. The hourly values making up the scatter plot are all nighttime values corresponding to hourly EA values that occur at least three hours after sunset and at least three hours before sunrise. Again the values are read in solar time units and converted to sidereal time before plotting. The resulting envelope curve corresponds to a typical sidereal day in 1966 free of any sun. The envelope value at 0204 is 26.8 EA units.

Using equation 95 with I_d equal to 21.8 EA units and I_q equal to 26.8 EA units results in .90 dB absorption.

To compute the average absorption for the hour 1700UT for April 1966 all the hourly EA values at 1700UT are compared to the April quiet day curve at the appropriate times and used as data if they meet the criteria of being less than 0.10 dB. The solar ionospheric absorption is then calculated for each of the data values found above by using the 1966 quiet night reference curve and equation 95. The mean of these values is the value used for the particular hour. For the hour 1700UT in April 1966 there are 10 data values that meet the criteria of less than 0.10 dB absorption giving an average value of solar ionospheric absorption equal to .82 dB with an uncertainty of $\pm$.07 dB. The same process is used for the other 23 hours in April. The EA values accepted as data here will be used as data in all the calculations in Section C of this Chapter. Figures 4 through 10 show the average solar ionospheric absorption versus time for seven different months in 1966 and 1967. Figure 11 shows the composite of the three months for 1966 and Figure 12 shows the composite for the four months of 1967. There is no data for January 1966 due to a malfunction of the riometer calibrator. Hours with missing values indicate that insufficient data was available to calculate a value.

Examination of the mean diurnal and seasonal variations of total solar ionospheric absorption indicate

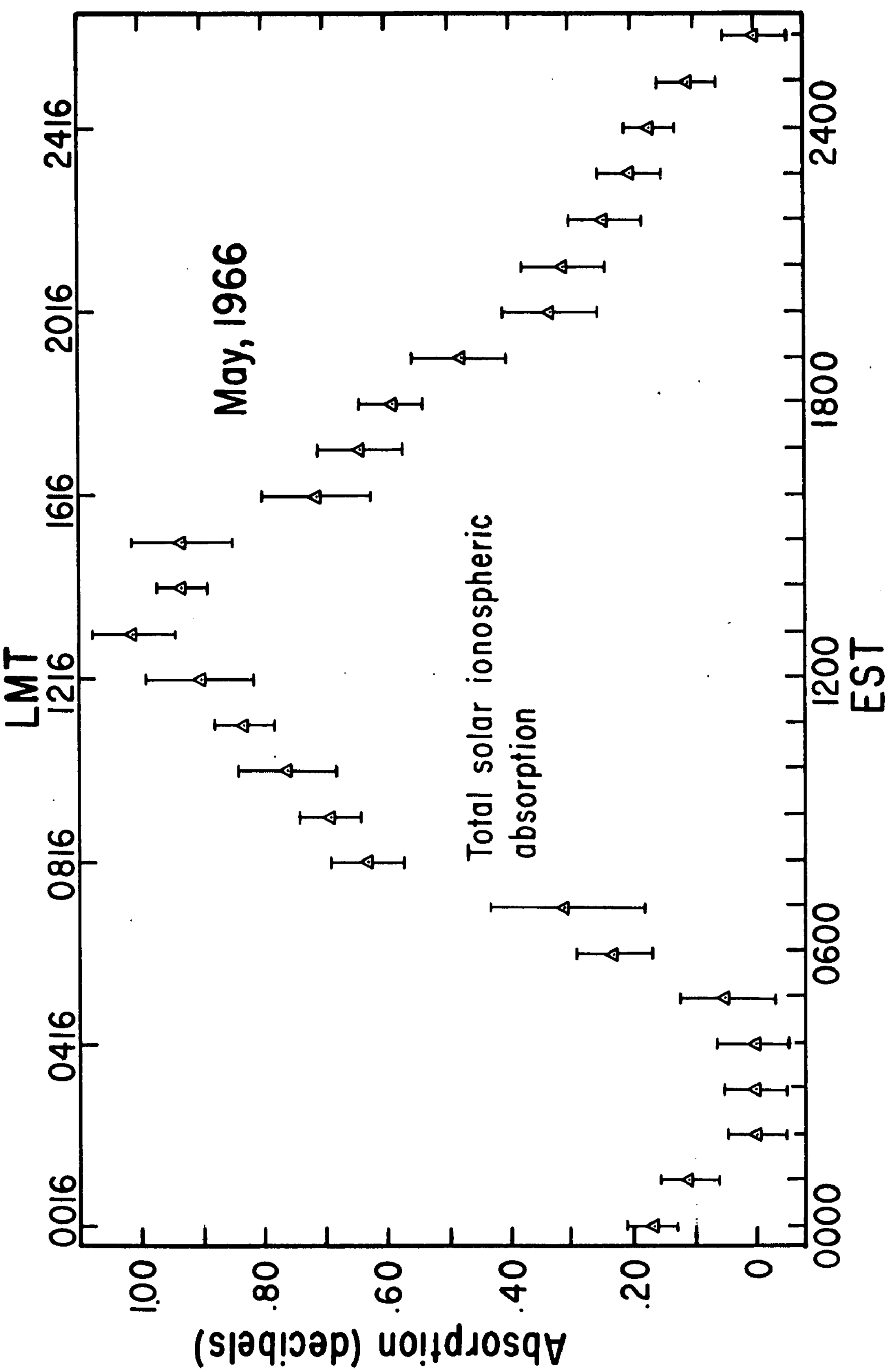
LMT
0016
0416
0816
1216
1616
2016
2416
May, 1966
Total solar ionospheric
absorption
0000
0600
1200
1800
2400
EST
1.00
.80
.60
.40
.20
0
Absorption (decibels)

Figure 4

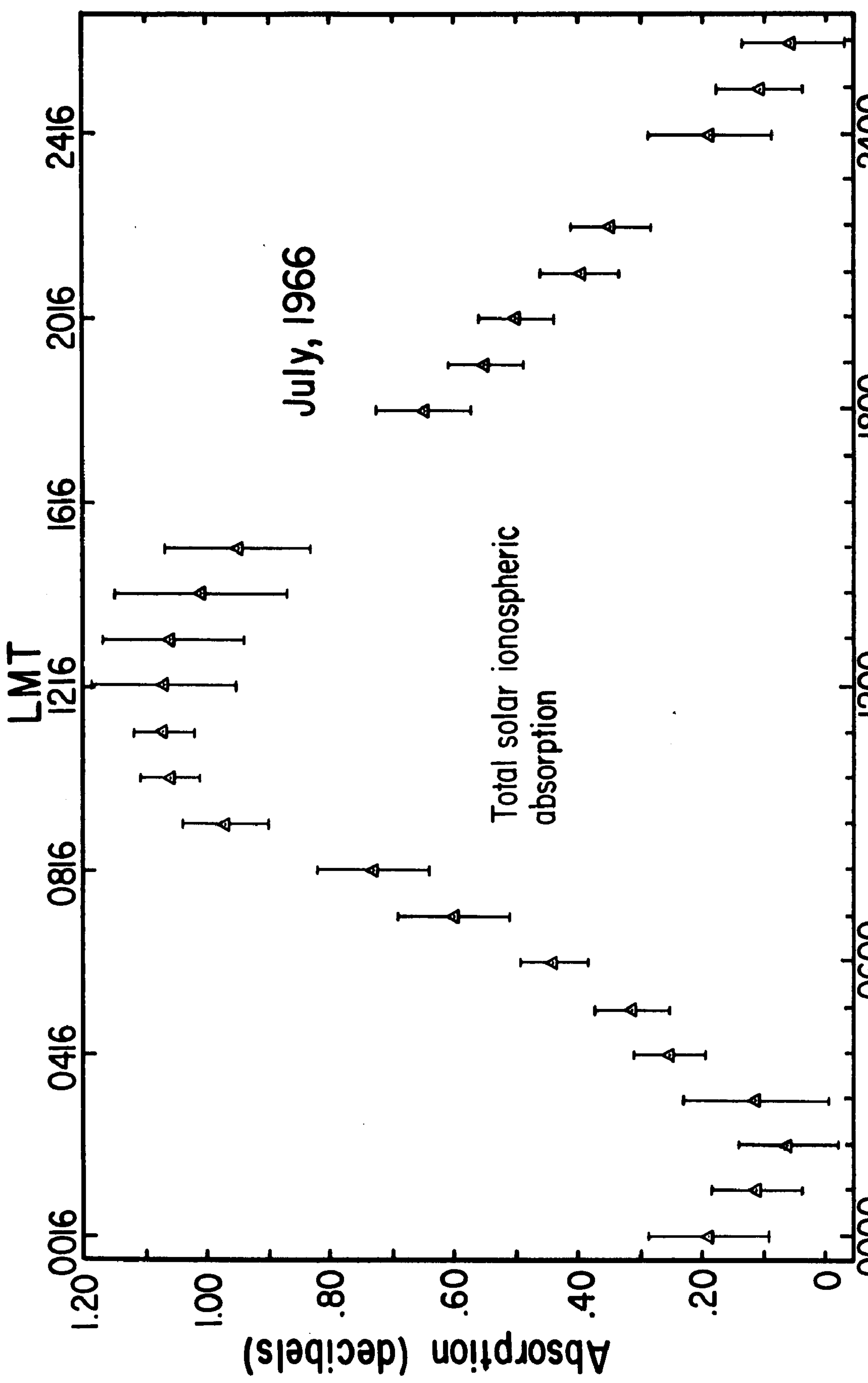
LMT
0016
0416
0816
1216
1616
2016
2416
July, 1966
Total solar ionospheric absorption
Absorption (decibels)
1.20
1.00
.80
.60
.40
.20
0
0000
0600
1200
1800
2400
EST

Figure 5

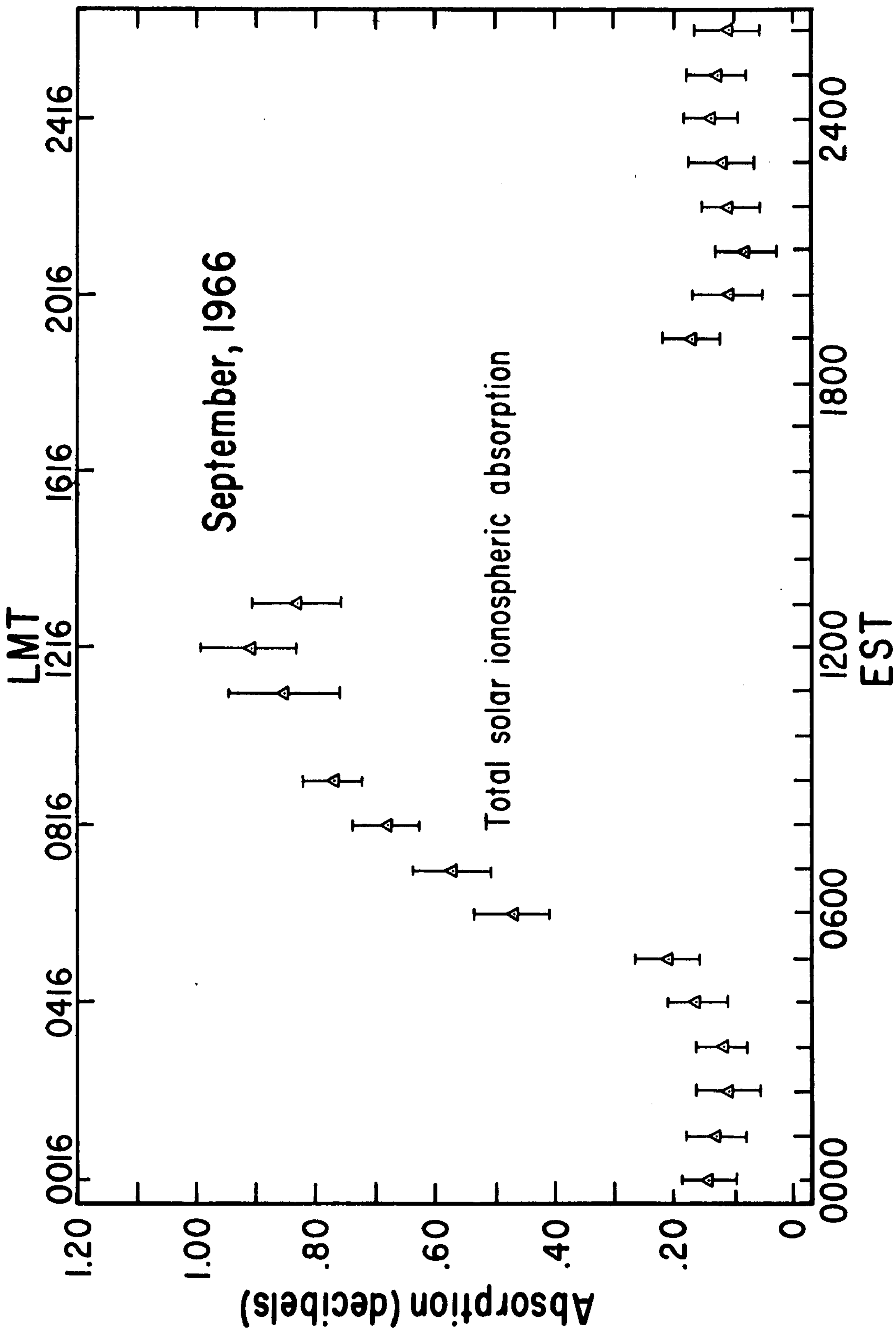

LMT
0016
0416
0816
1216
1616
2016
2416
September, 1966
Total solar ionospheric absorption
Absorption (decibels)
1.20
1.00
.80
.60
.40
.20
0
0000
0600
1200
1800
2400
EST

Figure 6

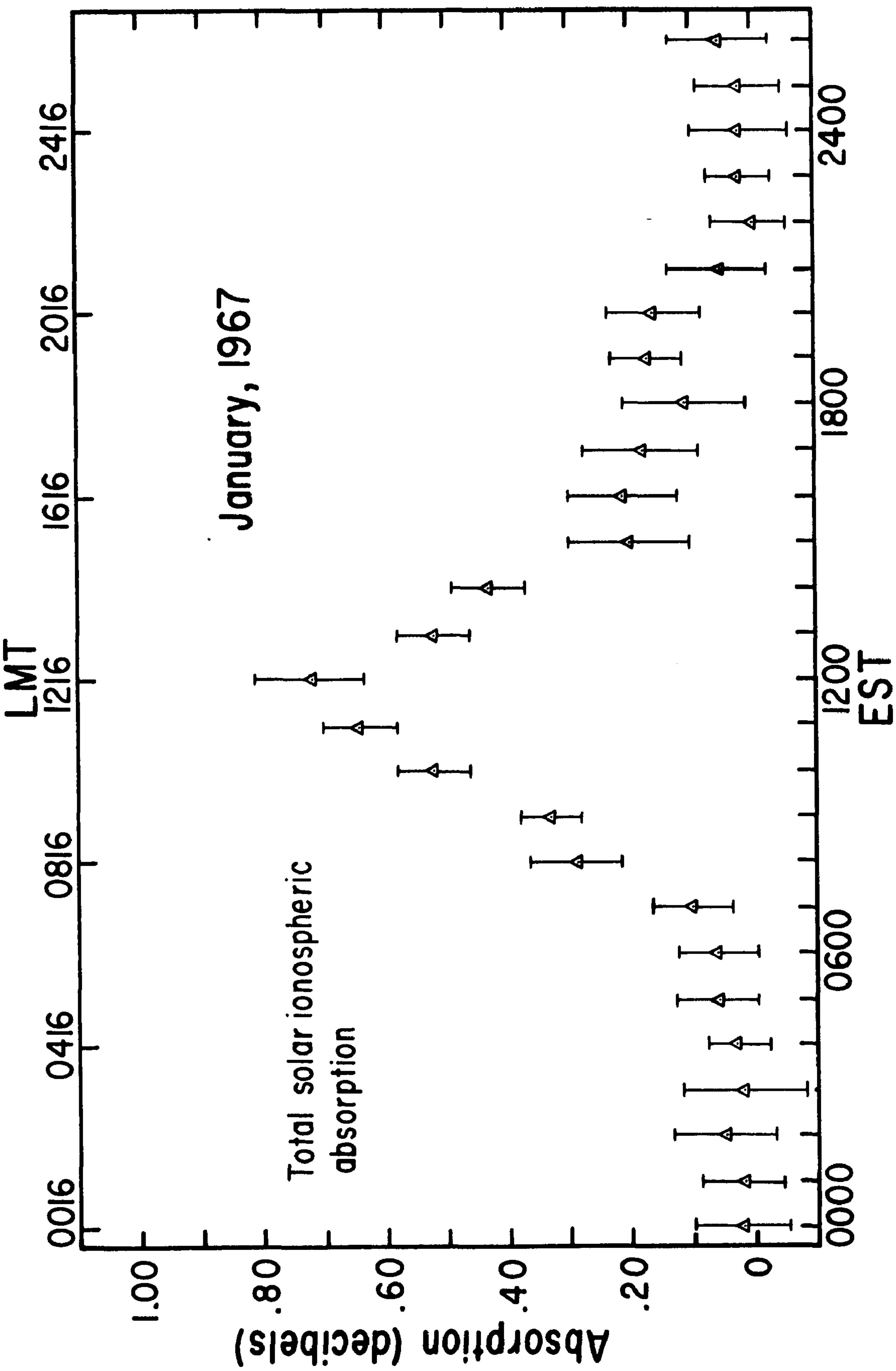
LMT
0016
0416
0816
1216
1616
2016
2416
January, 1967
Total solar ionospheric absorption
Absorption (decibels)
1.00
.80
.60
.40
.20
0
0000
0600
1200
1800
2400
EST

Figure 7

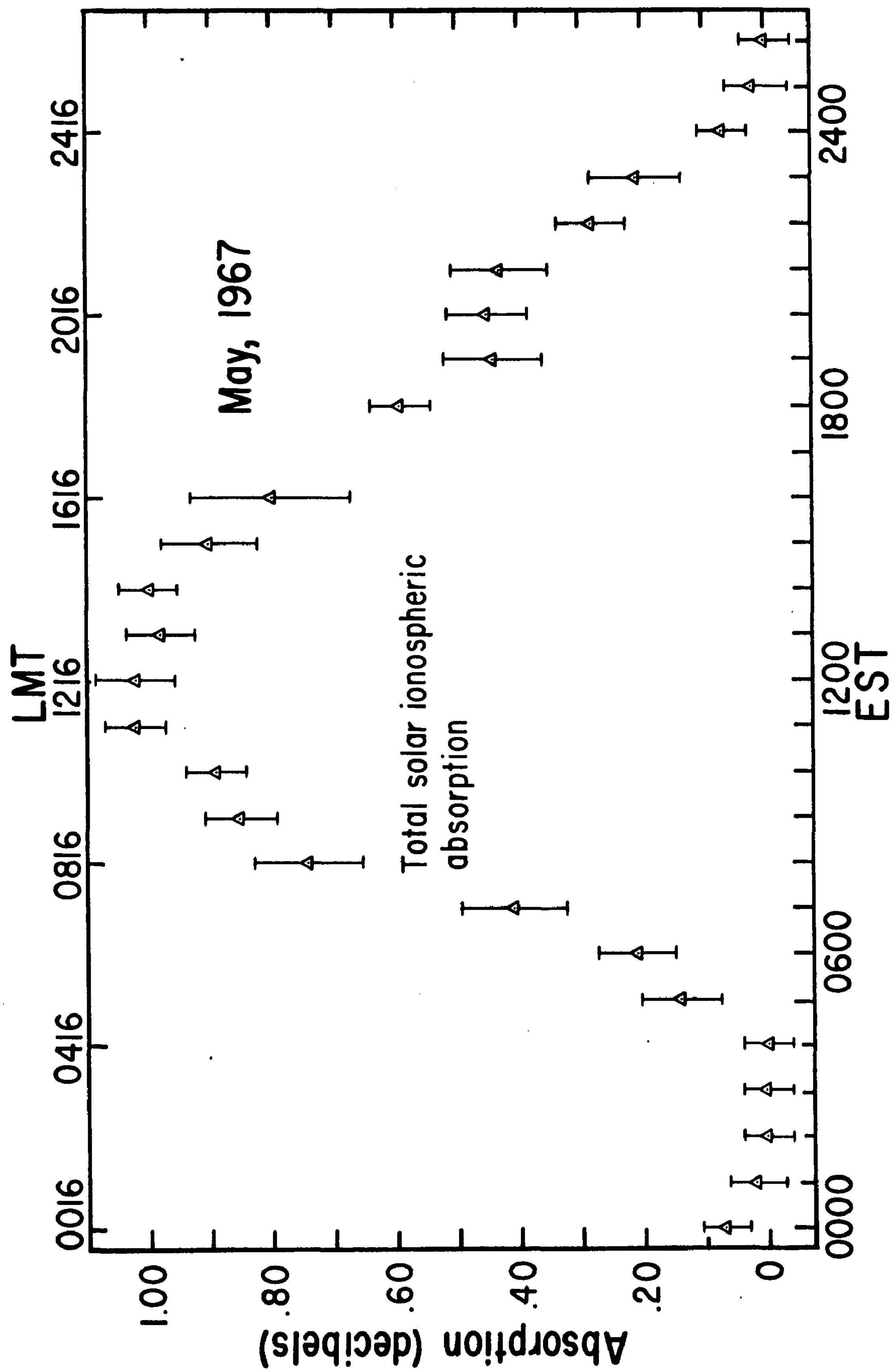
LMT
0016
0416
0816
1216
1616
2016
2416
May, 1967
Total solar ionospheric absorption
Absorption (decibels)
1.00
.80
.60
.40
.20
0
0000
0600
1200
1800
2400
EST

Figure 8

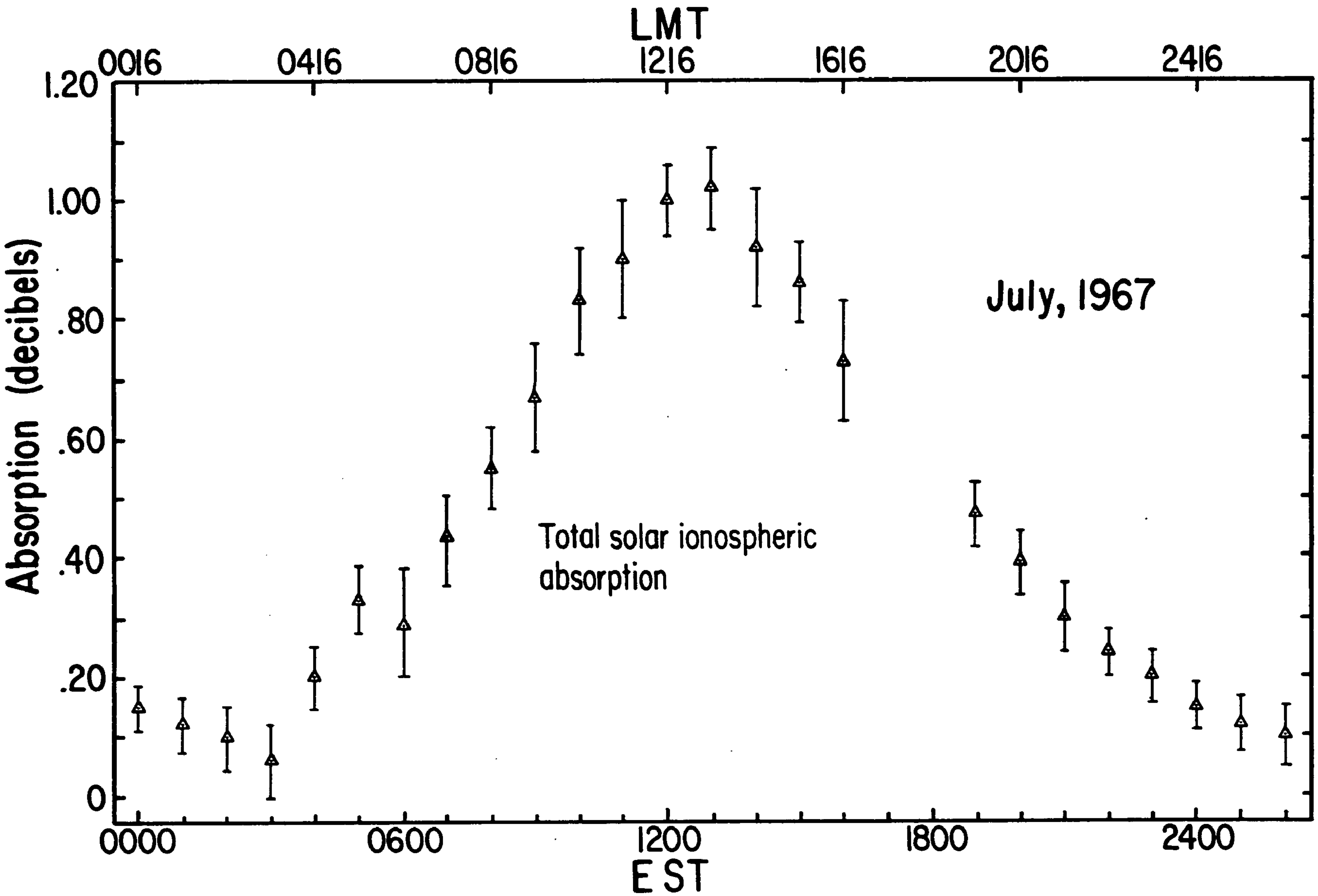
LMT
0016
0416
0816
1216
1616
2016
2416
1.20
1.00
.80
.60
.40
.20
0
Absorption (decibels)
July, 1967
Total solar ionospheric absorption
0000
0600
1200
1800
2400
EST

Figure 9

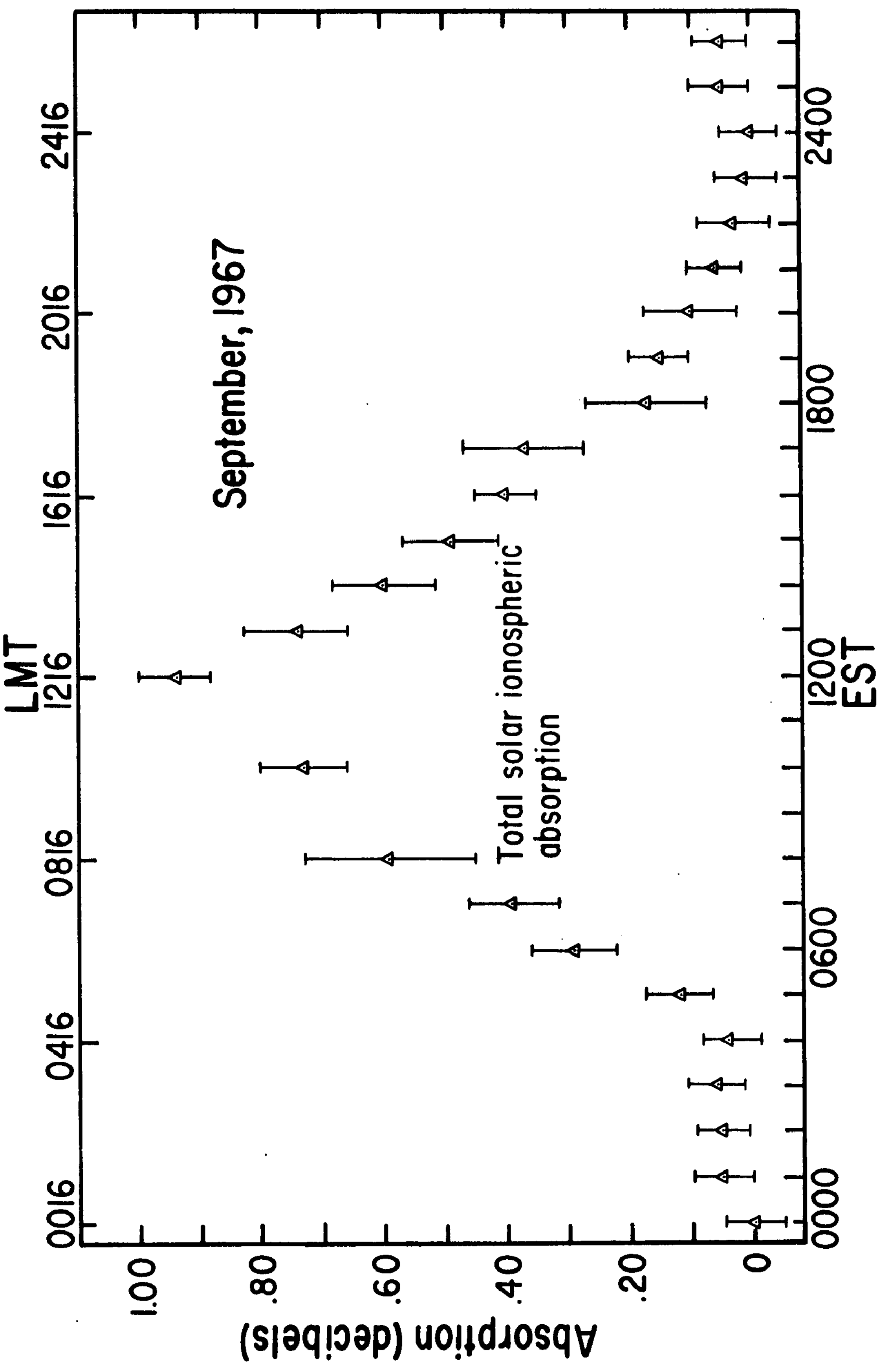
LMT
0016
0416
0816
1216
1616
2016
2416
September, 1967
Total solar ionospheric absorption
Absorption (decibels)
1.00
.80
.60
.40
.20
0
0000
0600
1200
1800
2400
EST

Figure 10

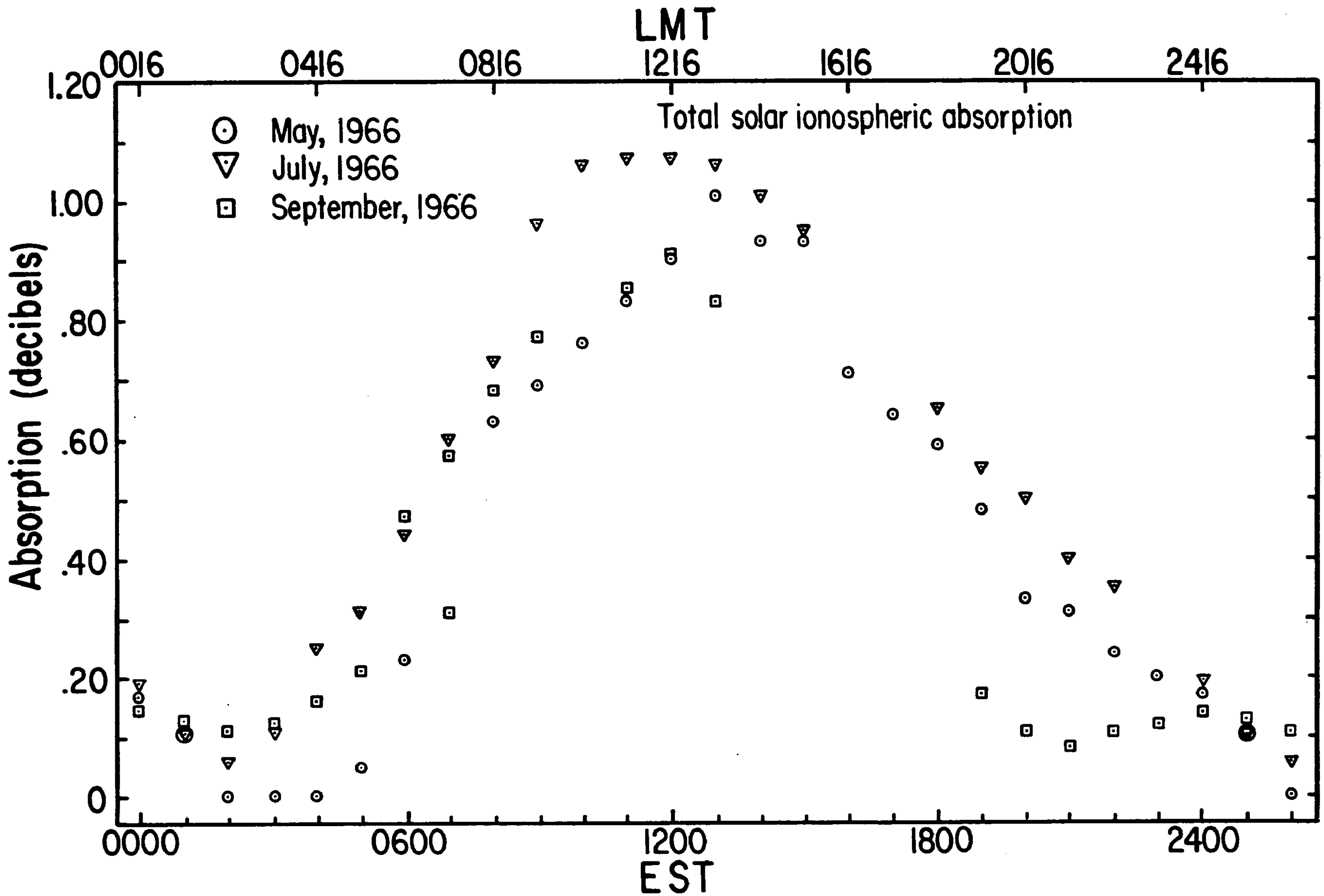
LMT
0016
0416
0816
1216
1616
2016
2416
Total solar ionospheric absorption
May, 1966
July, 1966
September, 1966
Absorption (decibels)
1.20
1.00
.80
.60
.40
.20
0
0000
0600
1200
1800
2400
EST

Figure 11

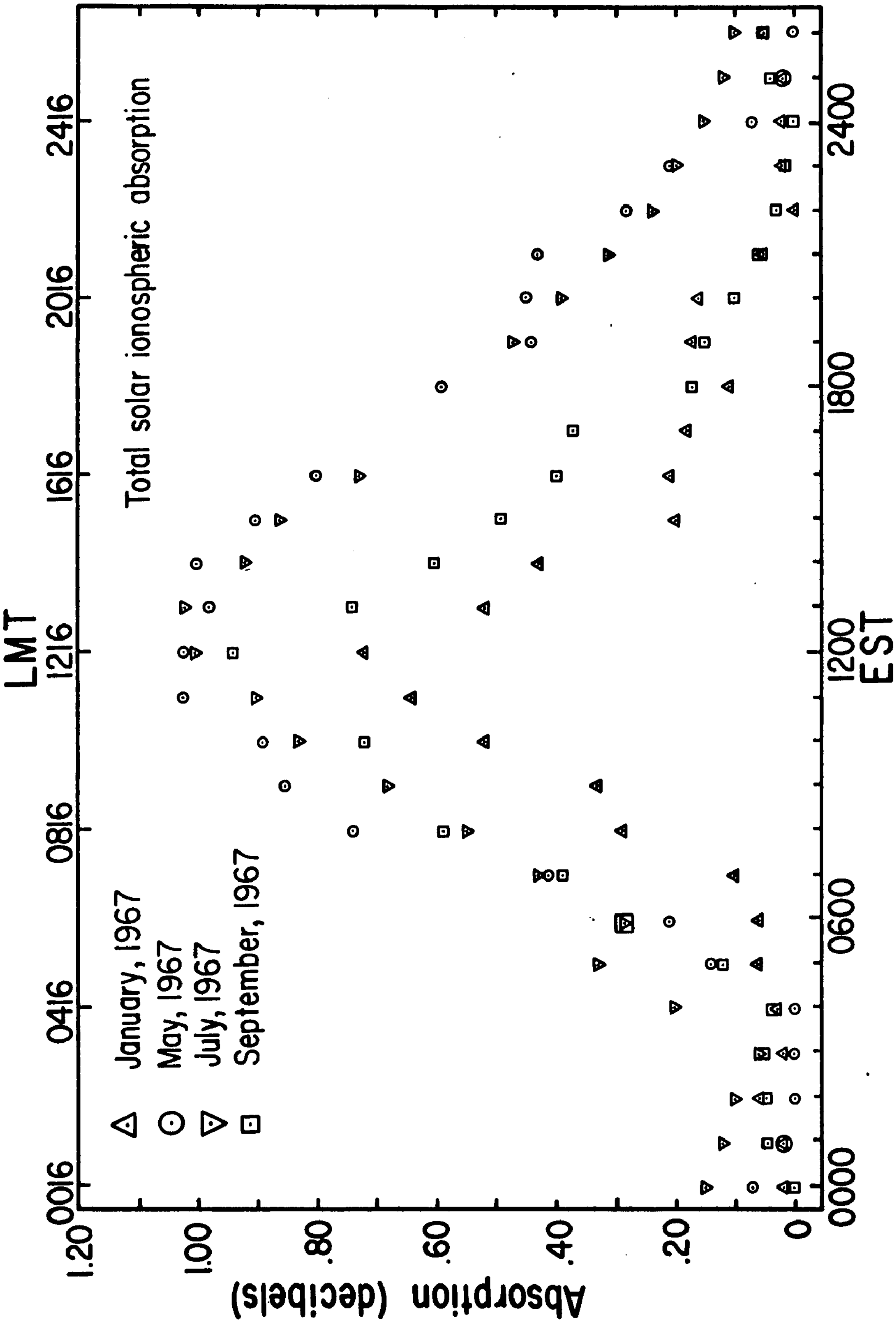
Total solar ionospheric absorption
LMT
0016
0416
0816
1216
1616
2016
2416
EST
0000
0600
1200
1800
2400
Absorption (decibels)
1.20
1.00
.80
.60
.40
.20
0
January, 1967
May, 1967
July, 1967
September, 1967

Figure 12

the following trends: (1) a single maximum in absorption occurring very close to local noon; (2) a larger magnitude of absorption in the summer months than in the winter months; (3) an assymetry around local noon with the decay to zero extending well into the nighttime; and (4) within experimental error the absorption does go to zero for part of the night. The duration of the zero level is much longer in winter than summer.

A closer look at these conclusions indicates that the single maximum in absorption occurring very close to local noon is indicative of solar control of the absorbing layer. The maximum absorption occurs when the solar zenith angle, χ, reaches its smallest value and the production function, q, reaches its largest value for a given height, as indicated in equation 37. The larger magnitude of absorption which occurs in the summer months as compared to the winter values is again explained by solar control. For this to occur, the sun is higher in the sky (smaller χ) in the summer than in the winter implying that q is larger at a given height in summer than in winter. Thus with a greater q there is a greater production of electrons and the characteristic absorption is greater.

The fact that the absorption does not go to zero when the sun sets indicates a more complex effect is taking place. Experimentally it is well known that the F-region electron density reaches its maximum in the late afternoon. Hence, one might expect that the absorption would not decay to zero at sunset but decay to zero only when the F-region solar induced electron density decreases to zero. The long time interval required for the absorption to decay to zero may be indicative of the slow rate of electron recombination in the F-region. Other nighttime values may indicate a disturbed condition flux of some kind. The preponderance of zero nighttime values gives confidence in the technique used.

3. Solar Induced Ionospheric Absorption Determined by Sunrise and Sunset at 150 Km Reference Curves

a. General Properties

As discussed in the beginning of this Chapter, the previous methods used to separate the absorption components in various regions of the ionosphere relied on a separate method of measurement, namely the use of ionospheric sounders. Here a new method is used to separate the absorption into that occurring in the upper ionosphere, defined to be at heights greater than 150 km, and the lower ionosphere, defined to be at heights less than 150 km. The method developed here utilizes reference curves that are found for sunrise at 150 km and sunset at 150 km. The sunrise at 150 km reference curve is a scatter plot of EA values versus sidereal time. The EA values correspond to the signal strength received by the riometer when the "real sun" reaches the height of 150 km on its way to ground sunrise.

The term real sun may be explained as follows [Skilling and Richardson, 1947]. The apparent eastward motion of the sun with respect to the stars is caused by the revolution of the earth around the sun. If the orbit of the earth were perfectly circular this motion would be uniform and the same day to day. This, however, is not the case. The earth moves in an elliptic orbit around the sun and results in the earth being about 3,000,000 miles nearer the sun in January than in July. According to Kepler's laws the earth is moving faster when it is closer to the sun. Also, the inclination of the earth's axis makes the equator oblique to the ecliptic. Hence the annual motion of the sun on the celestial sphere is sometimes parallel to the celestial equator and sometimes at an angle to the equator. Only motion along the celestial equator affects the length of day. For these reasons a clock keeping sun time would need to run at a non-uniform rate. Since this is mechanically unfeasible a mean or fictitious sun is defined which in one solar year travels the same distance as the real sun. Hence the true or apparent sun may occasionally be as much as six or eight times its own width to the east or west of its average position, the fictitious sun, by which clocks run. Early in February it is 14 1/2 minutes slow, and about November 1 it is 16 1/2 minutes fast.

Mitra [1952] derives an expression for the hours of sunrise and sunset at different atmospheric heights. This height is given by the expression

$$H = a\left(\frac{1}{\cos\theta} - 1\right) \tag{97}$$

where H is the height above the surface of the earth, a is the radius of the earth, and θ is the angle of depression of the sun below the horizon. The solar zenith angle, χ, is defined as

$$\chi = 90° + \theta + 50' \tag{98}$$

where the 50' represents 34' for horizontal refraction and 16' for the semi-diameter of the sun. Knowing χ, the hour angle of the sun, h, is determined by

$$\cosh = \frac{\cos\chi - \sin\phi \sin\delta}{\cos\phi \cos\delta} \tag{99}$$

where δ is the sun's declination, and ϕ is the latitude of the place of observation. Converting h in angular measure into time measure by means of the conversion factor 1 hour equal 15°, the real time of sunrise is defined to be

$$t = 12^h - h \tag{100}$$

and sunset by

$$t = 12^h + h \tag{101}$$

The sunrise curve will not include solar ionospheric absorption below the 150 km level since this region is still not illuminated. It will include solar ionospheric absorption in the upper atmosphere. However, depending on the time constants operating in the upper ionosphere, it is likely that this region has not built up to its daytime conditions. Thus the reference curve would not have the total upper ionosphere solar absorption included.

The sunset curve is determined as the sun is setting at 150 km. Hence the upper ionosphere is completely illuminated and should include all upper ionosphere solar absorption. The sun has just recently set in the lower ionosphere and the time constants here will determine if the region has decayed completely to a night condition. In the Introduction to this Chapter, the early work cited with respect to ionospheric absorption pointed out that the lower ionosphere closely follows the daily solar journey with little delay. Thus it is expected that the sunset reference curve will be largely free of the lower ionosphere solar absorption.

Therefore, solar ionospheric absorption as determined from the sunrise curve will include all the absorption from the lower ionosphere and possibly some solar ionospheric absorption from the upper ionosphere. The solar ionospheric absorption computed from the sunset curve will not include absorption from the upper ionosphere and possibly not all the absorption from the lower ionosphere. The sunset curve then sets a lower limit on the solar ionospheric absorption occurring in the lower ionosphere and the sunrise curve an upper limit on the solar ionospheric absorption occurring in the lower ionosphere.

To determine the solar ionospheric absorption occurring in the upper ionosphere, the average total solar ionospheric absorption for a given hour of a month is found. This was carried out in Section 2 of this Chapter. From this value the corresponding monthly hourly average value of absorption determined either from the sunrise or sunset curve is subtracted. The value obtained by subtracting the sunset value sets the upper limit of solar ionospheric absorption in the upper ionosphere. In a similar manner the value obtained by subtracting the sunrise value sets the lower limit of solar ionospheric absorption in the upper ionosphere.

Figure 13 shows the scatter plot versus sidereal time for the sunrise at 150 km reference curve for 1967. This curve is typical of a sunrise or sunset at 150 km curve. It should also be pointed out that although the times of sunrise and sunset vary only a few hours in solar time, a year of one data point per day will overlay a full 24 hours in sidereal time.

b. Results

Figures 14 through 20 show plots of the average hourly absorption values versus time for the total solar ionospheric absorption. The figures also show the lower ionosphere solar absorption determined from the sunrise curve and the sunset curve. It is to be emphasized that in an analysis of these figures the gross affects will be studied and not a point by point evaluation.

In most cases the total solar ionospheric absorption exceeds the absorption computed from the sunrise and sunset reference curves. In the few cases that show the absorption computed from the sunrise or sunset reference curve to be

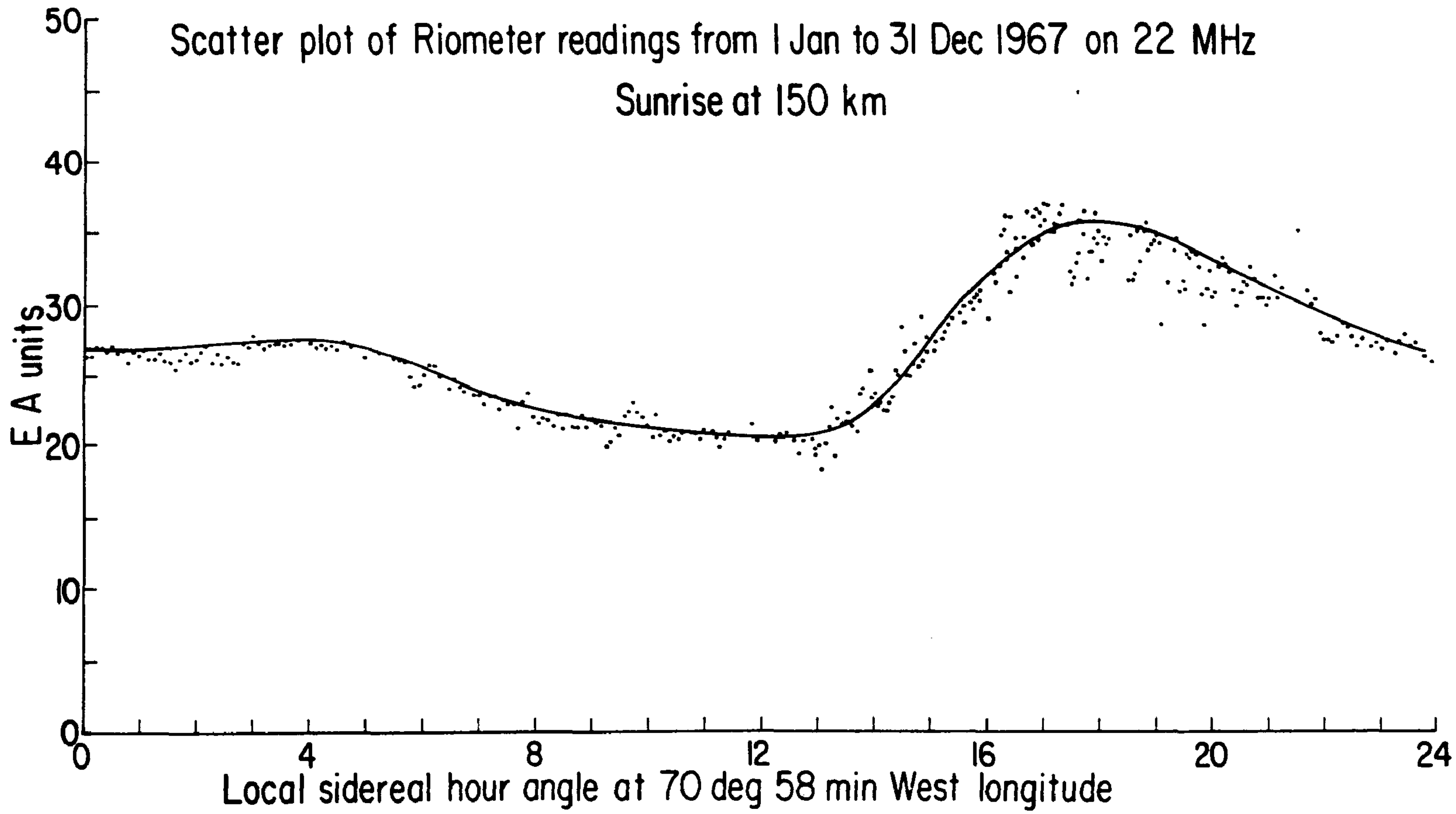
Scatter plot of Riometer readings from 1 Jan to 31 Dec 1967 on 22 MHz
Sunrise at 150 km
E A units
50
40
30
20
10
0
0
4
8
12
16
20
24
Local sidereal hour angle at 70 deg 58 min West longitude

Figure 13

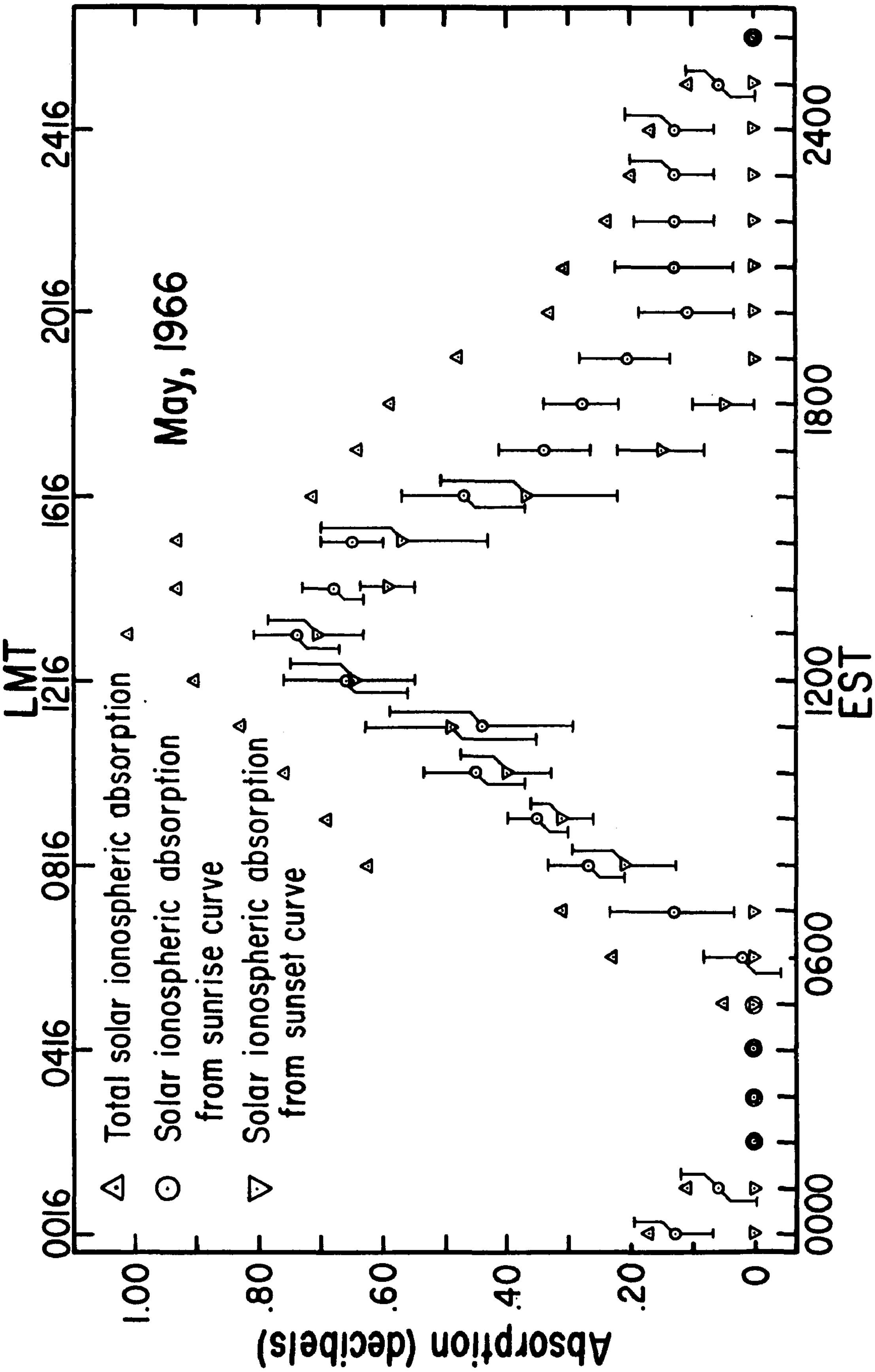
LMT
0016
0416
0816
1216
1616
2016
2416
Total solar ionospheric absorption
Solar ionospheric absorption from sunrise curve
Solar ionospheric absorption from sunset curve
May, 1966
Absorption (decibels)
1.00
.80
.60
.40
.20
0
0000
0600
1200
1800
2400
EST

Figure 14

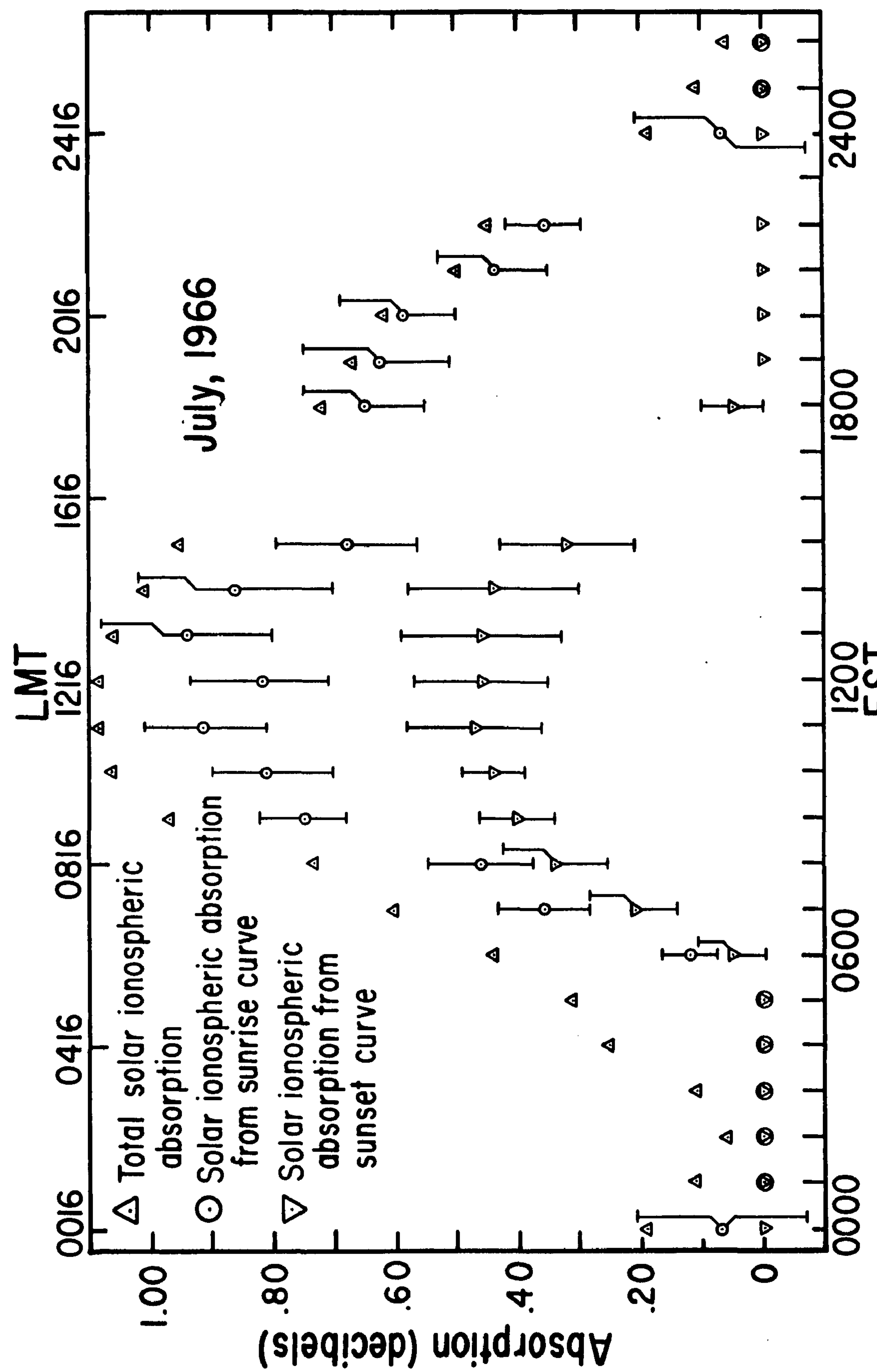
July, 1966
LMT
0016
0416
0816
1216
1616
2016
2416
0000
0600
1200
1800
2400
EST
Absorption (decibels)
1.00
.80
.60
.40
.20
0
Total solar ionospheric absorption
Solar ionospheric absorption from sunrise curve
Solar ionospheric absorption from sunset curve

Figure 15

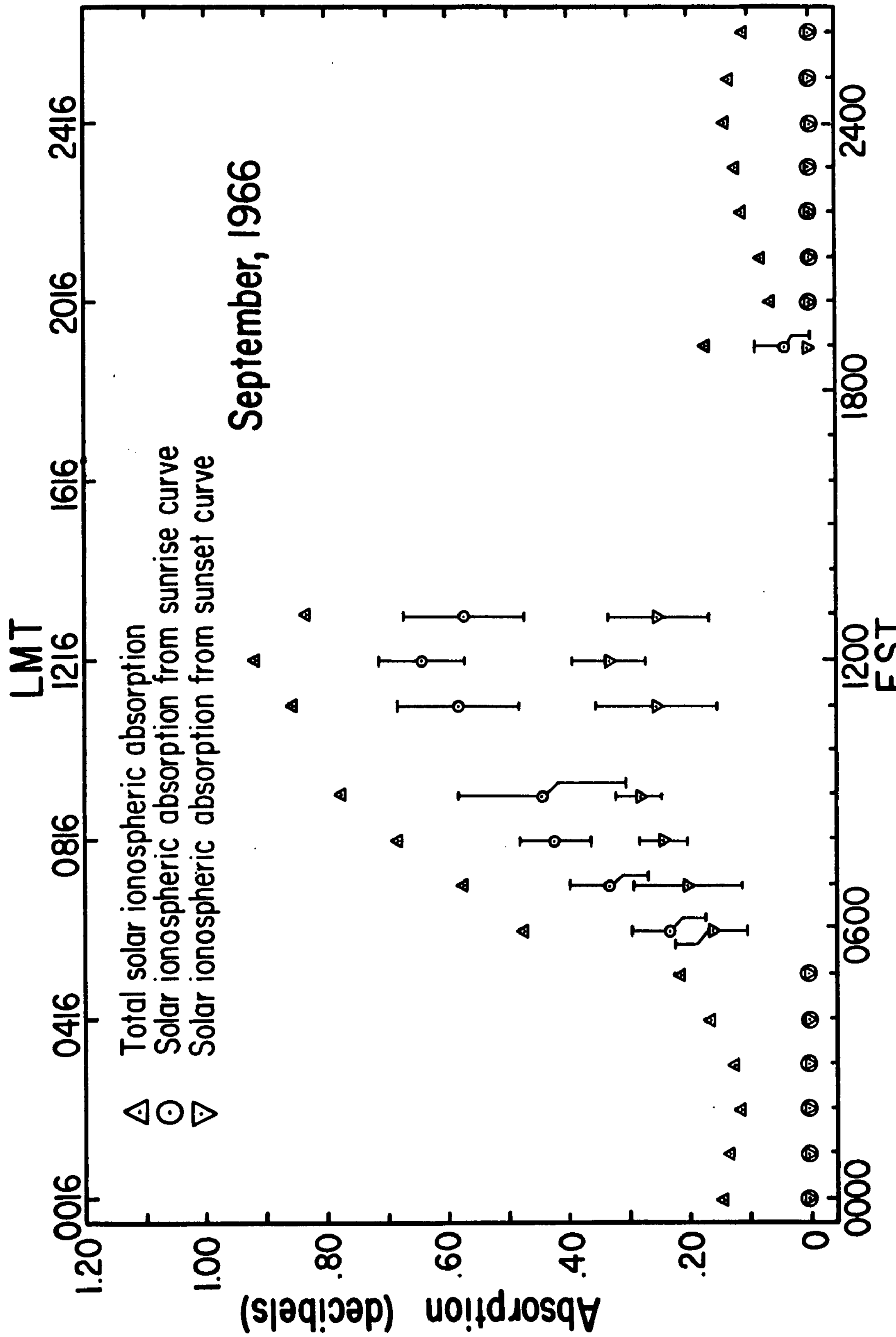
LMT
0016
0416
0816
1216
1616
2016
2416
Total solar ionospheric absorption
Solar ionospheric absorption from sunrise curve
Solar ionospheric absorption from sunset curve
September, 1966
Absorption (decibels)
1.20
1.00
.80
.60
.40
.20
0
0000
0600
1200
1800
2400
EST

Figure 16

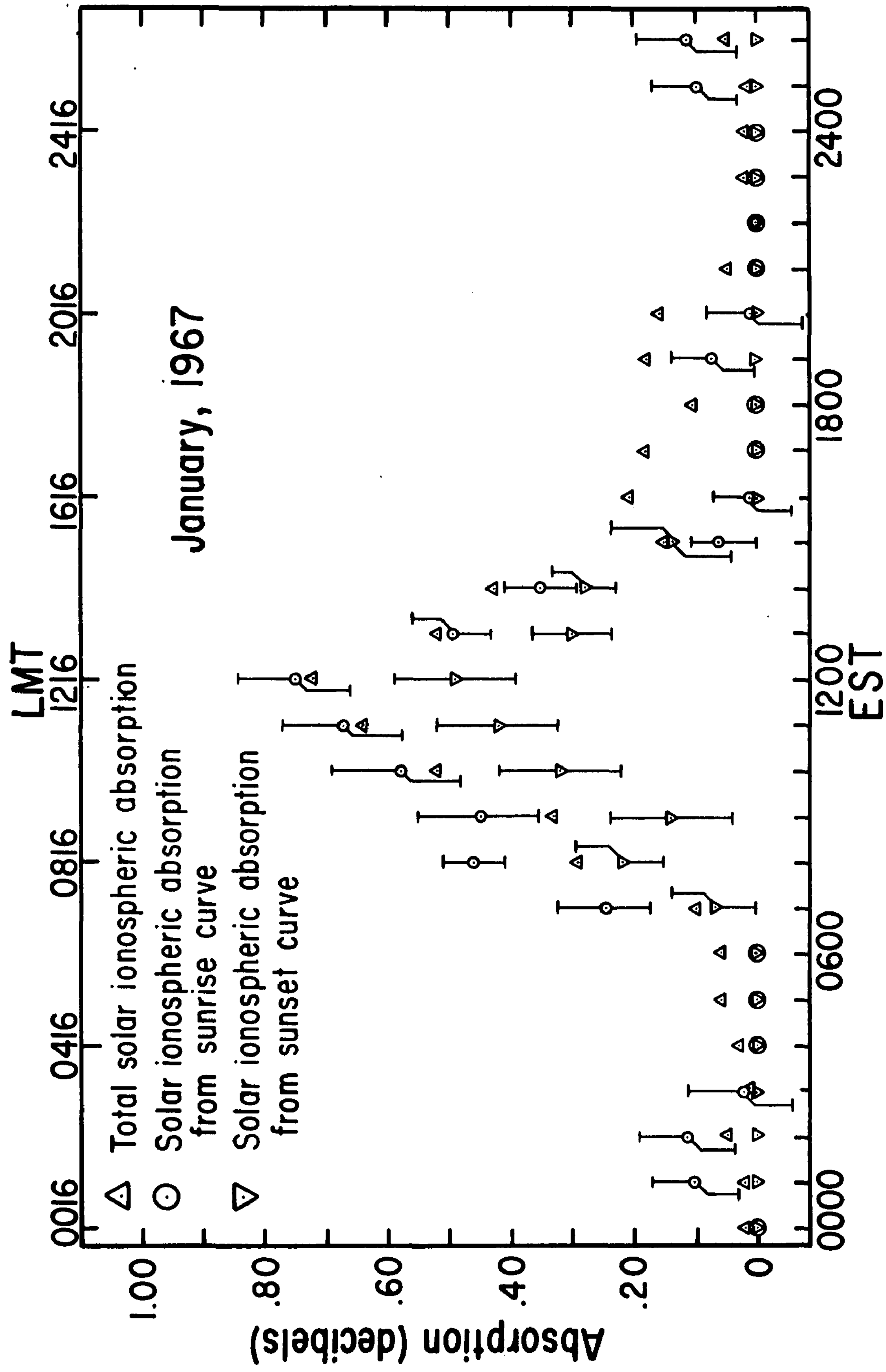
LMT
0016
0416
0816
1216
1616
2016
2416
January, 1967
Total solar ionospheric absorption
Solar ionospheric absorption from sunrise curve
Solar ionospheric absorption from sunset curve
Absorption (decibels)
1.00
.80
.60
.40
.20
0
0000
0600
1200
1800
2400
EST

Figure 17

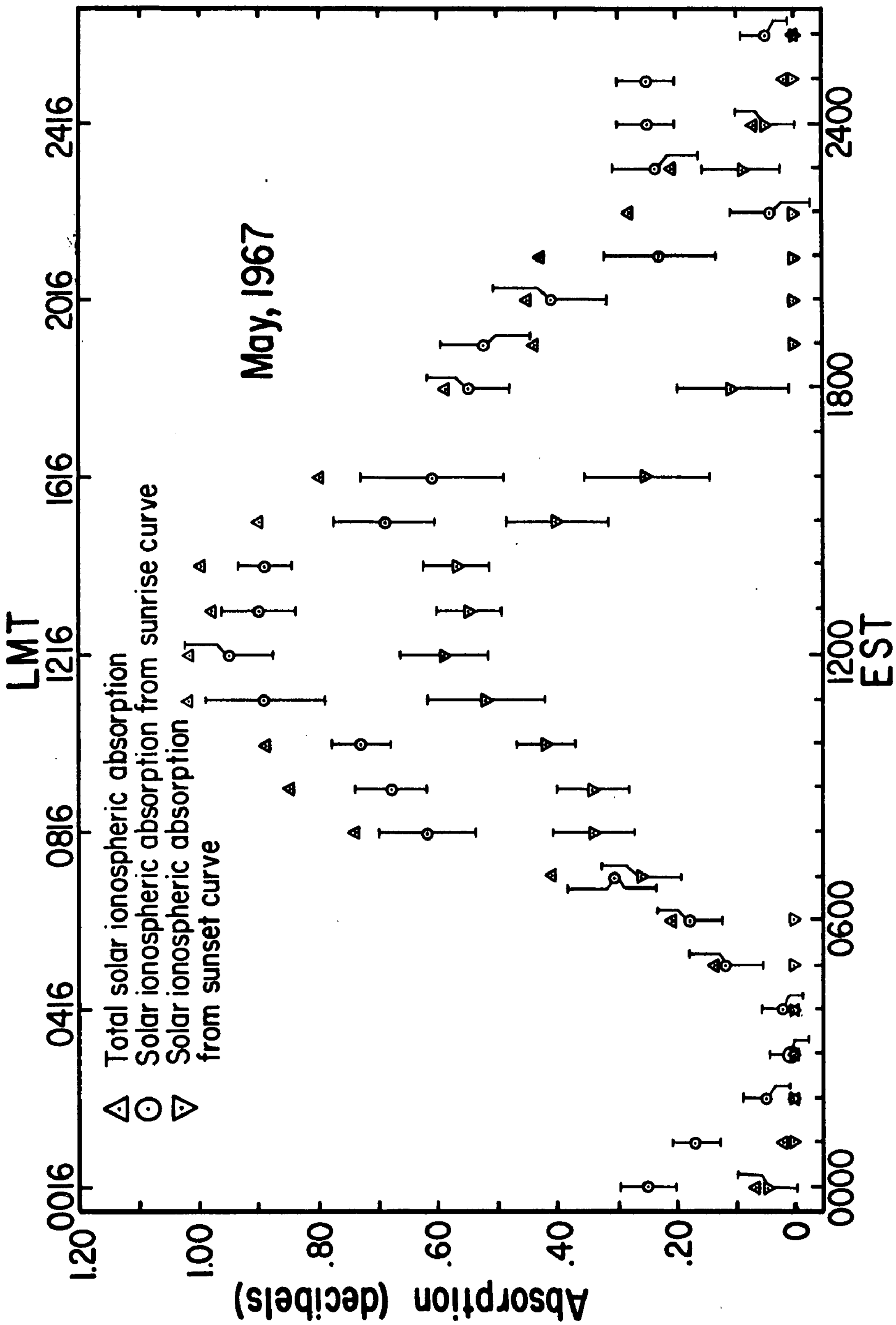
LMT
0016
0416
0816
1216
1616
2016
2416
May, 1967
Total solar ionospheric absorption
Solar ionospheric absorption from sunrise curve
Solar ionospheric absorption from sunset curve
Absorption (decibels)
1.20
1.00
.80
.60
.40
.20
0
0000
0600
1200
1800
2400
EST

Figure 18

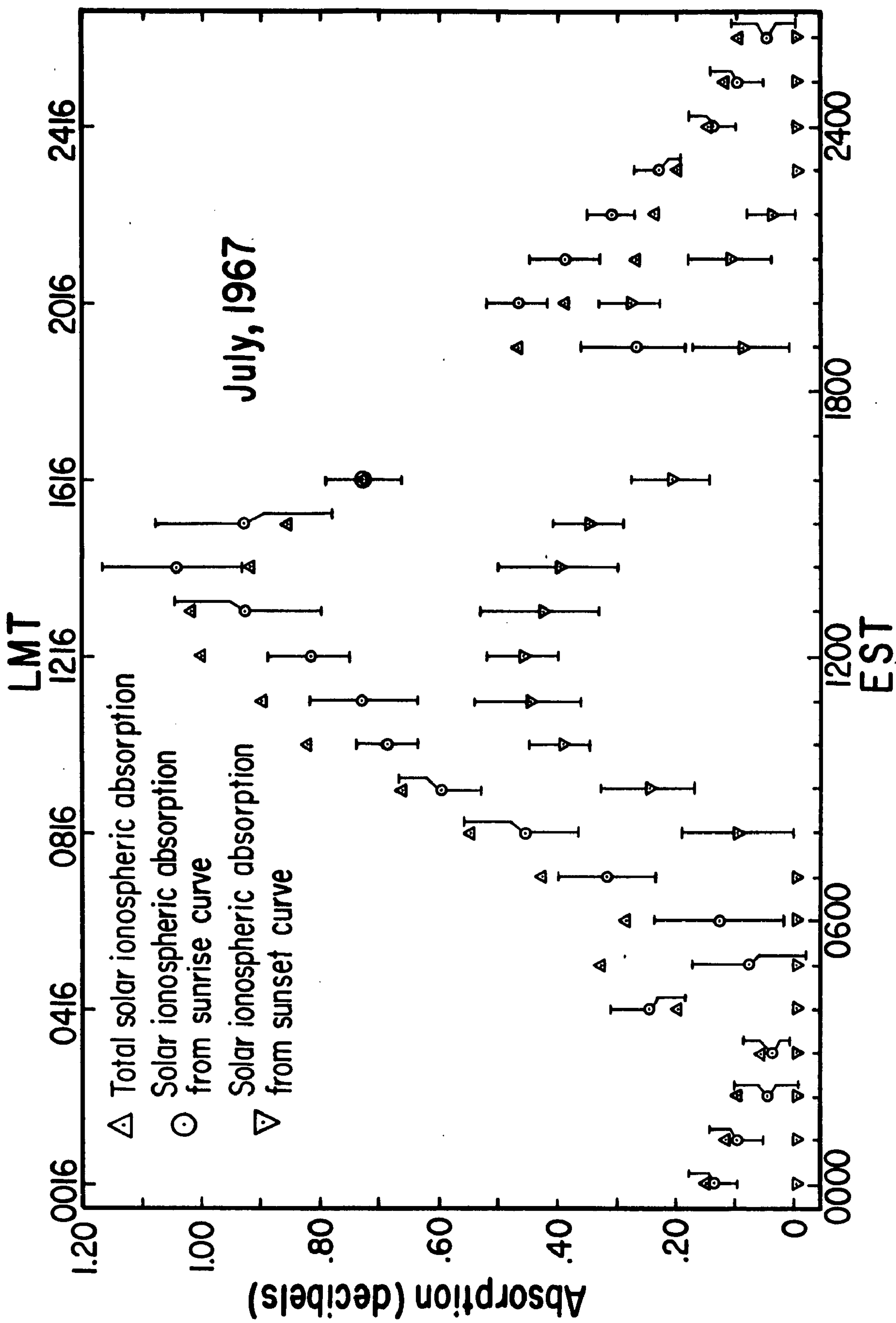
LMT
0016
0416
0816
1216
1616
2016
2416
July, 1967
Total solar ionospheric absorption
Solar ionospheric absorption from sunrise curve
Solar ionospheric absorption from sunset curve
Absorption (decibels)
1.20
1.00
.80
.60
.40
.20
0
0000
0600
1200
1800
2400
EST

Figure 19

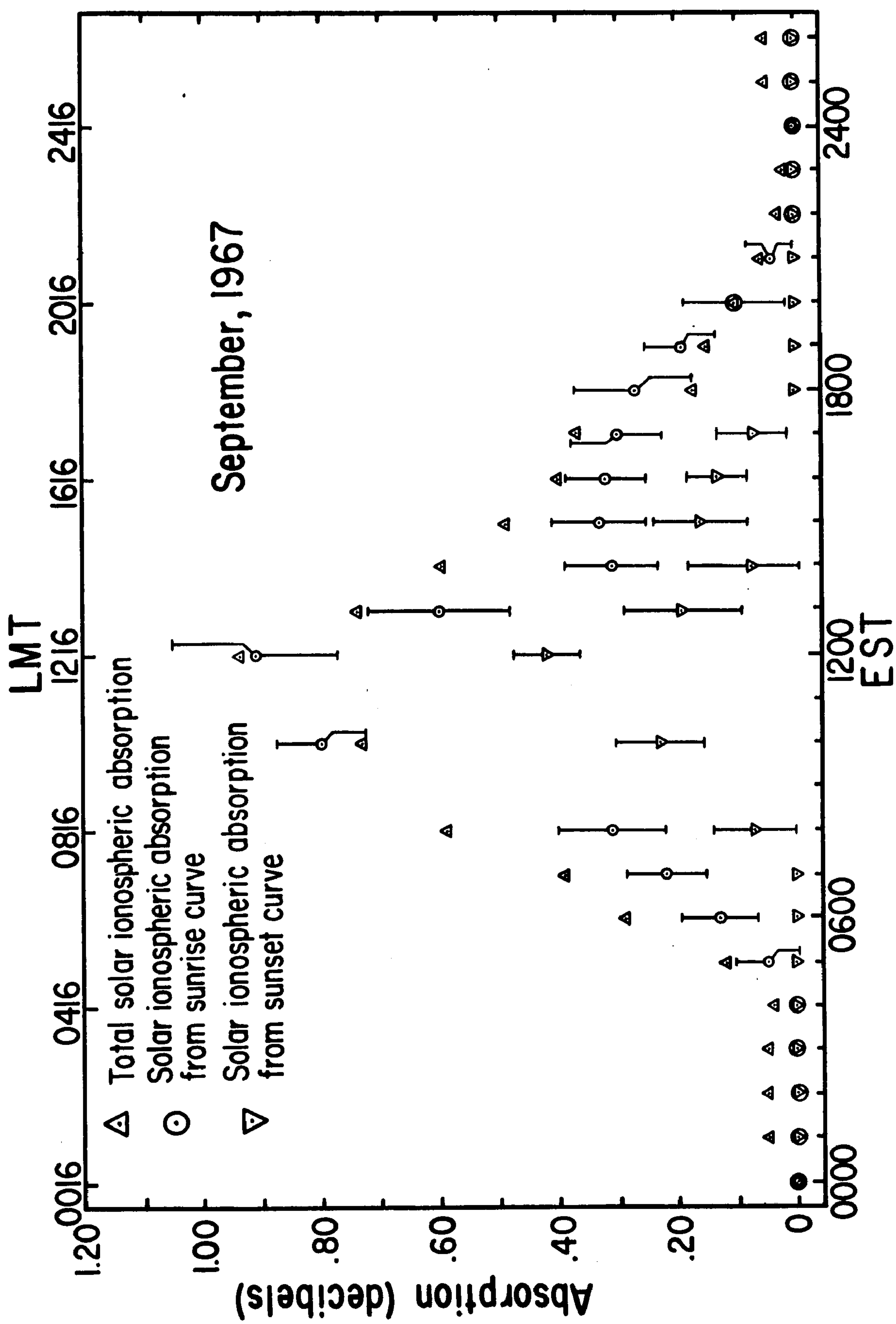
LMT
0016
0416
0816
1216
1616
2016
2416
Total solar ionospheric absorption
Solar ionospheric absorption from sunrise curve
Solar ionospheric absorption from sunset curve
September, 1967
Absorption (decibels)
1.20
1.00
.80
.60
.40
.20
0
0000
0600
1200
1800
2400
EST

Figure 20

greater than the total solar ionospheric absorption, the total absorption lies within the experimental uncertainty of the sunrise or sunset value.

However, in 1967 three particular sidereal hour values of absorption from the reference curve determined at sunrise are especially large. Because sidereal time advances 4 minutes/day with respect to local mean solar time, these three hour values result in a two hour per month advance of the inversion of sunrise values compared to the values determined from the quiet night reference curve.

The conclusions which may be drawn from these curves concerning solar ionospheric absorption are: (1) the absorption computed from the sunset reference curve is smaller than the absorption computed from the sunrise reference curve; (2) the absorption as computed by the sunrise reference curve continues to show the assymetric character of the total absorption around local noon; (3) the absorption computed from the sunset reference curve shows a much more symmetric effect about local noon.

The first conclusion is reasonable recalling that the sunrise reference curve does not include as much of the solar absorption as the sunset reference curve. Also conclusions two and three are explainable if the absorption as computed from the sunrise curve still contains F-region character and the absorption computed from the sunset curve does not contain any F-region character.

Figures 21 through 27 show plots of the average hourly absorption values versus time for the total solar

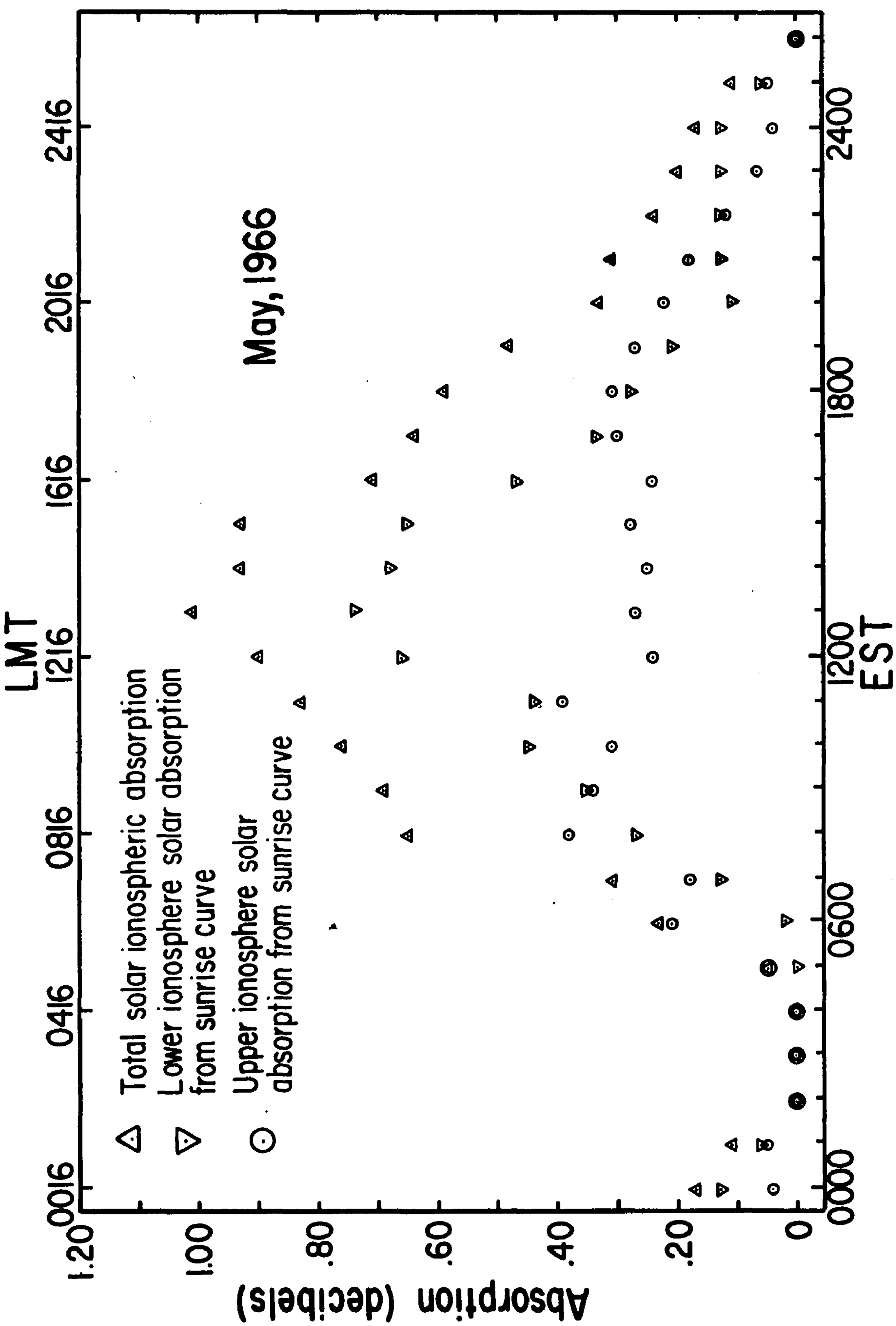
LMT
0016
0416
0816
1216
1616
2016
2416
Total solar ionospheric absorption
Lower ionosphere solar absorption from sunrise curve
Upper ionosphere solar absorption from sunrise curve
May, 1966
Absorption (decibels)
1.20
1.00
.80
.60
.40
.20
0
0000
0600
1200
1800
2400
EST

Figure 21

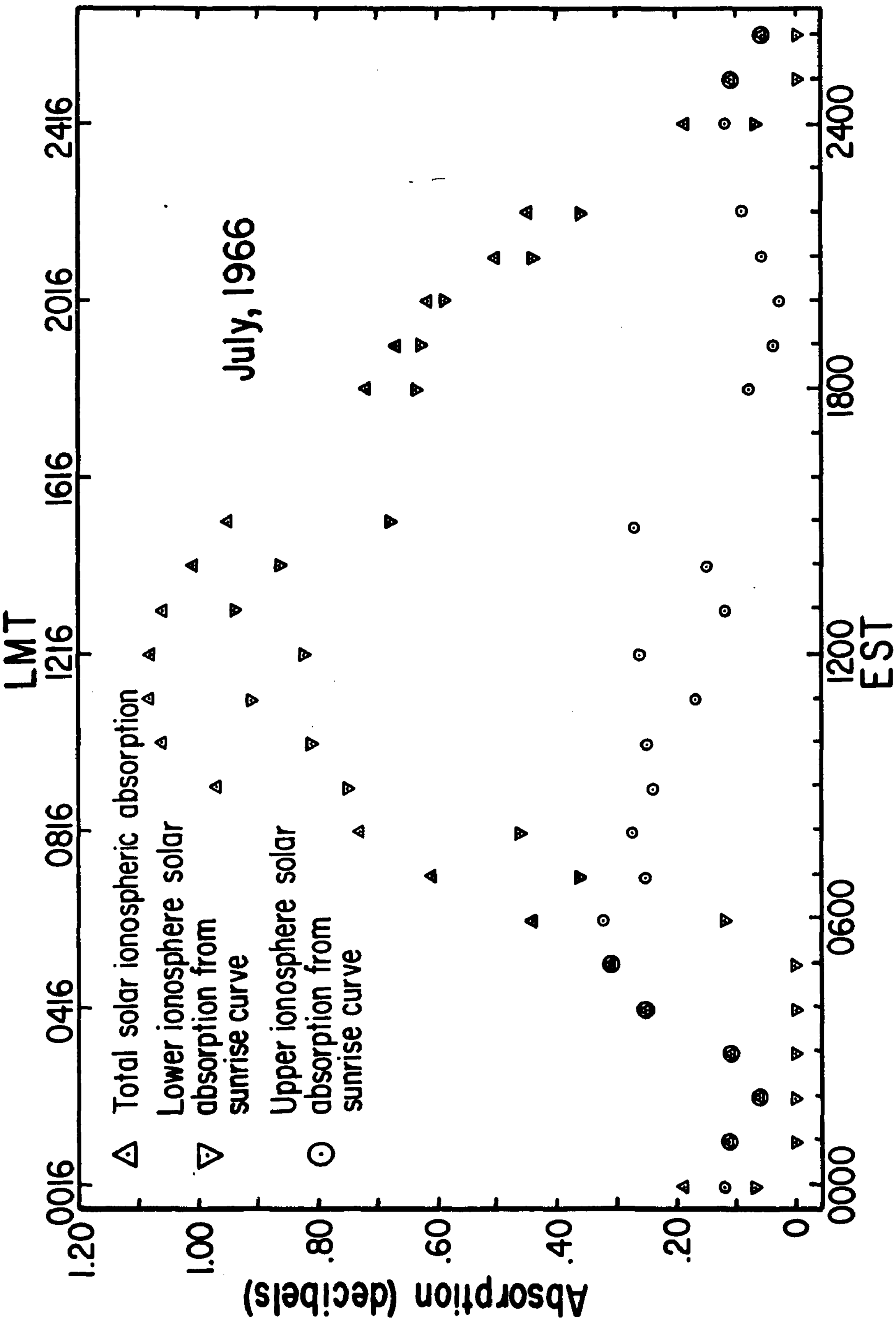
LMT
0016
0416
0816
1216
1616
2016
2416
Total solar ionospheric absorption
Lower ionosphere solar absorption from sunrise curve
Upper ionosphere solar absorption from sunrise curve
July, 1966
1.20
1.00
.80
.60
.40
.20
0
Absorption (decibels)
0000
0600
1200
1800
2400
EST

Figure 22

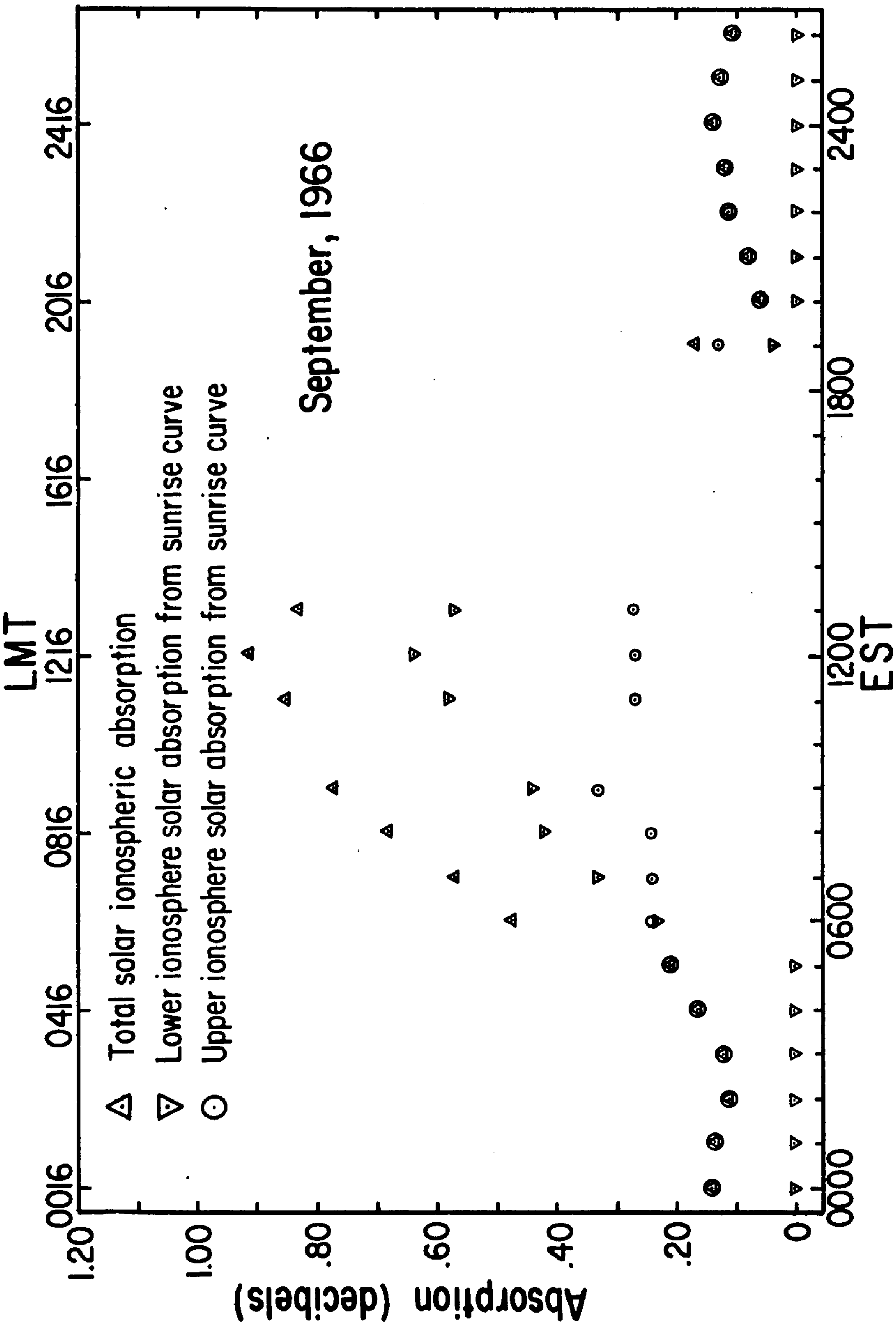
LMT
0016
0416
0816
1216
1616
2016
2416
Total solar ionospheric absorption
Lower ionosphere solar absorption from sunrise curve
Upper ionosphere solar absorption from sunrise curve
September, 1966
Absorption (decibels)
1.20
1.00
.80
.60
.40
.20
0
0000
0600
1200
1800
2400
EST

Figure 23

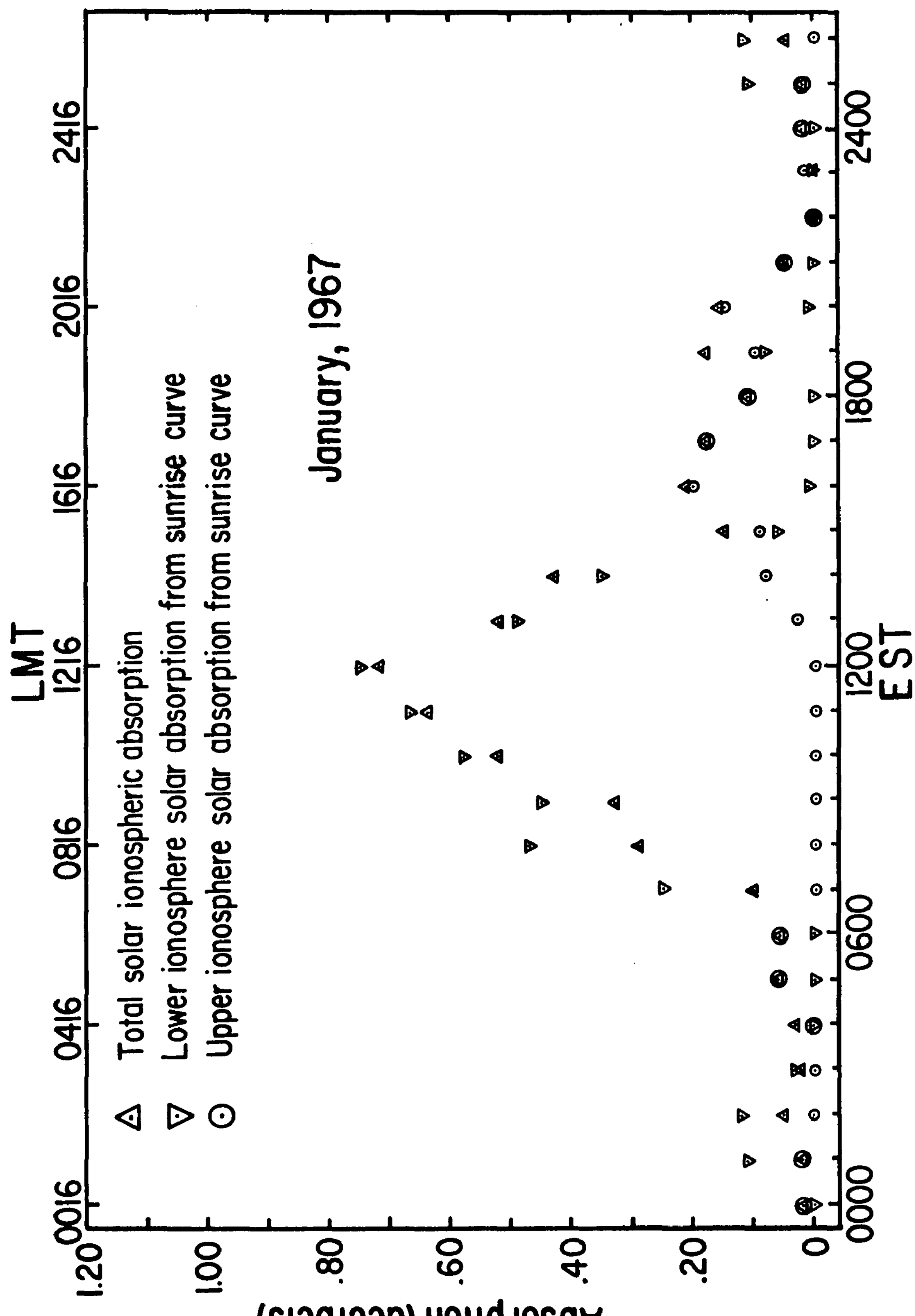

LMT
0016
0416
0816
1216
1616
2016
2416
Total solar ionospheric absorption
Lower ionosphere solar absorption from sunrise curve
Upper ionosphere solar absorption from sunrise curve
January, 1967
Absorption (decibels)
1.20
1.00
.80
.60
.40
.20
0
0000
0600
1200
1800
2400
EST

Figure 24

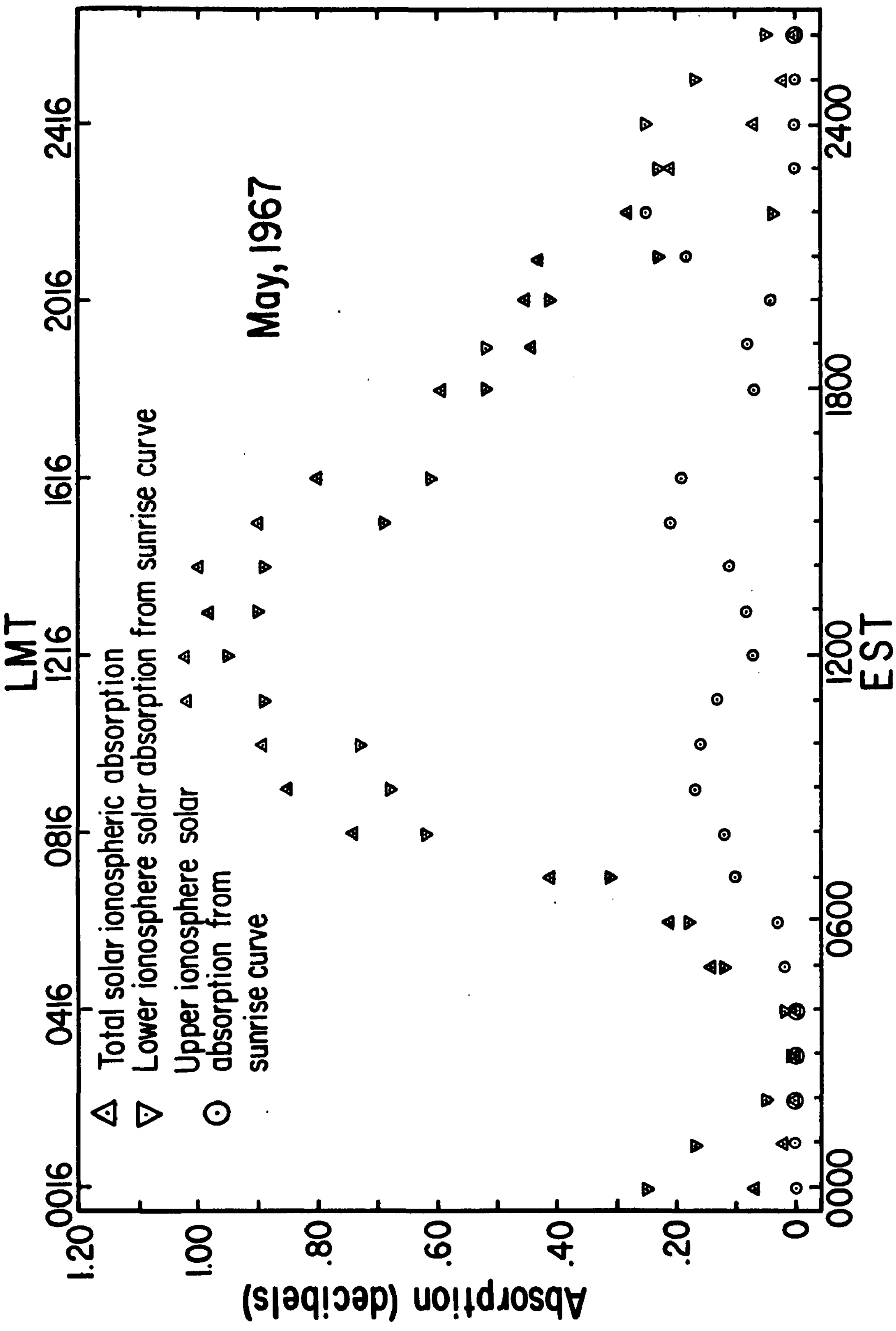
LMT
0016
0416
0816
1216
1616
2016
2416
Total solar ionospheric absorption
Lower ionosphere solar absorption from sunrise curve
Upper ionosphere solar absorption from sunrise curve
May, 1967
Absorption (decibels)
1.20
1.00
.80
.60
.40
.20
0
0000
0600
1200
1800
2400
EST

Figure 25

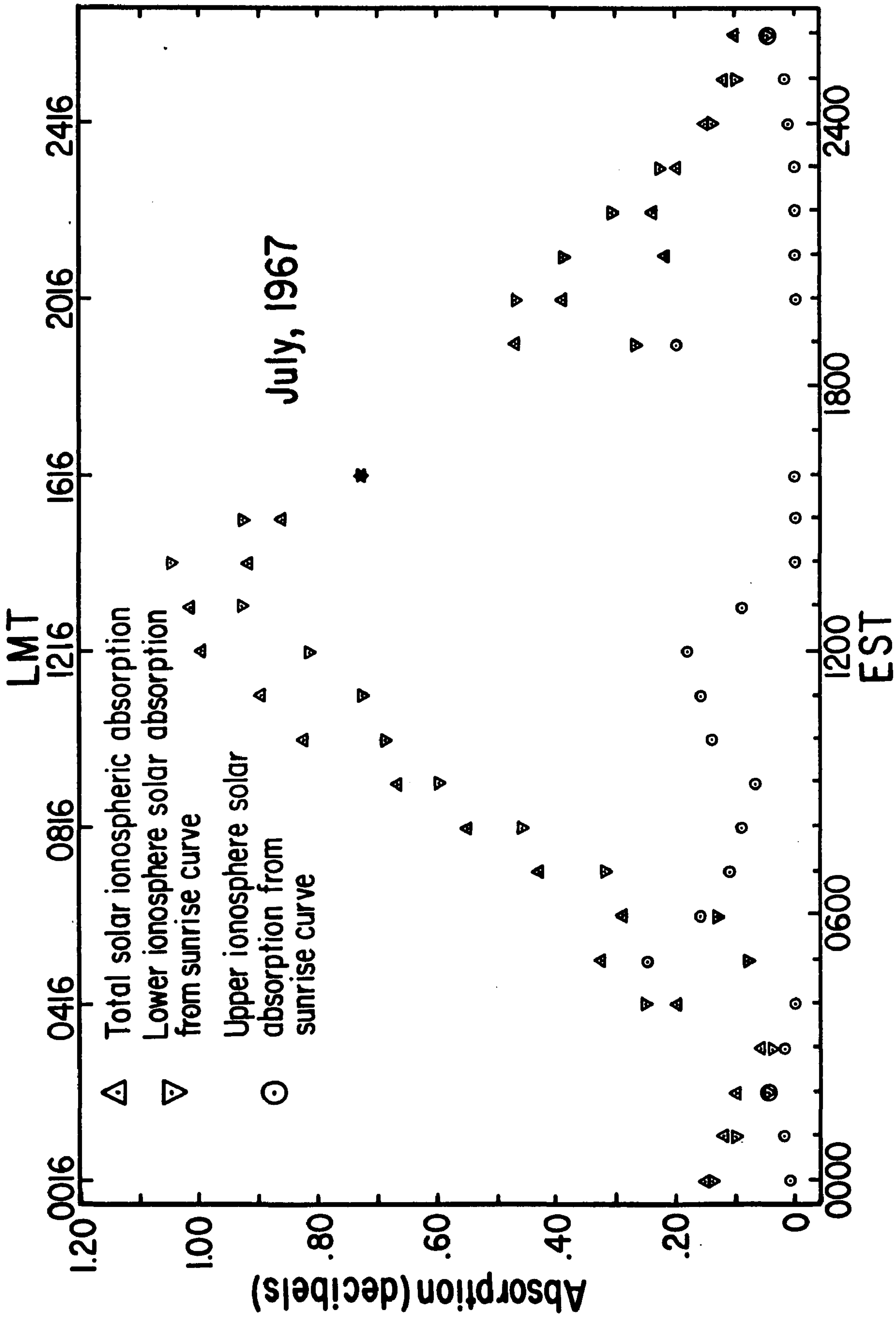
LMT
0016
0416
0816
1216
1616
2016
2416
Total solar ionospheric absorption
Lower ionosphere solar absorption from sunrise curve
Upper ionosphere solar absorption from sunrise curve
July, 1967
Absorption (decibels)
1.20
1.00
.80
.60
.40
.20
0
0000
0600
1200
1800
2400
EST

Figure 26

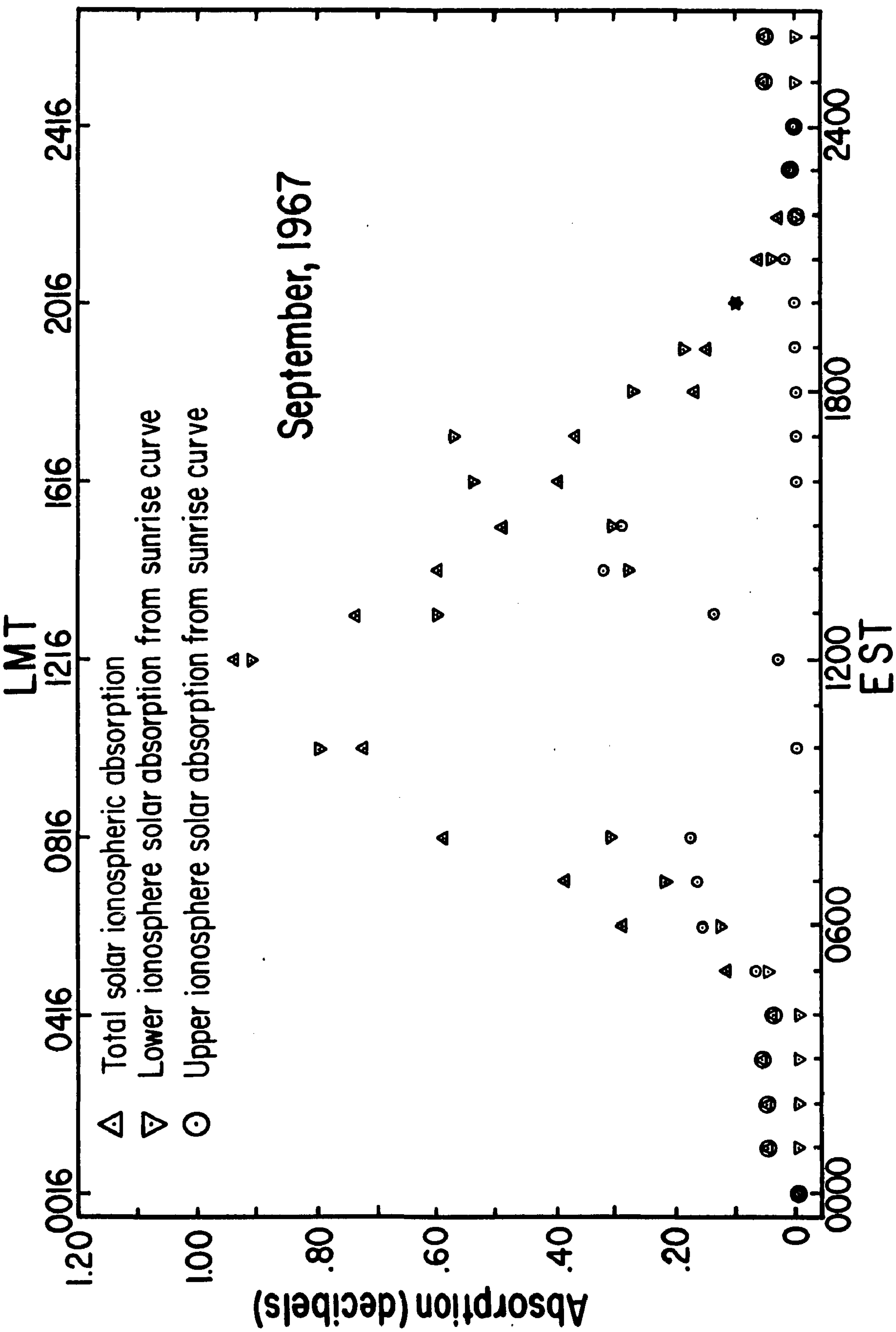
LMT
0016
0416
0816
1216
1616
2016
2416
Total solar ionospheric absorption
Lower ionosphere solar absorption from sunrise curve
Upper ionosphere solar absorption from sunrise curve
September, 1967
Absorption (decibels)
1.20
1.00
.80
.60
.40
.20
0
0000
0600
1200
1800
2400
EST

Figure 27

ionospheric absorption. The figures also show the lower ionosphere solar absorption determined from the sunrise curve, and the upper ionosphere solar absorption determined from the sunrise curve. These plots are for the same months as used previously for the years 1966 and 1967.

The main features exhibited by these plots are as follows: (1) the most prominent feature is that the upper ionosphere solar absorption rises to a plateau value in the morning, remains essentially at this value during the day, although some irregularity is usually present, and commences to decay by late afternoon; (2) the plateau value is greater in the spring, summer, and autumn months than the winter months. Little variation exists between spring, summer, and autumn; (3) the lower ionosphere solar absorption is is considerably greater than the upper ionosphere solar absorption.

Figure 28 shows a composite plot for 1966 and Figure 29 a composite for 1967. For convenience, the discussion of these and the above plots will follow the similar set of plots from the sunset reference curve to be described next.

Figures 30 through 36 show plots of the average hourly absorption values versus time for the total solar ionospheric absorption, the lower ionosphere solar absorption determined from the sunset curve, and the upper ionosphere solar absorption determined from the sunset curve. These plots are for the same months as used previously for the years 1966 and 1967. Figure 37 is a composite for 1966 and Figure 38 is a composite for 1967.

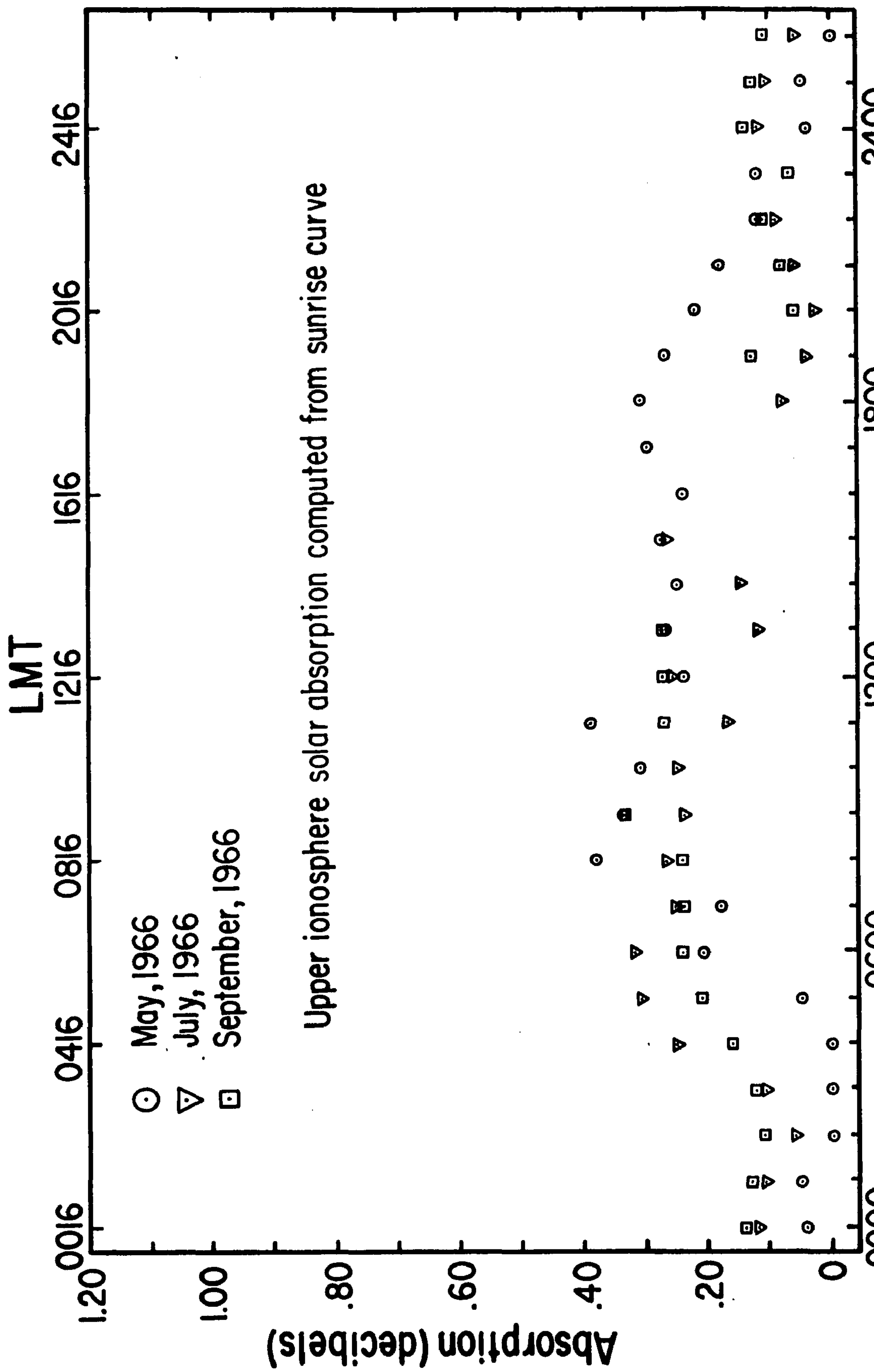
LMT
0016
0416
0816
1216
1616
2016
2416
○ May, 1966
▷ July, 1966
⊡ September, 1966
Upper ionosphere solar absorption computed from sunrise curve
Absorption (decibels)
1.20
1.00
.80
.60
.40
.20
0
0000
0600
1200
1800
2400
EST

Figure 28

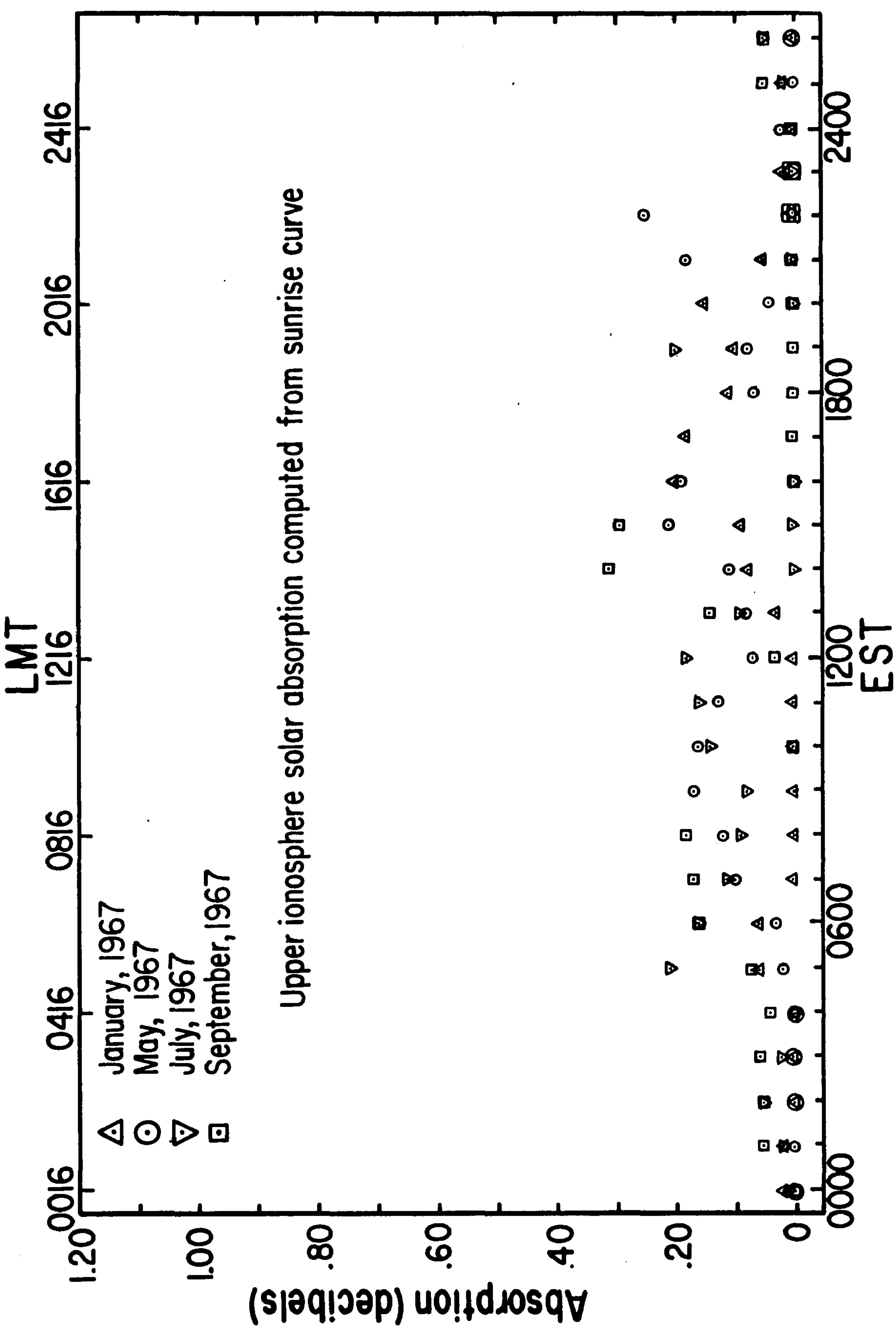
LMT
0016
0416
0816
1216
1616
2016
2416
January, 1967
May, 1967
July, 1967
September, 1967
Upper ionosphere solar absorption computed from sunrise curve
Absorption (decibels)
1.20
1.00
.80
.60
.40
.20
0
EST
0000
0600
1200
1800
2400

Figure 29

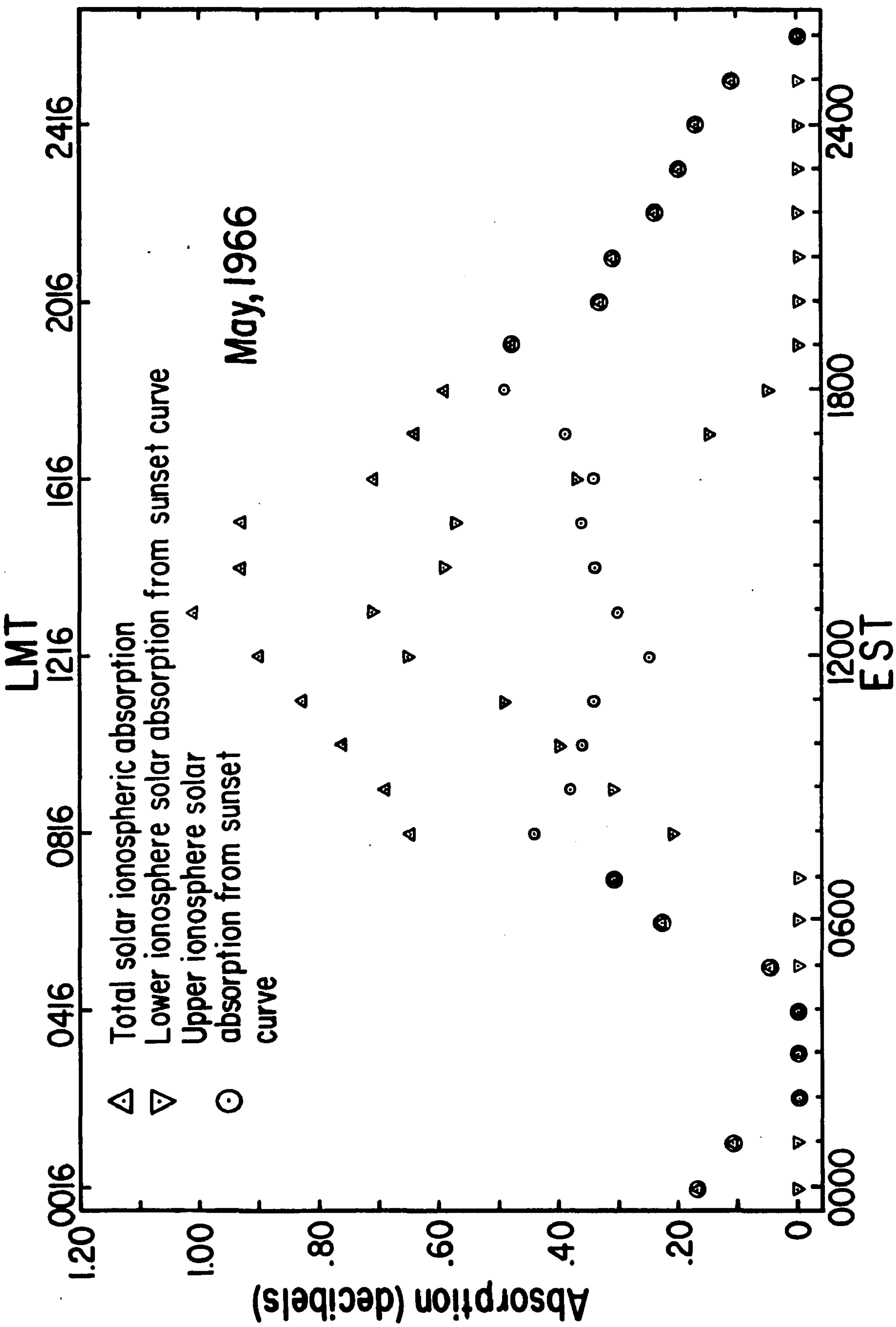
LMT
0016
0416
0816
1216
1616
2016
2416
Total solar ionospheric absorption
Lower ionosphere solar absorption from sunset curve
Upper ionosphere solar absorption from sunset curve
May, 1966
Absorption (decibels)
1.20
1.00
.80
.60
.40
.20
0
0000
0600
1200
1800
2400
EST

Figure 30

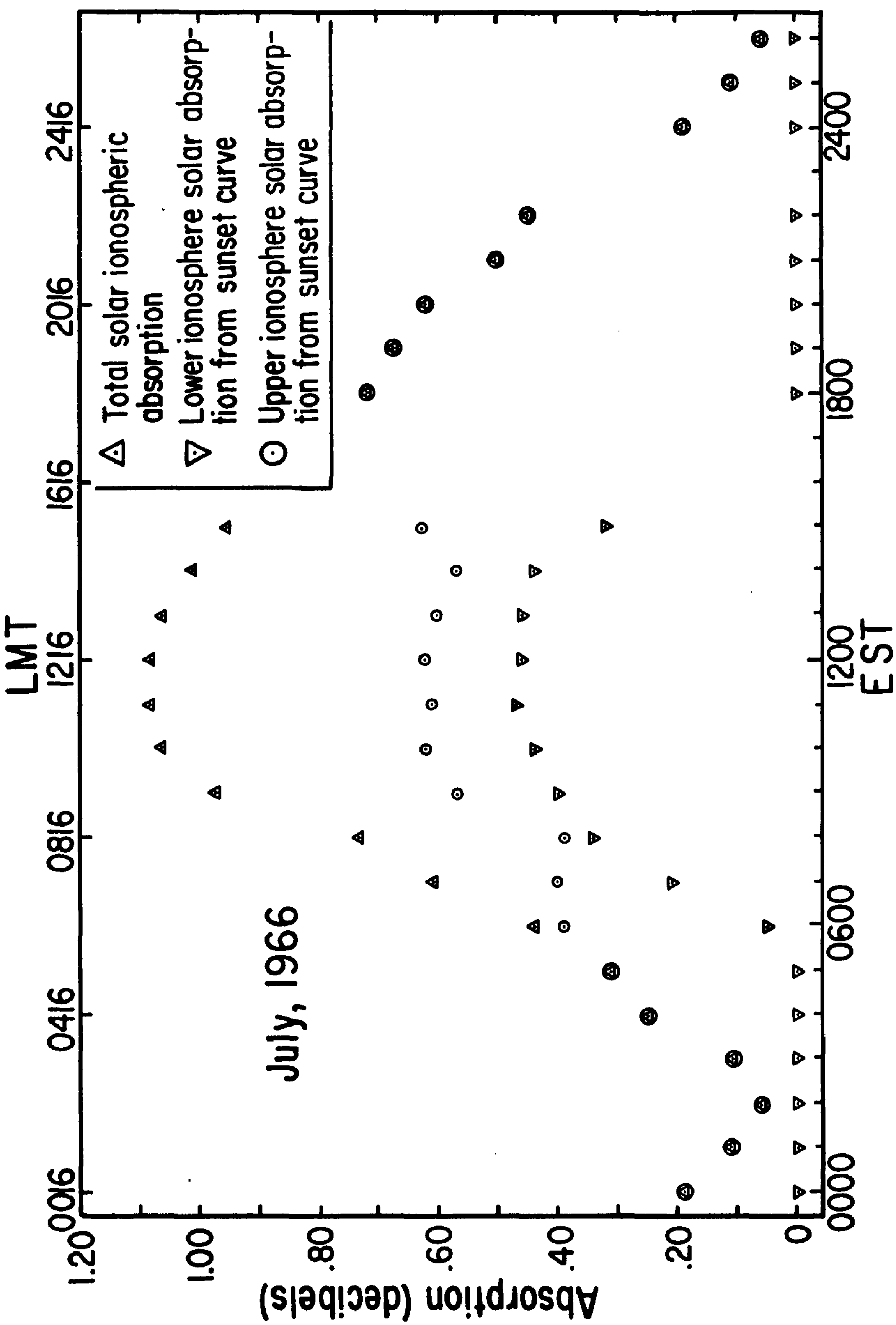
July, 1966
LMT
0016
0416
0816
1216
1616
2016
2416
EST
0000
0600
1200
1800
2400
Absorption (decibels)
1.20
1.00
.80
.60
.40
.20
0
Total solar ionospheric absorption
Lower ionosphere solar absorption from sunset curve
Upper ionosphere solar absorption from sunset curve

Figure 31

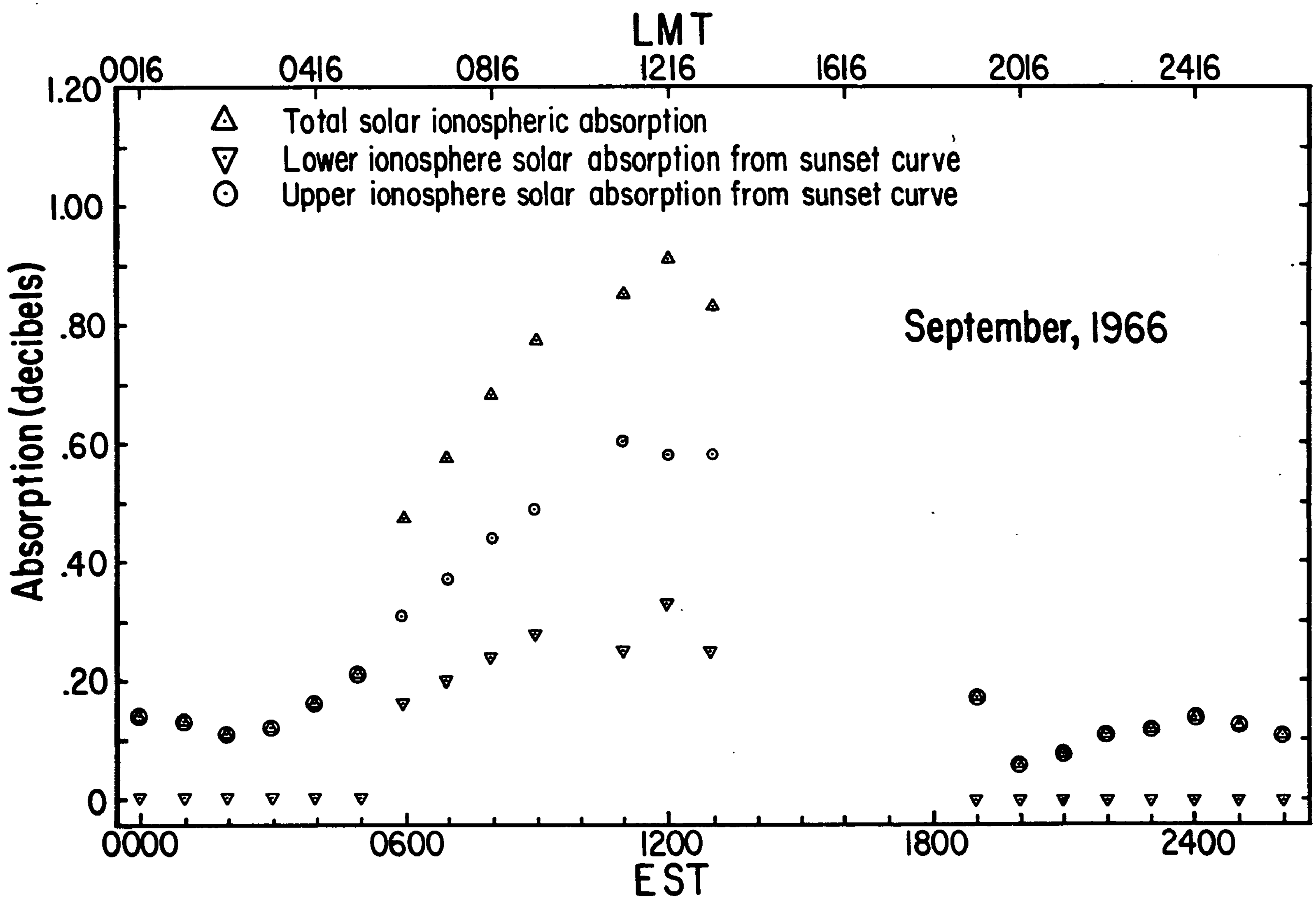
LMT
0016
0416
0816
1216
1616
2016
2416
Total solar ionospheric absorption
Lower ionosphere solar absorption from sunset curve
Upper ionosphere solar absorption from sunset curve
September, 1966
Absorption (decibels)
1.20
1.00
.80
.60
.40
.20
0
0000
0600
1200
1800
2400
EST

Figure 32

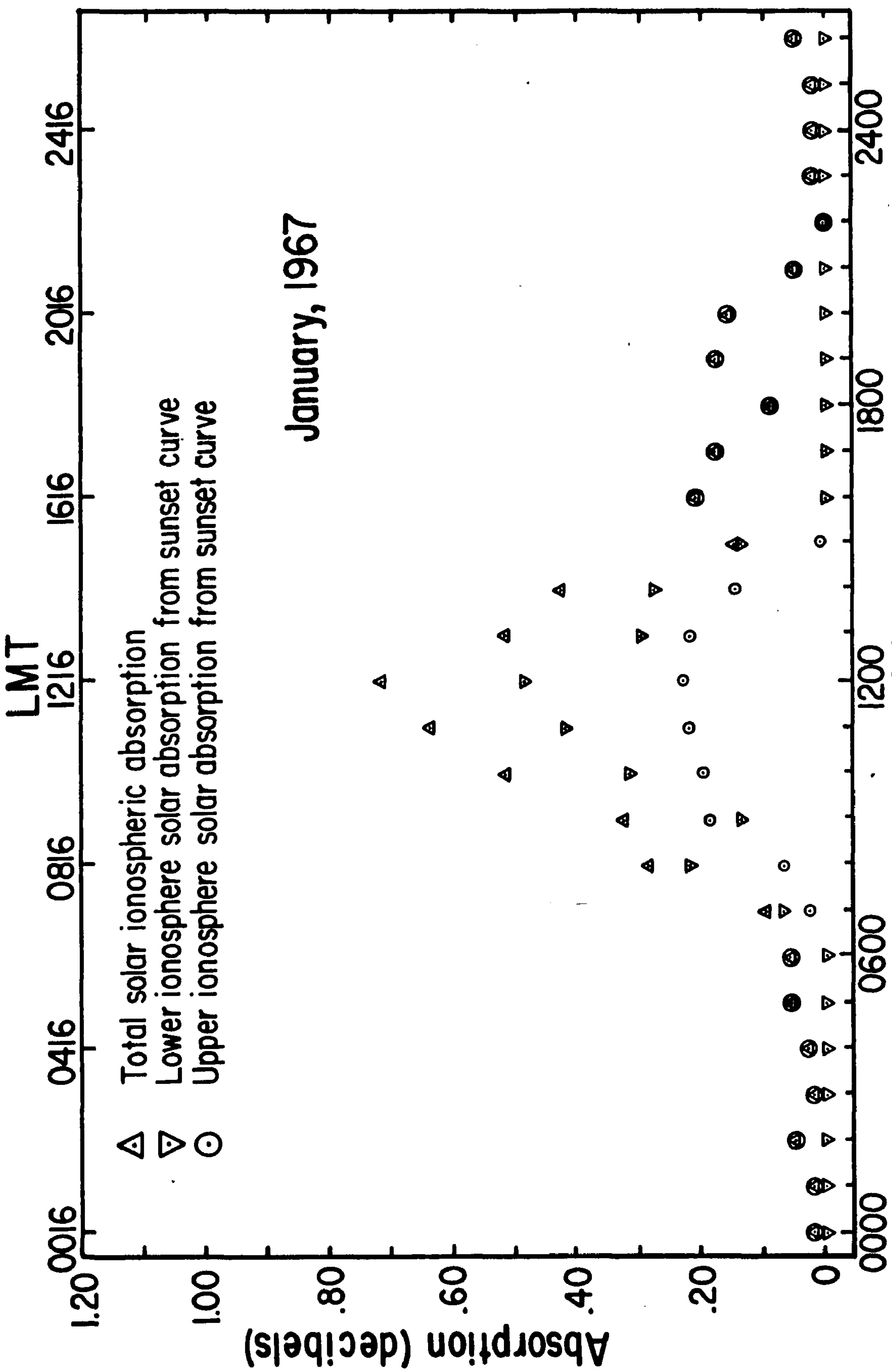
LMT
0016
0416
0816
1216
1616
2016
2416
Total solar ionospheric absorption
Lower ionosphere solar absorption from sunset curve
Upper ionosphere solar absorption from sunset curve
January, 1967
Absorption (decibels)
1.20
1.00
.80
.60
.40
.20
0
0000
0600
1200
1800
2400
EST

Figure 33

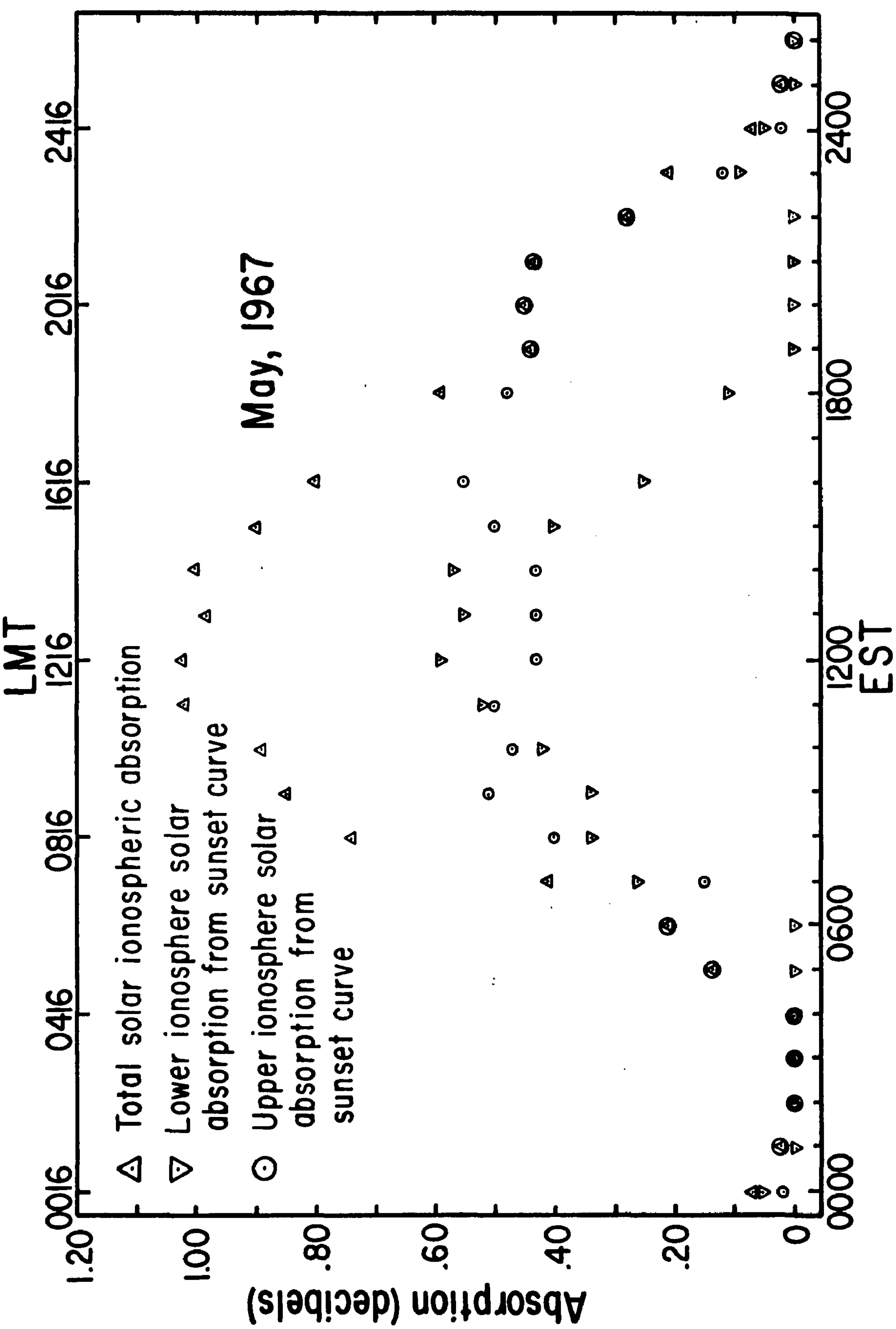
LMT
0016
0416
0816
1216
1616
2016
2416
Total solar ionospheric absorption
Lower ionosphere solar absorption from sunset curve
Upper ionosphere solar absorption from sunset curve
May, 1967
1.20
1.00
.80
.60
.40
.20
0
Absorption (decibels)
0000
0600
1200
1800
2400
EST

Figure 34

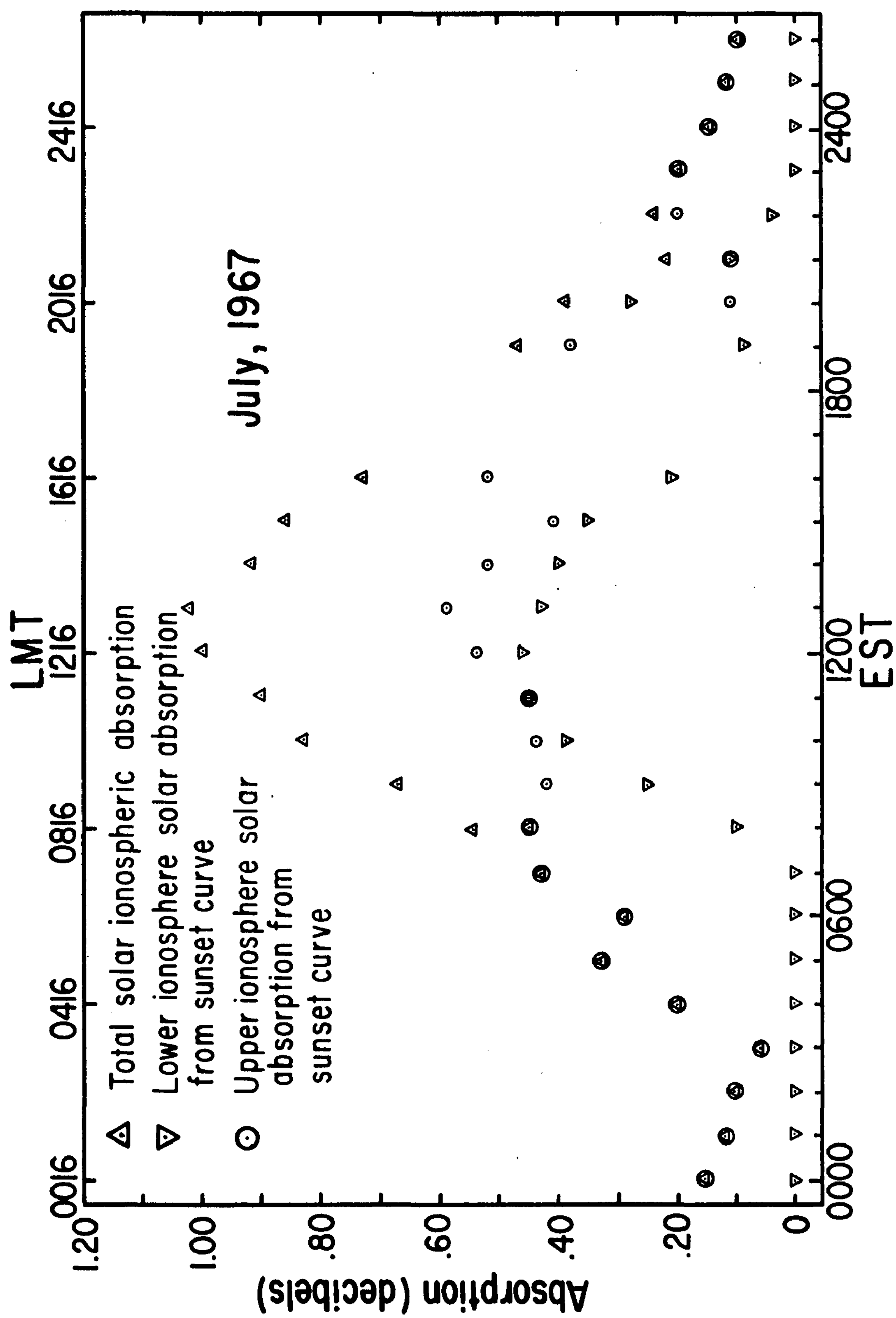
LMT
0016
0416
0816
1216
1616
2016
2416
Total solar ionospheric absorption
Lower ionosphere solar absorption from sunset curve
Upper ionosphere solar absorption from sunset curve
July, 1967
Absorption (decibels)
1.20
1.00
.80
.60
.40
.20
0
0000
0600
1200
1800
2400
EST

Figure 35

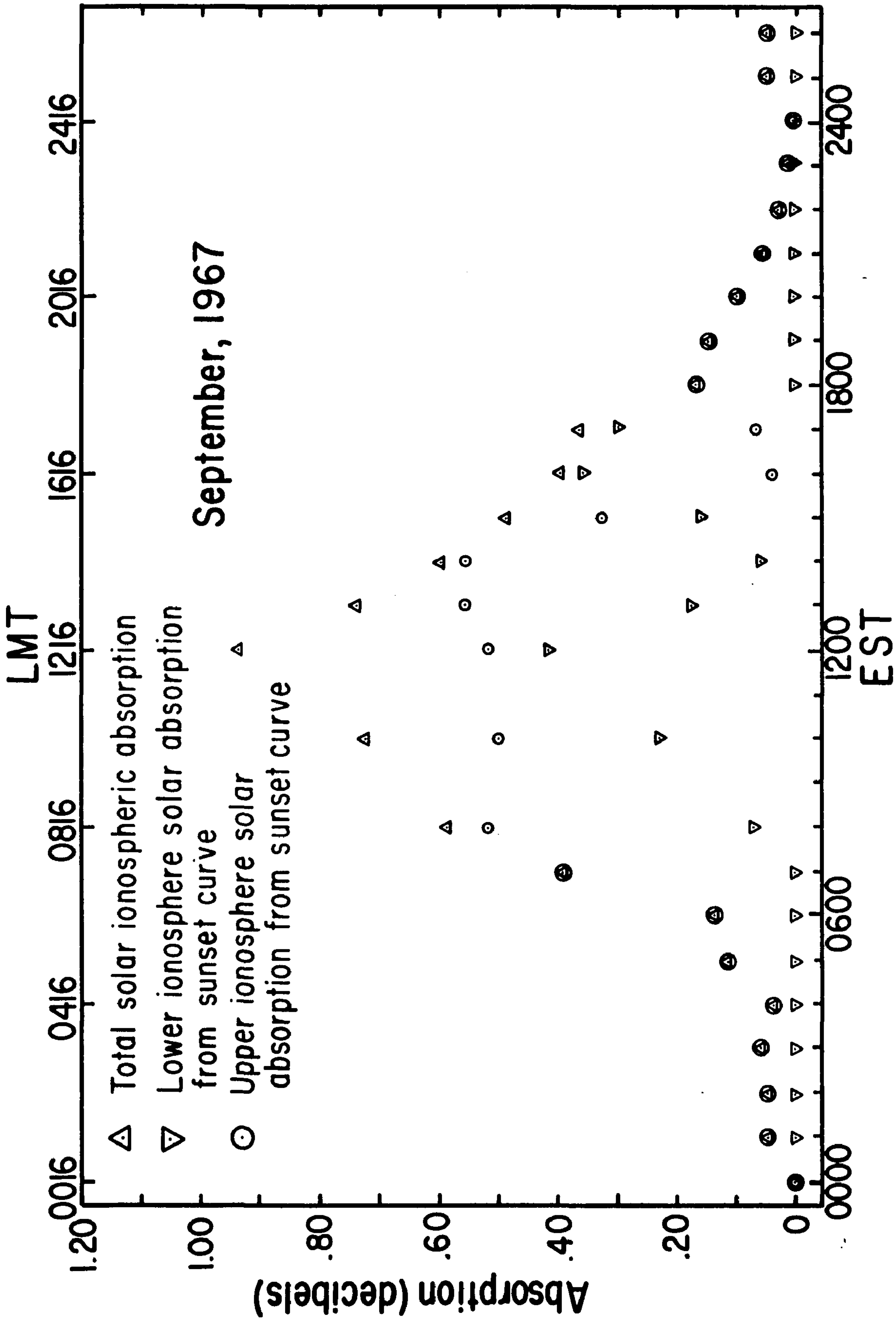
LMT
0016
0416
0816
1216
1616
2016
2416
Total solar ionospheric absorption
Lower ionosphere solar absorption from sunset curve
Upper ionosphere solar absorption from sunset curve
September, 1967
1.20
1.00
.80
.60
.40
.20
0
Absorption (decibels)
0000
0600
1200
1800
2400
EST

Figure 36

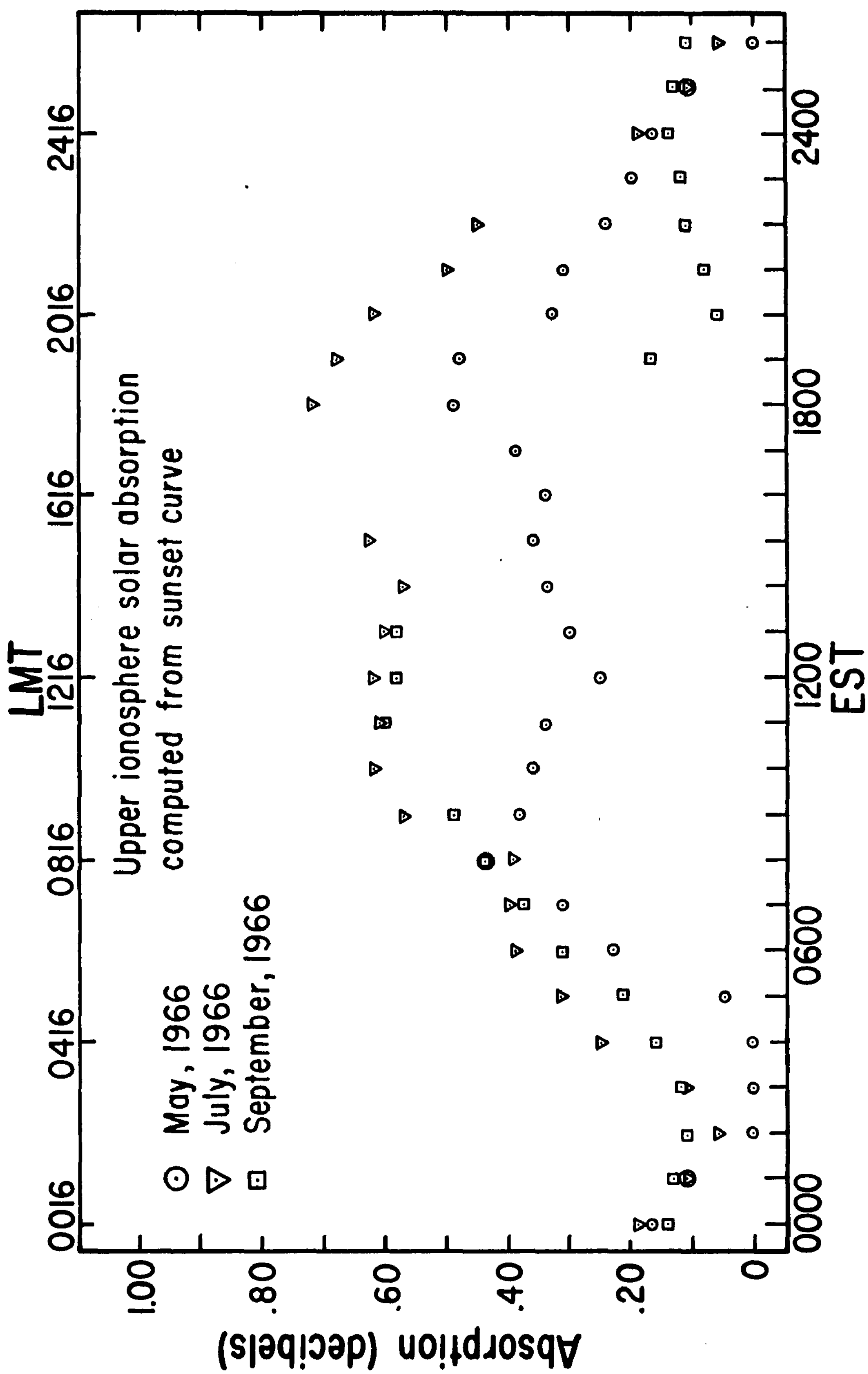
LMT
0016
0416
0816
1216
1616
2016
2416
Upper ionosphere solar absorption
computed from sunset curve
May, 1966
July, 1966
September, 1966
Absorption (decibels)
1.00
.80
.60
.40
.20
0
0000
0600
1200
1800
2400
EST

Figure 37

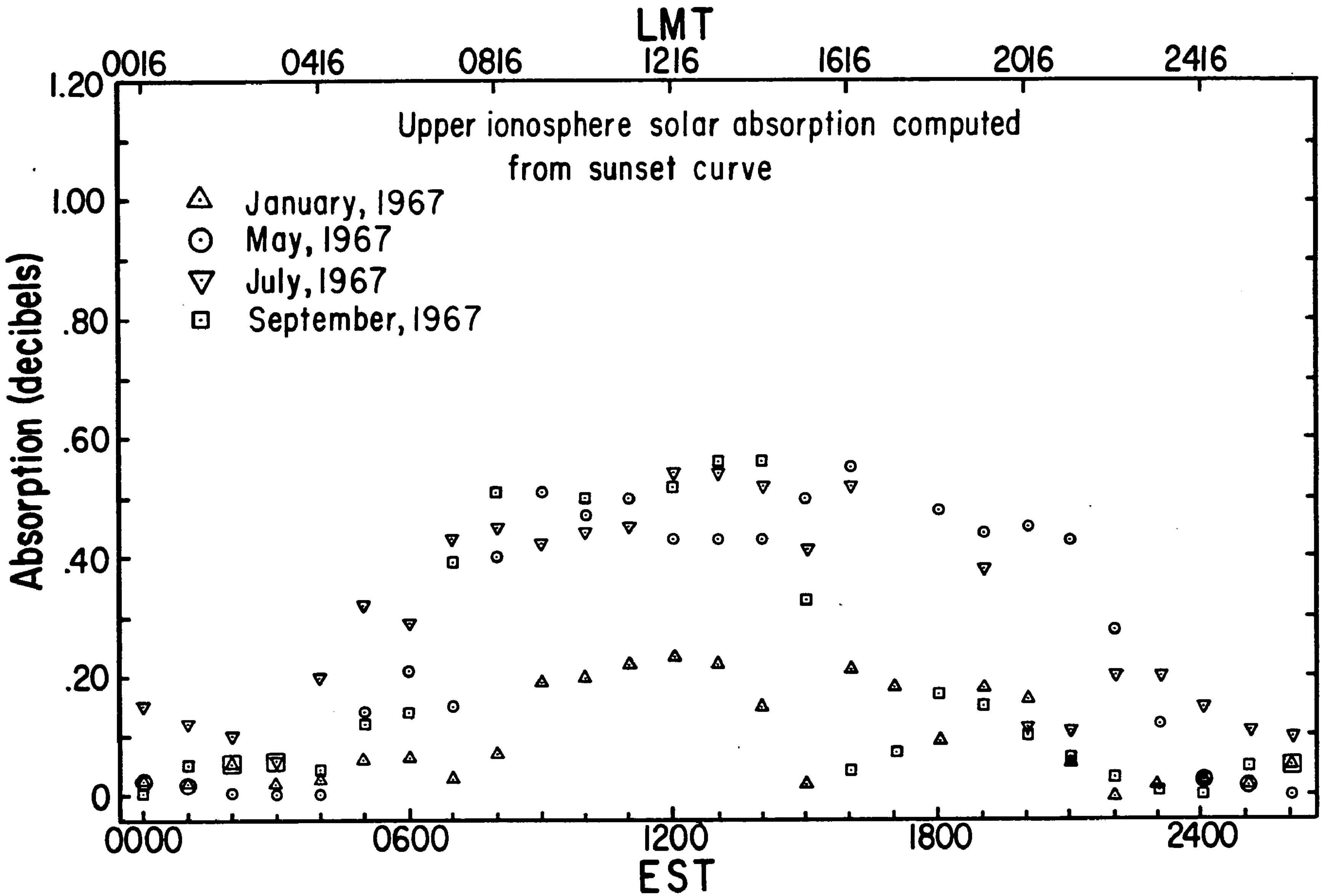
LMT
0016
0416
0816
1216
1616
2016
2416
Upper ionosphere solar absorption computed from sunset curve
January, 1967
May, 1967
July, 1967
September, 1967
Absorption (decibels)
1.20
1.00
.80
.60
.40
.20
0
0000
0600
1200
1800
2400
EST

Figure 38

The features of interest in these plots are: (1) the upper ionosphere solar absorption rises to a plateau, remains essentially at the same value during the day--although some irregularity is usually present--and commences to decay by late afternoon; (2) the plateau value is greater in the spring, summer, and autumn than the winter months with the former showing a tendency of being greater in July and September than May; (3) in the winter the lower ionosphere solar absorption is greater than the upper ionosphere solar absorption as is the case in May while in July and September the upper ionosphere absorption is greater than the lower ionosphere solar absorption.

The absorption calculated from the sunrise reference curve for the two years of data analyzed indicates 15 to 30 per cent of the solar absorption is occurring in the upper ionosphere with 70 to 85 per cent of the solar absorption taking place in the lower ionosphere near local noon. The value of 30 per cent for the upper ionosphere holds for the months of July and September (i.e. summer and autumn) while the value of 15 per cent holds for the months of January and May (i.e. winter and spring). An exception occurs in May 1966 where a value close to 30 per cent is obtained.

The absorption calculated from the sunset reference curve for two years of data analyzed shows 40 per cent of the absorption in the upper ionosphere and 60 per cent in the lower ionosphere for the month of May in the time period near local noon. These numbers also hold for January 1967. In

July and September of 1966 and 1967, the situation reverses and there is roughly 60 per cent of the absorption in the upper ionosphere and 40 per cent in the lower ionosphere around the time of local noon.

These results indicate that at least 15 per cent and not more than 60 per cent of the solar ionospheric absorption is taking place in the upper ionosphere at midday. It is thus reasonable that the faster response of the lower ionosphere to ionization changes would indicate the sunset reference curve has less lower ionosphere absorption remaining than the sunrise reference curve has upper ionosphere absorption. Hence, it would also follow that the actual amount of upper ionosphere absorption is closer to the higher value indicating possibly 35 to 50 per cent of the solar induced absorption taking place in the upper ionosphere during midday with larger amounts approaching 100 per cent in the early morning and early evening.

Another interesting point is that upper ionosphere solar absorption does show some dependence on the solar zenith angle χ as evidenced by the fact that the winter time absorption is less than the summer time absorption. However, this dependence is not as marked as the lower ionosphere solar absorption. The lower ionosphere solar absorption shows a peak at local noon while the upper ionosphere solar absorption does not peak at noon but indicates a fairly constant amount of absorption throughout the middle of the day.

4. Comparison of the Lower Ionosphere Absorption to a $\cos^n \chi$ Fit

Appleton and Piggott [1954] found experimentally that the diurnal variation of the D-region absorption is proportional to $\cos^n \chi$ where n is of the order of 0.75. Abdu et al. [1967] used this relationship to determine the D-region absorption at all hours by picking a value at one particular hour.

Calculating the solar zenith angle χ from equation 99 and using the $\cos^n \chi$ expression with n equal to both 0.75 and 0.95, the diurnal variation of the lower ionosphere solar absorption was calculated. This was accomplished by normalizing to the EA value at 1216 local mean time (1200 EST) and calculating the absorption at all other hours from the ratio of the $\cos^n \chi$ for 1216 to the $\cos^n \chi$ value for the local mean time under consideration. This diurnal variation was then compared with the diurnal variation of absorption for each month as determined from the sunrise and sunset reference curve.

Figure 39 shows a typical month compared to a sunrise reference curve while Figure 40 shows the comparison with the sunset curve. These two figures point out the general trend seen in all the plots. Namely, the $\cos^n \chi$ fit approximates the lower ionospheric absorption computed from the sunset reference curve much better than the absorption calculated from the sunrise reference curve. The discrepancy with the

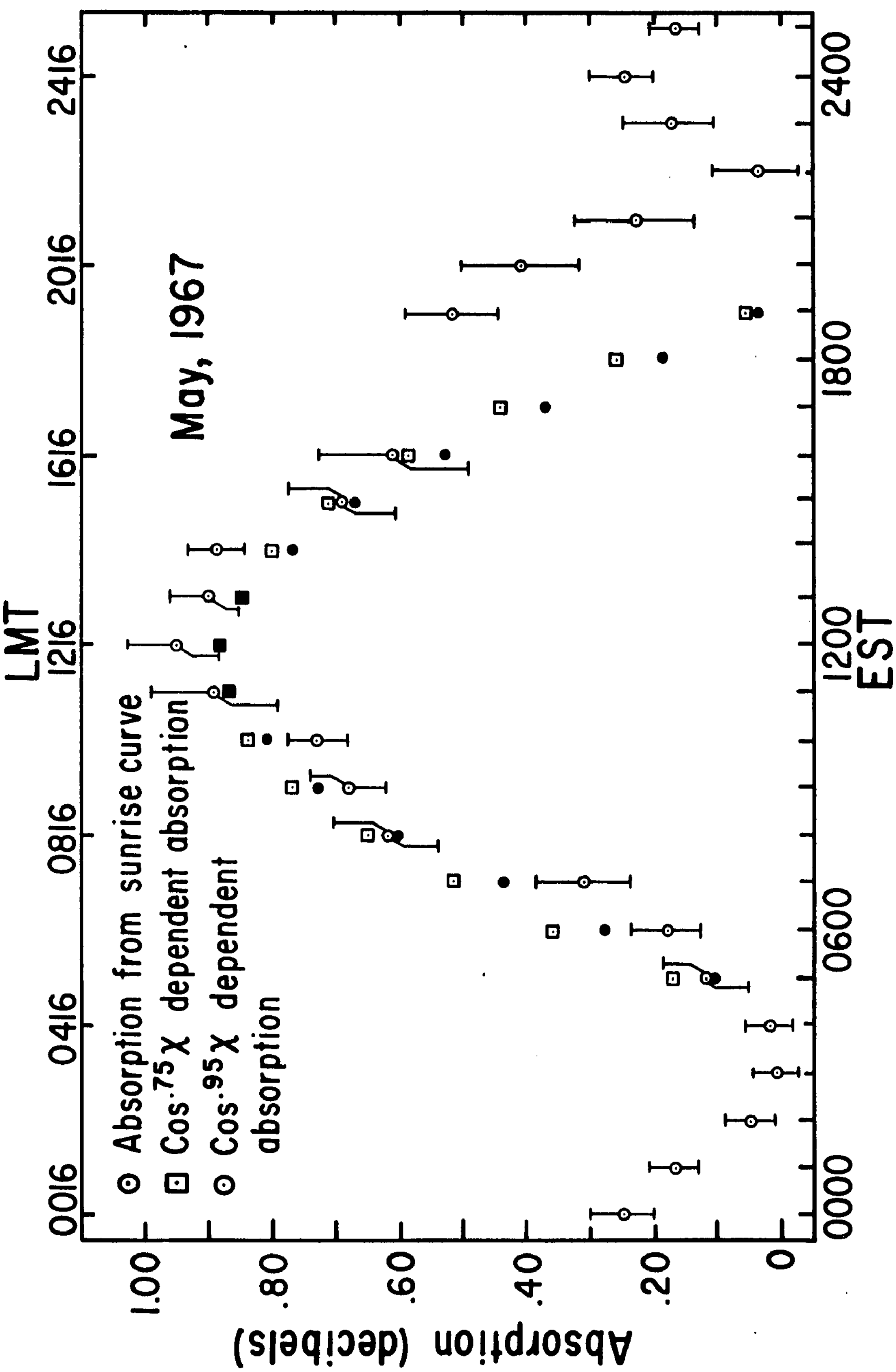

LMT
0016
0416
0816
1216
1616
2016
2416
May, 1967
Absorption from sunrise curve
Cos.75χ dependent absorption
Cos.95χ dependent absorption
1.00
.80
.60
.40
.20
0
Absorption (decibels)
0000
0600
1200
1800
2400
EST

Figure 39

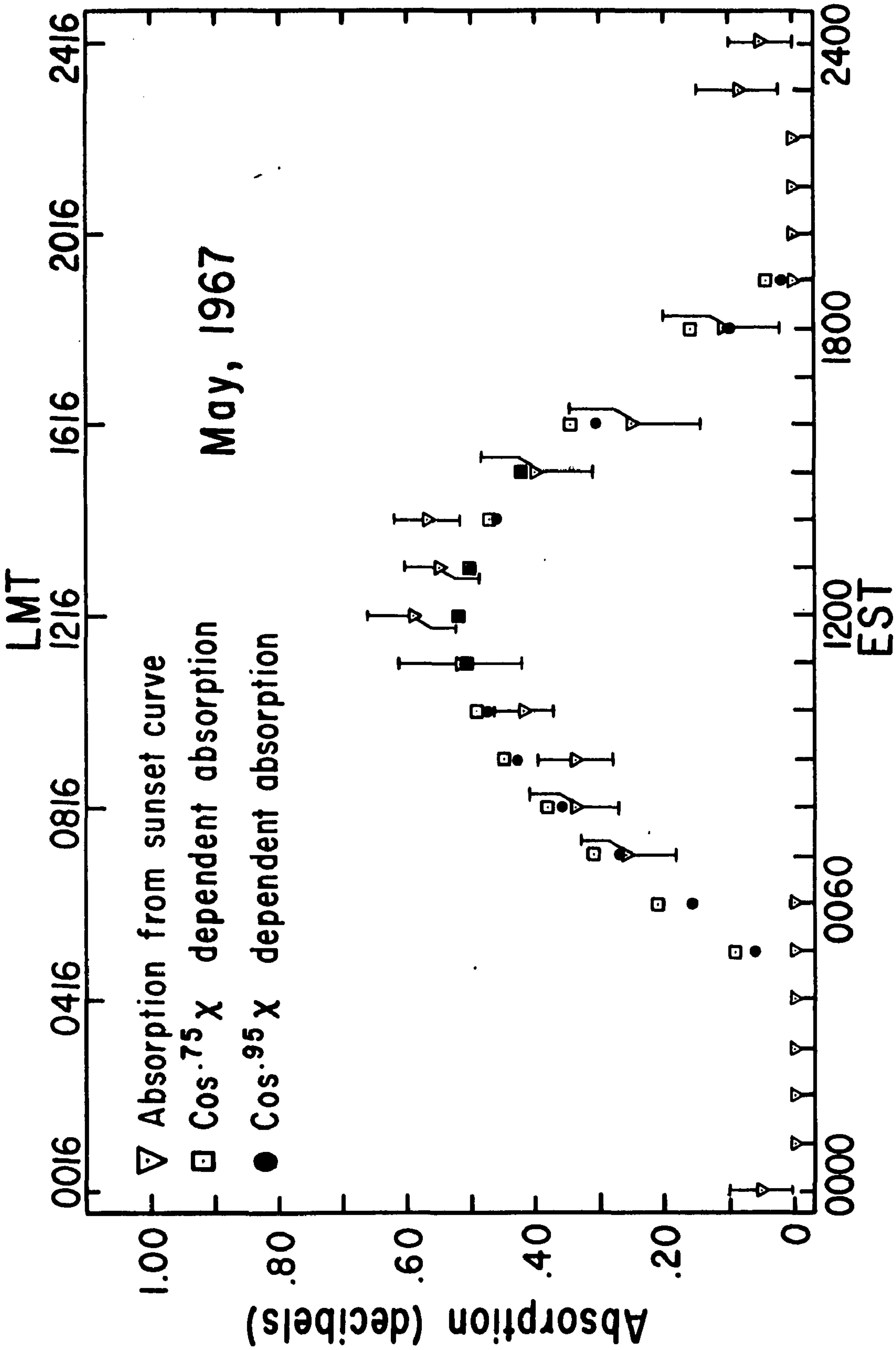

LMT
0016
0416
0816
1216
1616
2016
2416
May, 1967
Absorption from sunset curve
Cos$^{.75}$ X dependent absorption
Cos$^{.95}$ X dependent absorption
Absorption (decibels)
1.00
.80
.60
.40
.20
0
0000
0400
0800
1200
1600
1800
2400
EST

Figure 40

sunrise reference curve is largest in the late afternoon hours as might be expected. The choise of n equal 0.95 was used only to ascertain the difference in the effect of one n over another. The choice of n equal to 0.95 causes the diurnal variation to drop off a little faster.

The only conclusion one might draw from the above study is that the absorption calculated from the sunrise reference curve does not show pure D-region character and probably still contains some F-region character. This is one more point which indicates that the upper ionosphere absorption is larger than the 15 to 30 per cent calculated from the sunrise reference curve.

CHAPTER V

IONOSPHERIC ABSORPTION DURING A DISTURBED PERIOD

1. General Background

Polar cap absorption (PCA) is the name given to the intense absorption that HF and VHF frequencies undergo in propagating through the lower ionosphere under disturbed ionospheric conditions caused by solar disturbances. This absorption is caused by large increases in the ionization in the lower ionosphere. The ionization is caused by energetic charged particles coming from the sun and interacting with the earth's atmosphere. The charged particles are mostly protons in the energy range of a few Mev upwards to 100 Mev. The term PCA is misleading in that it describes the effect of this ionization on a particular range of radio frequencies. For example, at low frequencies radio signals are enhanced. The terms solar cosmic ray event or solar proton event, hereafter called SPE, are more appropriate and the latter is used in this study along with PCA.

It is necessary to give a general background of SPE's and their atmospheric effects. SPE's have their origin on the sun. They are closely associated with type IV centimeter and meter outbursts which are related to acceleration processes in the sun [Kundu and Haddock, 1960; Warwick and Haurwitz, 1962]. McCracken [1959] has pointed out that for relativistic particles ground level effects are noticeable if the solar flare occurs in the western hemisphere of the sun. Warwick and Haurwitz [1962] state that for PCA's this relation is not evident.

The propagation of the solar charged particles to the earth leads to the storage concept [Bailey, 1964]. This concept hinges on the idea that the process accelerating and ejecting particles at the sun is of short duration, usually a fraction of an hour. The duration of PCA's is typically several days. Consequently a large fraction of the particles must have been stored and released to reach the earth over such an extended period of time.

While still at some distance from the earth, the particles begin to deviate from their original paths because of the influence of the earth's geomagnetic field. The description of the motion of a charged particle in the geomagnetic field is difficult and was first solved by Störmer [1955] who assumed a simple dipole representation of the field.

In dealing with the effects of a magnetic field on the motion of a charged particle, the momentum of the particle is a more useful concept than kinetic energy, since particles with the same momentum and charge behave the same way in a magnetic field. If kinetic energy is defined in electron volts and momentum (p) in electron volts per velocity of light, then the dependence of momentum on charge can be eliminated if one defines a term known as rigidity. Hence, the relation

$$P = pc/z \tag{102}$$

where z is the numerical charge of the particles in units of electronic charge and P is the rigidity. Using the centered-dipole approximation, one obtains from Stormer theory the so called cutoff rigidity, defined as

$$P_c = \left[\frac{M \cos^4 \Phi}{R_r^2[1+(1-\sin\theta \sin\phi \sin\Phi)^{1/2}]}\right]^2 \tag{103}$$

where Φ is the geomagnetic latitude, θ the local zenith angle, ϕ the local azimuth angle, and R_r the radial distance from the dipole center to the point of observation. This equation states that for particular values of, Φ, θ, and ϕ at a given R_r the value of P_c calculated will be the smallest rigidity particle accessible to this region for these particular values of the variables. If θ=0, indicating vertically incident particles, one obtains

$$P_o = 14.8 \cos^4 \Phi \tag{104}$$

where R_r=R_o(6.4 x 10^3 km) and M=8.06 x 10^{25} gauss cm^3. P_o is measured in units of billions of volts.

Equation 103 shows that particles with rigidity less than P_o can reach the earth at latitude Φ at large zenith angles and certain azimuths. For latitudes greater than 40° the true minimum rigidity does not differ from P_o by more than 10% and at 70° by more than 1%. One can then regard P_o as a fairly sharp cutoff rigidity with all particles of rigidity less than P_o being confined to latitudes greater than Φ.

The interaction of solar protons in the earth's atmosphere and the characteristic riometer absorption may be calculated in a three step process. Initially, the solar protons interact with the atmospheric particles and produce ion-pairs described by a production function, q. By knowing the electron loss processes occurring in the atmosphere, the equilibrium electron density is determined. Finally, the ionospheric absorption for a particular frequency is calculated by using the equilibrium electron density in the generalized Appleton-Hartree equations.

Bailey [1959] was the first person to make a theoretical calculation of the magnitude of PCA expected from a given spectrum. He used an extrapolated spectrum derived from the neutron monitor data for relativistic particles of the February 23, 1956 event and calculated the production function and absorption at 10 km increments.

Whereas, Bailey used a power law in rigidity with an integral rigidity negative exponent of 2 and 6, Reid [1961] used a power law in energy with an integral energy negative exponent of 4. Reid calculated production functions and electron density distributions by using cutoff energies of 20 and 40 Mev for protons with the upper limit being 300 Mev. This study used different ionospheric rate parameters than did Bailey and did not attempt to compare a measured absorption event but studied only the general properties of day and night polar cap absorption assuming an isotropic distribution of protons.

Frier and Webber [1963] discuss the determination of the spectrum at different energy intervals by different methods. They note that the 1 - 50 Mev range is measured by rockets, satellites, and riometers, the intermediate energies (70 - 500 Mev) by emulsions from balloons and ion chambers, and the high energies greater than 500 Mev by neutron monitors. It is difficult to extrapolate such spectra over energy intervals covering several types of measurements. However, this does point out that riometers are sensitive only to the low energy particles. Bailey [1959] notes that in extrapolating a power law in energy to small energies of a few Mev one obtains far too many electrons at 100 km. It is known that these large electron densities are not observed at 100 km and hence the power law spectrum must be artificially cutoff or 'bent over'.

Being confronted with this problem, Frier and Webber [1963] suggested that the use of an exponential spectrum in rigidity would eliminate defining an artificial cutoff at some small energy. Webber [1962] used exponential rigidity spectrums to derive the production function and electron density for solar particle bombardment. Webber and Frier [1963], using exponential rigidity spectrums, derived the theoretical ionospheric absorption expected for a 30 MHz riometer for selected times of absorption events assuming only protons to be present. They found that the measured absorption was almost always greater than the calculated absorption indicating that alpha particles do contribute to the riometer absorption.

Since riometers measure total absorption, it is sometimes difficult to separate the PCA from the auroral absorption, particularly at night when electron attachment greatly reduces the PCA. The comparative uniformity and smooth variation with time of the PCA contrasts distinctly with the short-term fluctuations and spatial variations of auroral absorption, and permits some separation of the effects [Bailey, 1964]. It is found that there is a period of time lasting from several hours to as long as a few days following the onset of PCA during which auroral and magnetic activity are small. After the onset of severe magnetic disturbance, usually characterized by a sudden commencement, it is difficult to obtain quantitative measurement of a PCA. Leinbach et al. [1965] adopted the rule-of-thumb that the PCA contribution in the presence of auroral absorption is represented by the minimum value of absorption recorded over a several hour period. These authors also concluded that the polar cap can be divided into two regions. In the first, which includes latitudes north of geomagnetic latitudes 65° (L=5.5), the progress of the PCA event is dependent on the time variations of the solar particle flux, and is independent of geomagnetic activity. In the second zone, which extends from geomagnetic latitudes 64° down to 55° the characteristics of the PCA are dominated by the influence of the geomagnetic field. For instance, at King Salmon (L=3.3) it is seldom possible to observe PCA before the magnetic storm, and the absorption approaches that recorded at Thule (L=220.1) only when D_{st} is greater than 200 γ.

PCA is characterized by nighttime recoveries of absorption [Leinbach, 1962]. Leinbach et al. [1965] state that the nighttime recovery usually sets in at solar zenith angles of 88-90°, while the morning increase begins at about 102°. During PCA events in the polar cap region the primary ionizing source often remains almost constant in intensity over a period of many hours [Reid, 1964]. This indicates that the change from daytime to nighttime conditions is an atmospheric phenomenon and is attributed to the lack of photodetachment occurring at night. The result is more negative ions due to the attachment of electrons to molecules. The change from daytime to nighttime is very marked with the ratio of daytime to nighttime absorption measured by a riometer being of the order of 4 to 6.

PCA measurements have given rise to two important anomalies; the twilight and the midday recovery anomalies. Reid [1964] has attempted to explain the twilight anomaly. If the dominant negative ion is O_2^-, or any other negative ion requiring visible sunlight for detachment, the transition to nighttime conditions should follow the shadow of the earth. The observations, however, show the transition occurring when the shadow of the earth traverses altitudes 0 to 50 km. Observations of the ionizing particles show on the other hand that most of the absorption is taking place above 50 km. It was pointed out that much better agreement could be obtained if the effective screening region were the ozone layer [Ericksen et al., 1965; Reid and Leinbach, 1961]. This implies that the radiation responsible for photodetachment is ultraviolet rather than visible. The ultraviolet absorption by the ozone layer sets in at about 3000 A or a quantum energy of 4 electron volts. Since the highest acceptable value of electron affinity for O_2^- is roughly 0.6 electron volts, it seems unlikely that O_2^- is the dominant negative ion. Thus, twilight observations of PCA indicate a negative ion with a very high electron affinity. With this large electron affinity it is difficult to explain the large nighttime electron densities which have been attributed to collisional detachment. However, it is possible that this unknown negative ion may be of importance only at twilight and O_2^- may be the dominant negative ion during the day and night. There has been no positive identification of the negative ion to date.

The other anomaly observed by PCA riometer measurements is the midday recovery [Leinbach, 1962]. He attributes this recovery of the cosmic noise signal toward its undisturbed value to a local increase in geomagnetic cutoff. In a later paper Leinbach [1967] points out the current observations of midday recoveries. The recoveries peak in the local time period of 0800 to 1500 and mostly between 1000 and 1200 local time. The recoveries are not observed deep inside the polar cap, are most noticeable at the edge of the polar cap, and move southward with the edge of the polar cap during the geomagnetic storm. He states that satellite data during midday recoveries indicates that particles with pitch angles small enough to penetrate into the atmosphere were depleted. Such action points toward the development of an anisotropy in the pitch angle distribution of the protons rather than an increase in cutoff. On the other hand, Brown and Parthasaratly [1967] state that the PCA midday recovery of September 2, 1966 corresponded to a change in the particle flux with the higher energy particles increasing before the lower energies, indicating a cutoff change.

2. Theoretical

a. Calculation of Theoretical Riometer Absorption from a Proton Spectrum

The calculation of the theoretical riometer absorption begins with the calculation of the number of ion-pairs produced at a particular altitude. The general expression for calculating the electron production rate, q, is given by

$$q = \frac{1}{.000036} \int_{E(\theta,h)}^{\infty} \int_{\theta=0}^{\Pi/2} \int_{\phi=0}^{\Pi 2} \frac{dJ}{dE} \frac{dE}{dX} \rho(h) dE \sin\theta d\theta d\phi \qquad (105)$$

where $\frac{dJ}{dE}$ is the differential energy spectrum expressed in number of protons/(cm^2 sec ster Mev), $\frac{dE}{dx}$ is the proton energy loss in Mev/gm/cm^2 in traversing the atmosphere, ρ is the atmospheric density in gm/cm^3, θ is the zenith angle (attack angle) of the particle, ϕ is the azimuth angle, .000036 Mev is the average ionization potential in the lower atmosphere, and q is the number of electrons produced per cm^3 sec. In this calculation the atmospheric density is given by the United States Standard Atmosphere [1962] and the proton energy loss parameters in air by Bethe and Ashkin [1953]. The assumption is made that air has the same composition throughout the atmosphere below 100 km.

Recent satellite measurements have obtained proton particle spectrums at an altitude of 1100 km. One must determine how many of these particles will arrive at 100 km to interact with the atmosphere. If one considers a single particle in a static magnetic field there is no work done on the particle. Hence, the flux, Φ, linking the orbit of a particle rotating about a field line is constant [Spitzer, 1962]. Therefore

$$\Phi = B \Pi R_c^2 = \text{constant} \tag{106}$$

where B is the magnetic field and R_c is the cyclotron radius. The particle's perpendicular energy is given by

$$E_\perp = 1/2 \, mv_\perp^2 \tag{107}$$

or

$$E_\perp = e^2 B^2 R_c^2/2mc^2 \tag{108}$$

Rewriting the expression for Φ, one obtains

$$\Phi = \text{constant} = 2\Pi \, mc^2 \, E_\perp/e^2 B \tag{109}$$

Therefore,

$$E_\perp/B = \text{constant} = \mu \tag{110}$$

The constant μ is the magnetic moment due to the particle's motion around the field line. Now

$$E_\perp = mv_\perp^2/2 \tag{111}$$

or

$$E_\perp = mv^2 \sin^2\alpha/2 \tag{112}$$

where v is the speed of the particle and α is the pitch angle defined to be the angle between the velocity vector and the field line. This expression then gives the following relation at two different points along the field line.

$$\sin^2\alpha_1/B_1 = \sin^2\alpha_2/B_2 = \text{constant} \tag{113}$$

While the last expression was derived for a single particle it will also apply to an isotropic distribution of many particles. Furthermore, the expression shows that the particles will move into a region of increasing B field until $\sin\alpha = 1$ when they stop and move out of the region of increasing B field.

In this study the assumption of 2Π isotropy will be used. If

$$\alpha_1 = \alpha_{100\text{ km}} \tag{114}$$

and

$$\alpha_2 = \alpha_{1100\text{ km}} \tag{115}$$

and if α_1, is set equal to 90° indicating that the mirroring is taking place at 100 km, one obtains

$$\sin^2\alpha_{1000\ km} = B_{1100\ km}/B_{100\ km} \tag{116}$$

The values of $B_{1100\ km}$ and $B_{100\ km}$ may be obtained from <u>Roederer</u> <u>et</u> <u>al</u>. [1965] and are taken as .35 gauss and .52 gauss respectively for Durham. As a consequence all the particles with pitch angles greater than $\alpha_{1100\ km}$ will mirror before reaching 100 km. This angle corresponds to 55°36'.

The surface area that is accessible at 100 km is given as

$$\text{surface area} = r^2 \int_0^{\alpha_{1000\ km}} \sin\alpha\, d\alpha \int_0^{2\Pi} d\phi \tag{117}$$

and upon integration

$$\text{surface area} = 2\Pi\, r^2\, [1-\cos\alpha] \tag{118}$$

In solid angle measure one obtains

$$\Omega = 2\Pi\, (1-\cos\alpha) \tag{119}$$

steradians which indicates this is the solid angle available at 100 km. For an α of 55°36' this corresponds to

$$\Omega = (.434)\, 2\Pi \tag{120}$$

or put another way, 43.4% of the particles that are at 1100 km reach 100 km. This value will be adopted in the work that follows to correct for the mirroring particles above 100 km.

As the particles at 100 km begin their descent into the atmosphere, the spectrum that represents them at 100 km will change due to atmospheric attenuation. The method of Maeda [1963] will be utilized to correct for this change.

Using the energy loss expression of Bethe and Ashkin [1953] for protons in air one obtains

$$-\frac{dE}{dR} = 236E^{-.78} \tag{121}$$

with dE/dR representing the rate of energy loss E per unit depth of air R expressed as Mev/(gm cm^{-2}). Using a differential energy spectrum in a power law in energy gives

$$j(E)dE = \alpha E^{-n}\, dE \tag{122}$$

To convert the differential energy spectrum into a range spectrum the following transformation is required.

Integrating $\frac{dE}{dR}$ results in

$$\int_{o}^{R} dR = \int_{E}^{o} -\frac{dE}{236}\, E^{.78} \tag{123}$$

yielding

$$R = \frac{E^{1.78}}{236(1.78)} \tag{124}$$

Now

$$E = (450.1\ R)^{-\frac{1}{1.78}} \tag{125}$$

and

$$E^{-n} = (450.1\ R)^{-\frac{n}{1.78}} \tag{126}$$

Substituting into equation 122, one obtains

$$j(R)dR = kR^{-\ell}dR \tag{127}$$

where

$$k = \alpha 236^{-\frac{(n-1)}{1.78}}(1.78)^{-\ell}$$

and

$$\ell = (n+.78)/1.78$$

Since the rate of energy loss of protons penetrating into the atmosphere is larger for protons of lower energy than for high energy protons, the form of the differential spectrum will change with increasing depth in the atmosphere. The omnidirectional differential range spectrum at the top of the atmosphere is given by

$$i_o(R)dR = 2\Pi j(R)dR \tag{128}$$

and at an atmospheric depth $x(gm/cm^2)$ by

$$i_x(R)dR = 2\Pi \int_0^{\Pi/2} j(R+x/\cos\alpha)\sin\alpha\ d\alpha \tag{129}$$

where α is the pitch angle. Substituting $R = R + \frac{x}{\cos\alpha}$ in equation 127, one obtains

$$i_x(R)dR = 2\pi \int_0^{\pi/2} k \left(R + \frac{x}{\cos\alpha}\right)^{-\ell} \sin\alpha \, d\alpha \quad (130)$$

Let

$$\mu = \cos\alpha \quad (131)$$

so that

$$d\mu = -\sin\alpha \, d\alpha \quad (132)$$

resulting in

$$i_x(R)dR = 2\pi \; k \; R^{-\ell} \; dR \; (1+\eta/\mu)^{-\ell} d\mu \quad (133)$$

where

$$\eta = x/R$$

Changing from range to energy, the omnidirectional differential energy spectrum becomes

$$i_x(E)dE = 2\pi \; k \; (E^{1.78}/450.1)^{-\ell} \left(\frac{E^{.78}}{236}\right) dE \int_0^1 (1+\eta/\mu)^{-\ell} \, d\mu \quad (134)$$

The production function is then written as

$$q = \frac{1}{.000036} \int_{E_{lower}}^{E_{upper}} i_x(E) \; dE/dx \; \rho(h) \; dE \quad (135)$$

In this dissertation, the atmospheric depth is obtained from the atmospheric pressure as defined by the United States Standard Atmosphere [1962]. If the atmospheric pressure is measured in cm of mercury, the atmospheric depth, x, is found by the equation

$$x = (\text{density of mercury}) \times (\text{pressure in cm mercury}) \tag{136}$$

The calculations do not take account of nuclear reactions and the ionization produced in the atmosphere by the secondary particles from these reactions. Hofmann and Winckler [1963] made a theoretical calculation of the γ-ray production for protons interacting in air. They found, for example, that for 20 Mev protons only about one proton in two hundred produces a nuclear reaction. Each reaction leads to the release of about four γ-ray photons, so for every 50 protons of 20 Mev energy one γ-ray photon of typical energy 2 Mev is produced. At 10 Mev there is only one γ-ray photon for every 200 protons while at 50 Mev there is only one γ-ray photon for every 25 protons. Bailey [1964] shows that for a 2 Mev γ-ray photon, if all the energy were to be dissipated by ionization at heights from 59 to 70 km, then only about 0.2 per cent, at most, of the total ionization resulting from incident protons of 20 Mev could be attributed to γ-rays. Consequently, this source of ionization is negligible.

The electron production function has been calculated every kilometer from 20 km to 100 km for the spectrum data available. The equilibrium electron density has been calculated at one kilometer increments using Webber's [1962] effective recombination coefficients for nighttime conditions.

The computer program for the above calculation is discussed in Appendix F.

Having found the equilibrium electron density, the ionospheric absorption is calculated at one km increments. The ionospheric absorption coefficient, k, is determined every km for a 22 MHz electromagnetic wave in both the ordinary and extraordinary mode from equation 64 and ds is taken as one km. The total absorption is then the sum of all these incremental absorptions. The computer program for the above calculation is discussed in Appendix G. It should be pointed out that the absorption coefficient k is inversely proportional to the mass and results in the positive ions making a completely negligible contribution to the absorption compared to the electrons.

The determination of the collision frequency is taken from Larson [1967] and is given as

$$\nu = (9 \times 10^7) \times (p) \tag{137}$$

where p is the atmospheric pressure in mm of mercury and is obtained from the United States Standard Atmosphere [1962]. Larson reports that these values agree well with the earlier experimentally determined values of Kane [1961].

Webber [1962] states that the electron collision frequency with neutral particles, ν, may change slightly from day to night as the atmospheric temperature and density change. However, he notes this effect is only a few per cent and much less than a factor of two even in the case of high electron production. Also, Lerfald et al. [1964] report that during disturbed auroral periods the electron collision frequencies are not changed drastically. Therefore, this study will assume that the electron-neutral collisions do not change under disturbed conditions.

The experimental values of absorption to be used here are the average of the two modes produced by the birefringence of the ionosphere. Adams [1965] states that the riometer has equal sensitivity to both modes and that the unabsorbed strengths of both modes are equal.

b. Correction of Experimental Broad-Beam Antenna to Pencil-Beam Antenna Absorption

Leinbach [1962] describes a method for the correction of the experimental broad-beam antenna absorption to a pencil-beam antenna absorption or absorption per unit vertical column. The increased absorption is the result of the greater path length through the absorbing region for waves entering the beam at a zenith angle θ as compared to vertically incident waves.

If there is no absorption, the cosmic radio noise received by the antenna is written as

$$\int_0^{2\Pi} \int_0^{\Pi/2} P(\theta,\phi)F(\theta,\phi) \sin\theta \, d\theta \, d\phi$$

where $P(\theta,\phi)$ is the distribution of the cosmic radio noise as a function of the zenith angle θ and the azimuth angle ϕ, and $F(\theta,\phi)$ is the power polar diagram of the antenna. If an absorbing layer is added, so that only a fraction $T(\theta,\phi)$ of the incident cosmic radio noise power reaches the antenna from a given direction, the cosmic radio noise reaching the antenna under these conditions is

$$\int_0^{2\pi}\int_0^{\pi/2} P(\theta,\phi)\ T(\theta,\phi)\ F(\theta,\phi)\ \sin\theta\ d\theta\ d\phi$$

The measured absorption in decibels is given by

$$A(dB) = 10\log_{10}\frac{\int_0^{2\pi}\int_0^{\pi/2} PTF\ \sin\theta\ d\theta\ d\phi}{\int_0^{2\pi}\int_0^{\pi/2} PF\ \sin\theta\ d\theta\ d\phi} \qquad (138)$$

It is very difficult to write an analytic expression for the product TF because of the complex nature of the cosmic radio noise and the antenna power polar pattern. $P(\theta,\phi)$ varies with time due to the rotation of the sky through the fixed antenna pattern and at any time is a complicated function of position.

The assumptions made here are a uniform cosmic radio noise distribution, a symmetrical antenna power polar pattern with a $\cos^2\theta$ power response, and a horizontal and uniform absorbing layer over the antenna. The transparency of the absorbing layer, T, is represented as

$$T = e^{-a\sec\theta} \qquad (139)$$

where a is the integral of the vertical absorption coefficient and secθ compensates for the increase of path length with increasing zenith angle. Assuming azimuthal symmetry the expression for absorption becomes

$$A(\mathrm{dB}) = 10 \log_{10} \frac{\int_0^{\Pi/2} e^{-a \sec\theta} \cos^2\theta \sin\theta \, d\theta}{\int_0^{\Pi/2} \cos^2\theta \sin\theta \, d\theta} \tag{140}$$

where

$$a = \frac{10^3}{c} \int_{h_1(\mathrm{km})}^{h_2(\mathrm{km})} \frac{\omega_p^2 \, r}{\omega^2 + \nu^2} \, dh$$

with c the velocity of light, ω_p the plasma frequency, ω the operating frequency, and ν the collision frequency.

To integrate the numerator of the absorption expression let $z = a \sec\theta$. Expressing the differential of θ in terms of z gives

$$d\theta = \frac{dz}{a \sec\theta \tan\theta} \tag{141}$$

giving in turn

$$\int_a^{\infty} \frac{e^{-z}}{\sec^2\theta} \sin\theta \frac{dz}{a \sec\theta \tan\theta} \tag{142}$$

which leads to

$$\int_a^\infty \frac{a^3 e^{-z} dz}{a^4 \sec^4\theta} \tag{143}$$

and finally

$$\int_a^\infty \frac{a^3 e^{-z} dz}{z^4} \tag{144}$$

Integration by parts yields

$$A(dB) = 10 \log_{10} \left\{ e^{-a}[1-a/2(1-a)]^{-a^2/2} E_1(a) \right\} \tag{145}$$

where

$$E_1(a) = \int_a^\infty \frac{e^{-z} dz}{z}$$

and $E_1(a)$ may be evaluated from Abramowitz and Stegun [1965]. The ratio of broad beam absorption to vertical column absorption is roughly 1.33 in the absorption range 0-15 dB.

3. Experimental

a. Introduction

During late August and early September, 1966 two solar proton events occurred. The first event began on August 29, 1966 and is attributed to an importance 3B flare at 1531UT [Solar-Geophysical Data, 1966]. The second event commenced on September 2, 1966 and is attributed to an importance 3B flare at 0538UT.

The protons from these two events were detected by satellite 1963 38C which was launched September 28, 1963 into a nearly circular orbit at 1100 km altitude [Bostrom et al., 1967].

b. Satellite Results

The satellite is magnetically stabilized to within ~5° of the local magnetic field direction. The protons are detected by two proton spectrometers, one looking parallel (θ=180°) and one perpendicular (θ=90°) to the magnetic alignment axis. The parallel unit looks away from the earth in the northern hemisphere.

Each spectrometer consists of two fully depleted surface barrier solid-state detectors each 500 microns thick by 50 mm^2 in area. The minimum shielding excluding the aperature is sufficient to stop 50 Mev protons with additional shielding which prevents electrons of less than

100 Mev from entering the telescope in the reverse direction. A permanent magnet that serves as part of the collimator prevents electrons of energy less than ~200 kev from reaching the detector. By proper discriminator settings and coincidence four energy channels are set for protons: 1.2 to 2.2 Mev, 2.2 to 8.2 Mev, 8.2 to 25.0 Mev, and 25.0 to 100 Mev. The proton spectrometers do not distinguish protons from other heavy ions, such as alpha particles, but Bostrom [private communication, 1968] states this contribution is less than 10% and the background negligible compared to the counts observed during disturbed times.

The satellite data is plotted in units of invariant latitude, Λ, which is derived from the McIlwain coordinates [McIlwain, 1964]. These coordinates are used to describe the trapped radiation in the earth's magnetic field and are related to the adiabatic motion of charged particles in the earth's magnetic field. The coordinates are expressed in the local magnetic field, B, and the shell parameter, L. L is defined so that it remains constant (to within 1%) along any given geomagnetic field line, and represents the height to which the field line rises on crossing the geomagnetic equatorial plane (measured in earth radii from the center of the earth). Field lines characterized by a specific value of L then constitute a toroidial shell about the geomagnetic axis, and L is termed the shell parameter.

The pseudo-polar coordinates (R_r, Λ) are defined as

$$R_r = L \cos^2 \Lambda \tag{146}$$

where R_r is the radial distance in earth radii to the point of interest, and Λ is the invariant latitude. The pseudo-polar coordinates must be used with caution since their relation to true polar coordinates is indirect. At Durham the invariant latitude is 56.5° and the geomagnetic latitude is 55°.

The period of late August and early September shows only three passes in which protons above background reach the invariant latitude, Λ, of Durham (Λ=56.5°). These passes occur at northbound passes 2342UT on September 3, 1966 and 0406UT on September 4, 1966 and a southbound pass at 2353UT on September 3, 1966. During this period the local time of the satellite corresponded to a midday-midnight orbit. Therefore, pass 0406UT is within one hour of local time at Durham while pass 2342UT is within five hours. Pass 2353UT is on the dayside of the earth and is seven hours different in local time from Durham. It is also on the other side of the polar cap.

Figures 41, 42, and 43 show the counts per second averaged over one degree versus Λ for the 90° proton detector in the energy range 2.2 to 8.2 Mev for the passes 2342UT, 2353UT, and 0406UT. In each of the three cases the count rate (counts per second) at Λ=56.5° is approaching the knee of the curve. In the 2353UT pass the count rate at Λ=56.5° has almost reached the plateau value. The plateau value of the curves indicates equal accessibility of the protons to all latitudes greater than that defined at the knee.

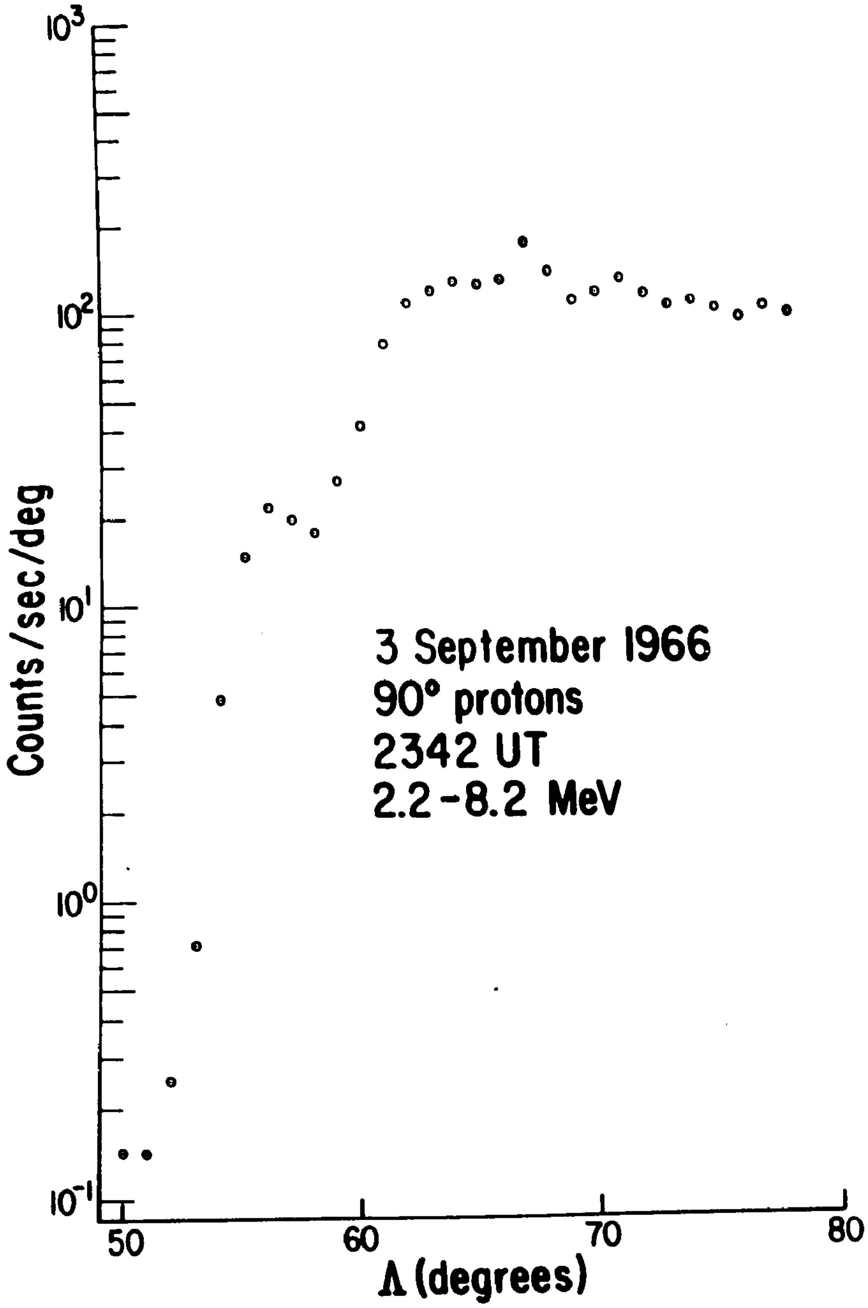

10^3
10^2
10^1
10^0
10^{-1}
Counts/sec/deg
3 September 1966
90° protons
2342 UT
2.2-8.2 MeV
50
60
70
80
Λ (degrees)

Figure 41

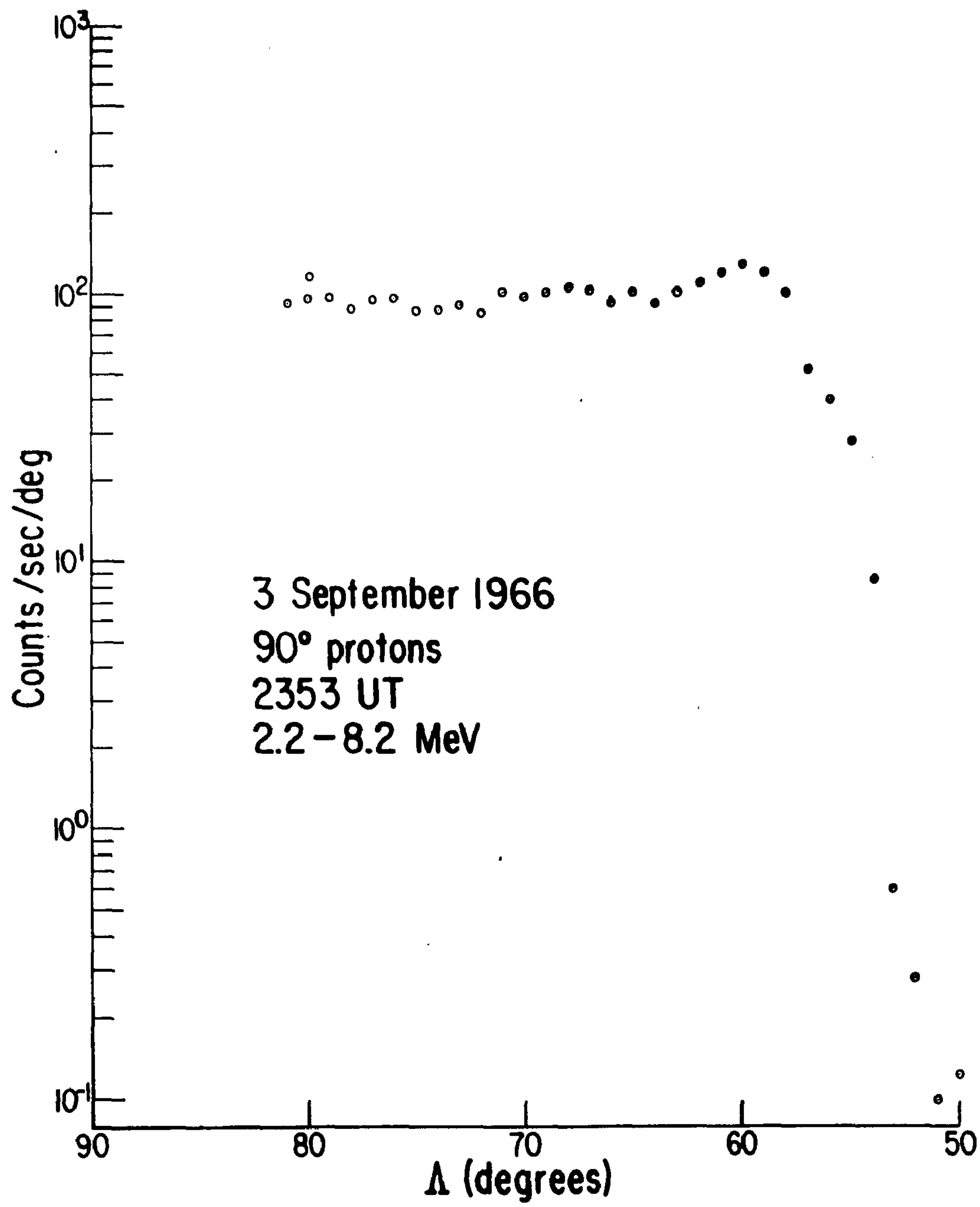
10³
10²
10¹
10⁰
10⁻¹
Counts /sec/deg
3 September 1966
90° protons
2353 UT
2.2-8.2 MeV
90
80
70
60
50
Λ (degrees)

Figure 42

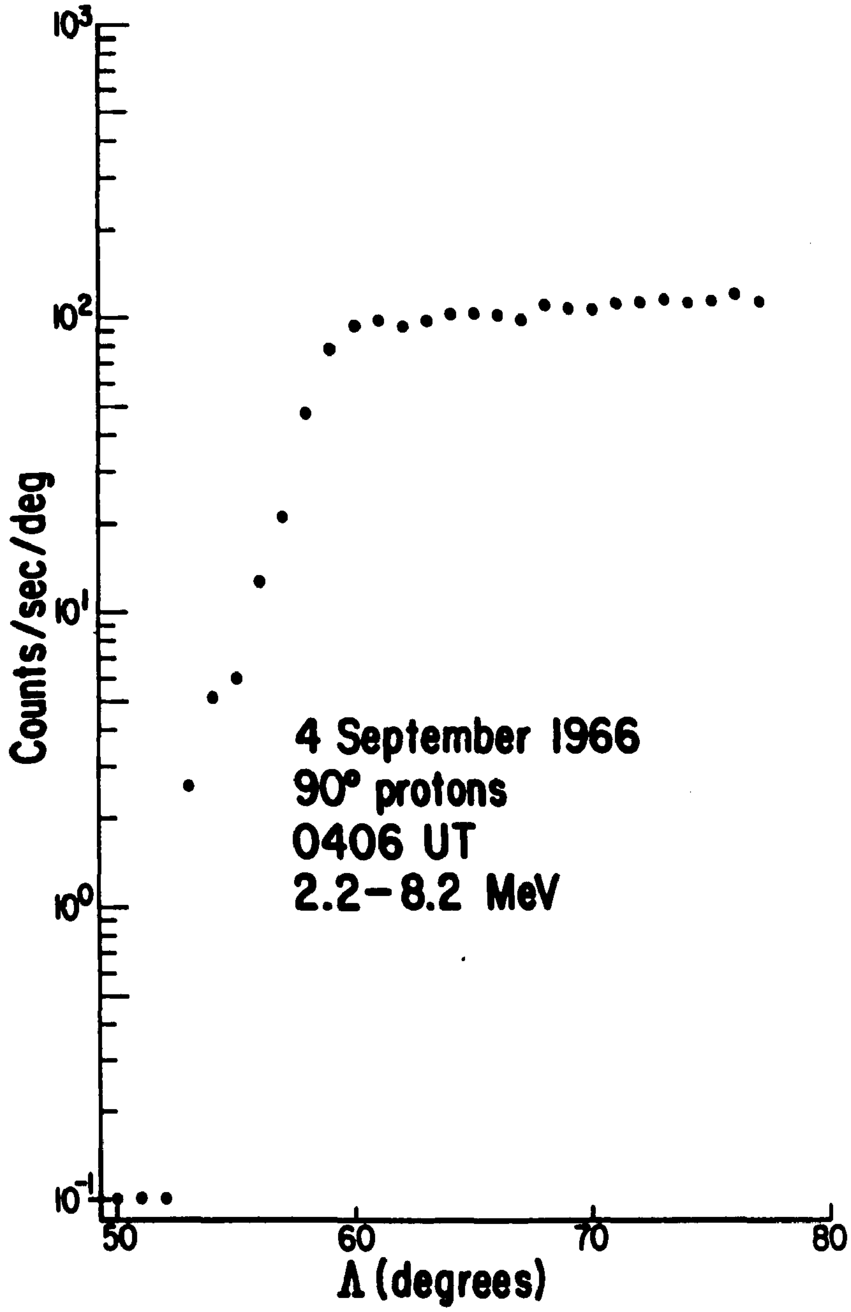
10^3
10^2
10^1
10^0
10^-1
Counts/sec/deg
4 September 1966
90° protons
0406 UT
2.2-8.2 MeV
50
60
70
80
Λ (degrees)

Figure 43

Figure 44 shows the counts per second, before averaging over one degree, versus Λ for the 90° proton detector in the energy range 2.2 to 8.2 Mev for the pass 1922UT on September 2, 1966. The plateau value found in the above four figures is typical of all energy ranges in both the 90° and 180° directions.

The spectrum for each of the three passes where protons reach the atmosphere above Durham is described by a negative exponent power law in energy with the exponent for the two lowest energy channels being different than the exponent for the two highest energy channels. Bostrom [private communication, 1968] states that the data has been found to fit a negative exponent power law in energy better than any other type of spectrum. Figure 45 shows the integral spectrum for the three passes, 2342UT, 2353UT, and 0406UT. In Figure 46 the omnidirectional differential spectrum for pass 2342UT is shown at various altitudes in the atmopshere indicating the change in the spectrum as it penetrates into the atmosphere.

Pass 2342UT is represented by differential energy spectrums in the energy range 1.2 to 8.2 Mev as

$$\frac{dJ}{dE} = 3.224 \times 10^3 \; E^{-2.399} \tag{147}$$

and in the energy range 8.2 to 100 Mev as

$$\frac{dJ}{dE} = 5.15 \times 10^2 \; E^{-1.796}$$

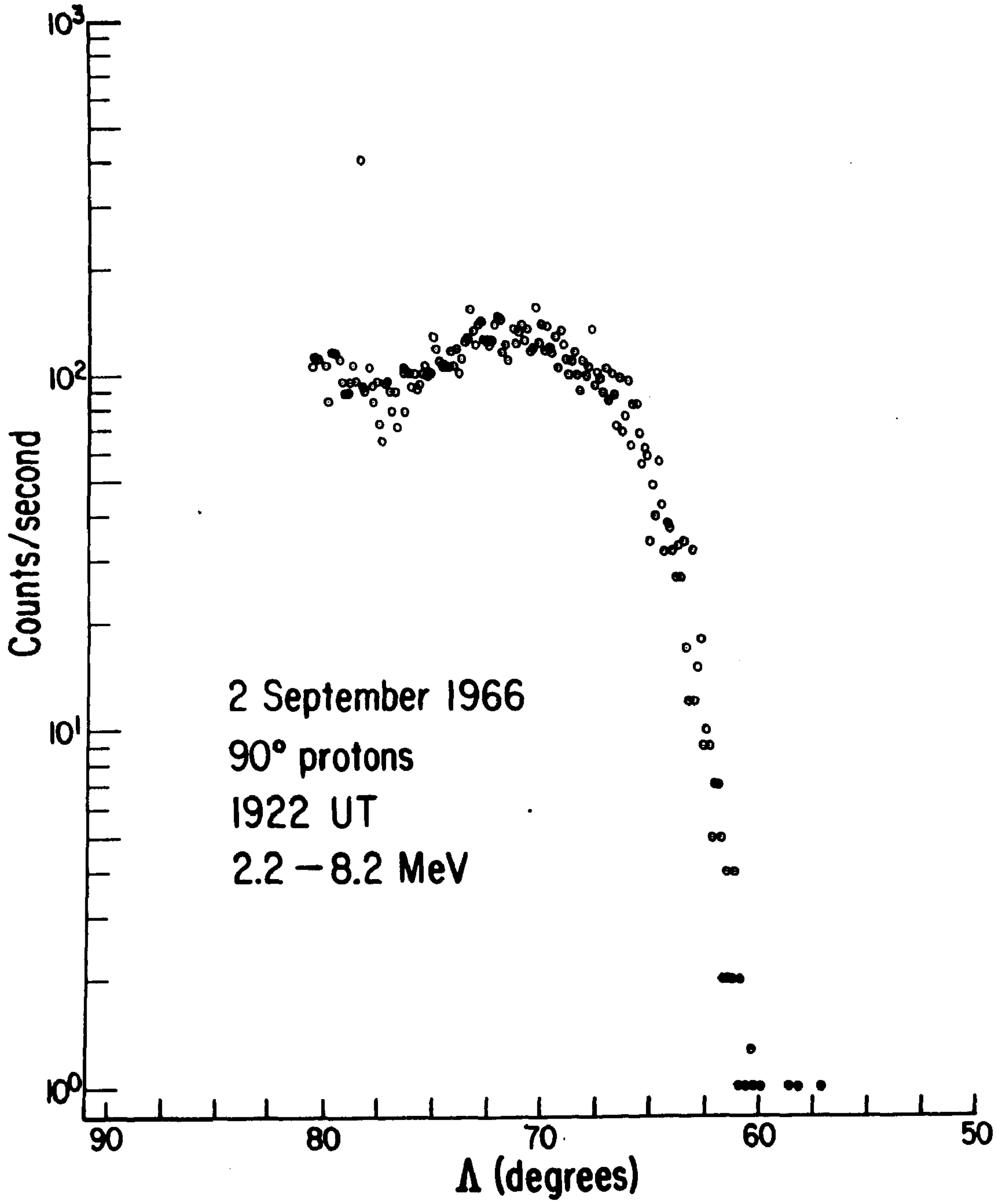

Counts/second
10^3
10^2
10^1
10^0
90
80
70
60
50
Λ (degrees)
2 September 1966
90° protons
1922 UT
2.2 – 8.2 MeV

Figure 44

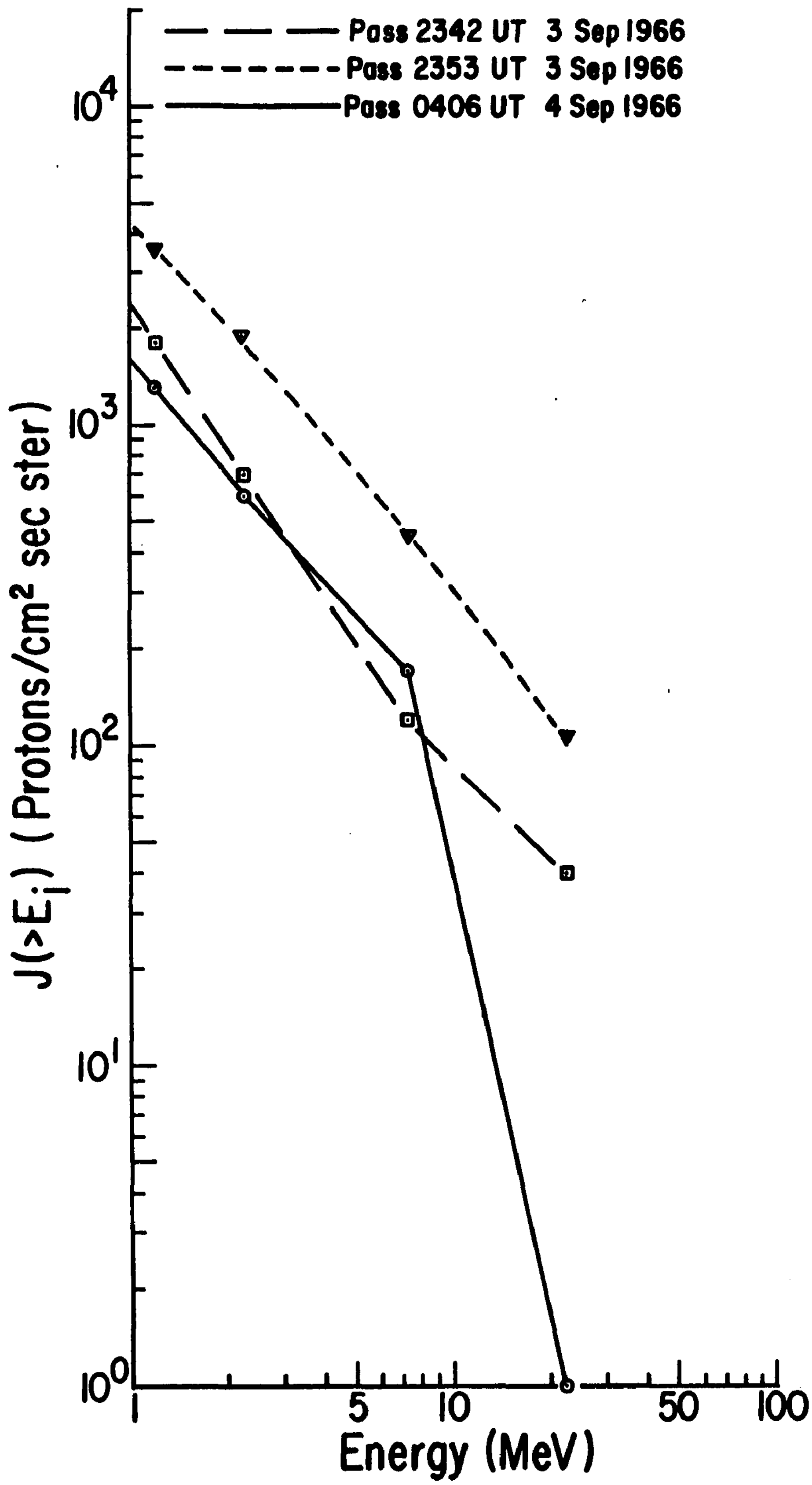

Pass 2342 UT 3 Sep 1966
Pass 2353 UT 3 Sep 1966
Pass 0406 UT 4 Sep 1966
10^4
10^3
10^2
10^1
10^0
J(>E$_i$) (Protons/cm^2 sec ster)
1
5
10
50
100
Energy (MeV)

Figure 45

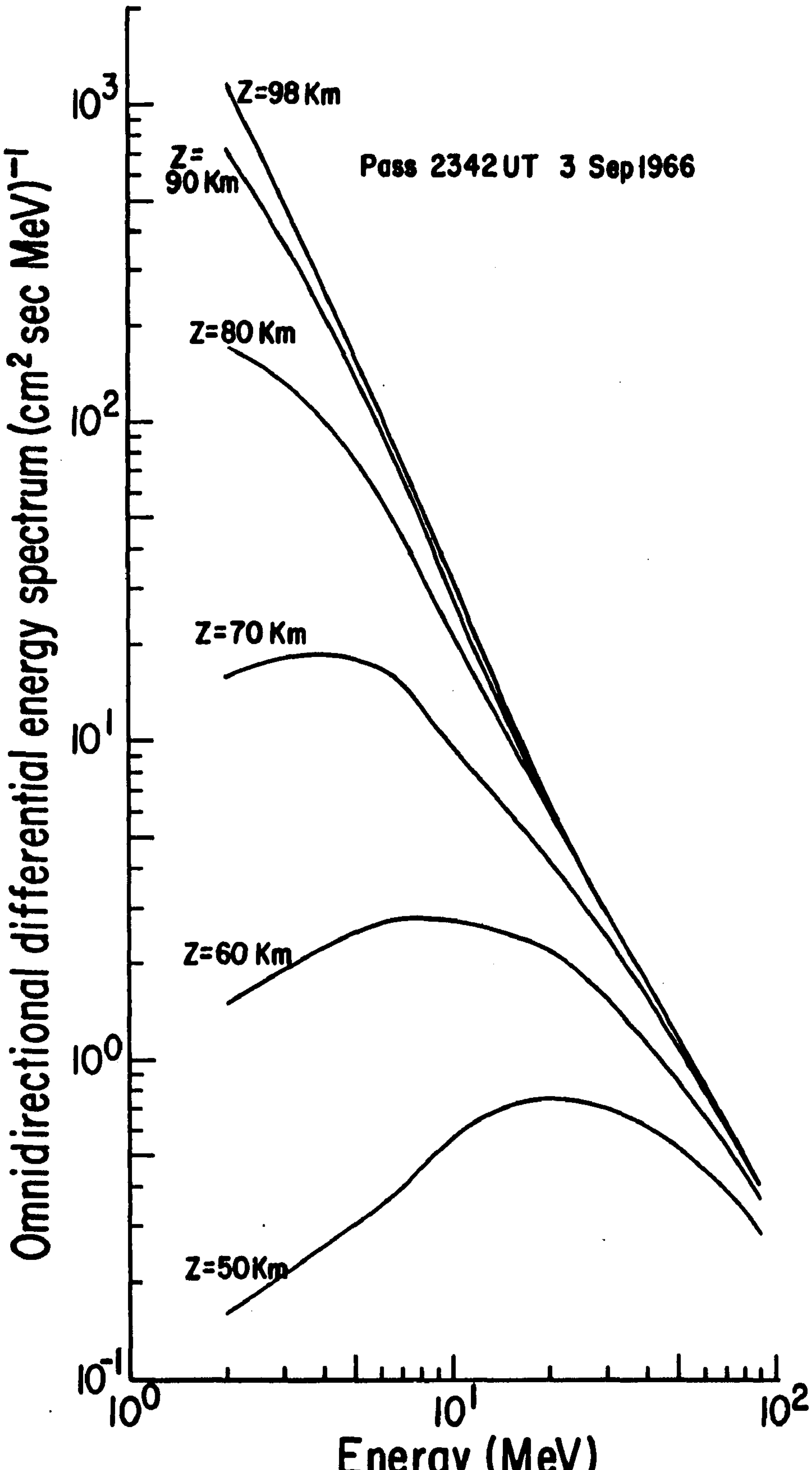

Z=98 Km
Z=
90 Km
Pass 2342 UT 3 Sep 1966
Z=80 Km
Z=70 Km
Z=60 Km
Z=50 Km
10^3
10^2
10^1
10^0
10^{-1}
10^0
10^1
10^2
Omnidirectional differential energy spectrum (cm^2 sec MeV)$^{-1}$
Energy (MeV)

Figure 46

Pass 2353UT is represented by differential energy spectrums in the energy range 1.2 to 8.2 Mev as

$$\frac{dJ}{dE} = 5.331 \times 10^3 E^{-2.063} \tag{149}$$

and in the energy range 8.2 to 100 Mev as

$$\frac{dJ}{dE} = 1.6144 \times 10^5 E^{-2.444} \tag{150}$$

Pass 0406UT is represented by differential energy spectrums in the energy range 1.2 to 8.2 Mev as

$$\frac{dJ}{dE} = 1.871 \times 10^3 E^{-2.136} \tag{151}$$

and in the energy range 8.2 to 100 Mev as

$$\frac{dJ}{dE} = 1.32694 \times 10^7 E^{-5.620} \tag{152}$$

The units of these spectra are protons/(cm^2 sec ster Mev) and the spectra as given are for the altitude of the satellite. They must be multiplied by the factor 43.4% to obtain the correct numbers at 100 km. Figure 47 shows the production function for three passes at 2342UT, 2353UT, and 0406UT. Figure 48 shows the resulting electron densities for the passes at 2342 UT, 2353UT, and 0406 UT.

This study will assume a cutoff of 1.2 Mev to prevent an excessive number of particles for energies less than one Mev. Two reasons make this assumption plausible. One reason is that no data is available for energies less than 1.2 Mev. The other reason is that the ionization produced by protons of

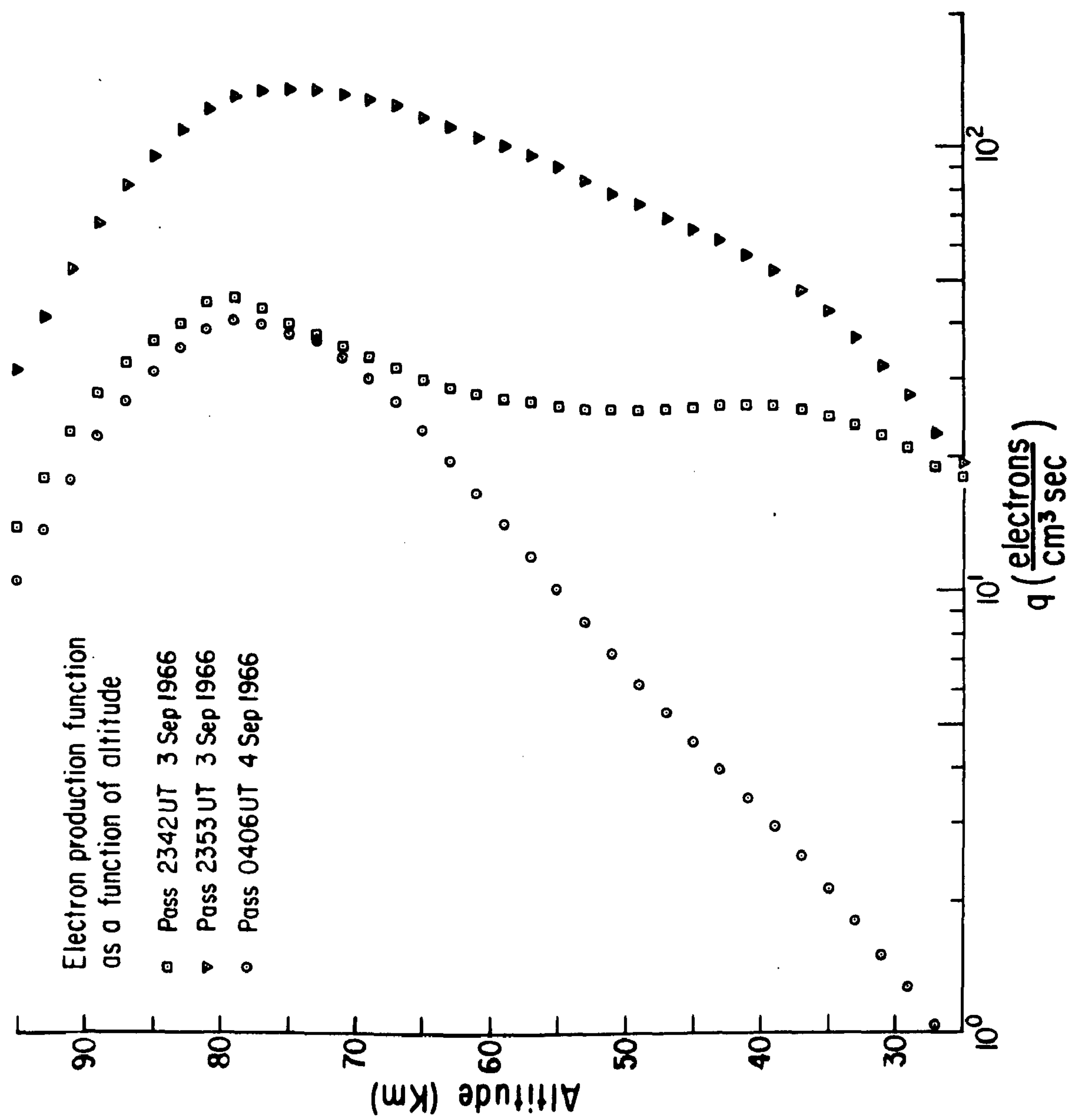

Electron production function
as a function of altitude
Pass 2342UT 3 Sep 1966
Pass 2353UT 3 Sep 1966
Pass 0406UT 4 Sep 1966
Altitude (Km)
90
80
70
60
50
40
30
10^0
10^1
10^2
$q\left(\frac{\text{electrons}}{\text{cm}^3\,\text{sec}}\right)$

Figure 47

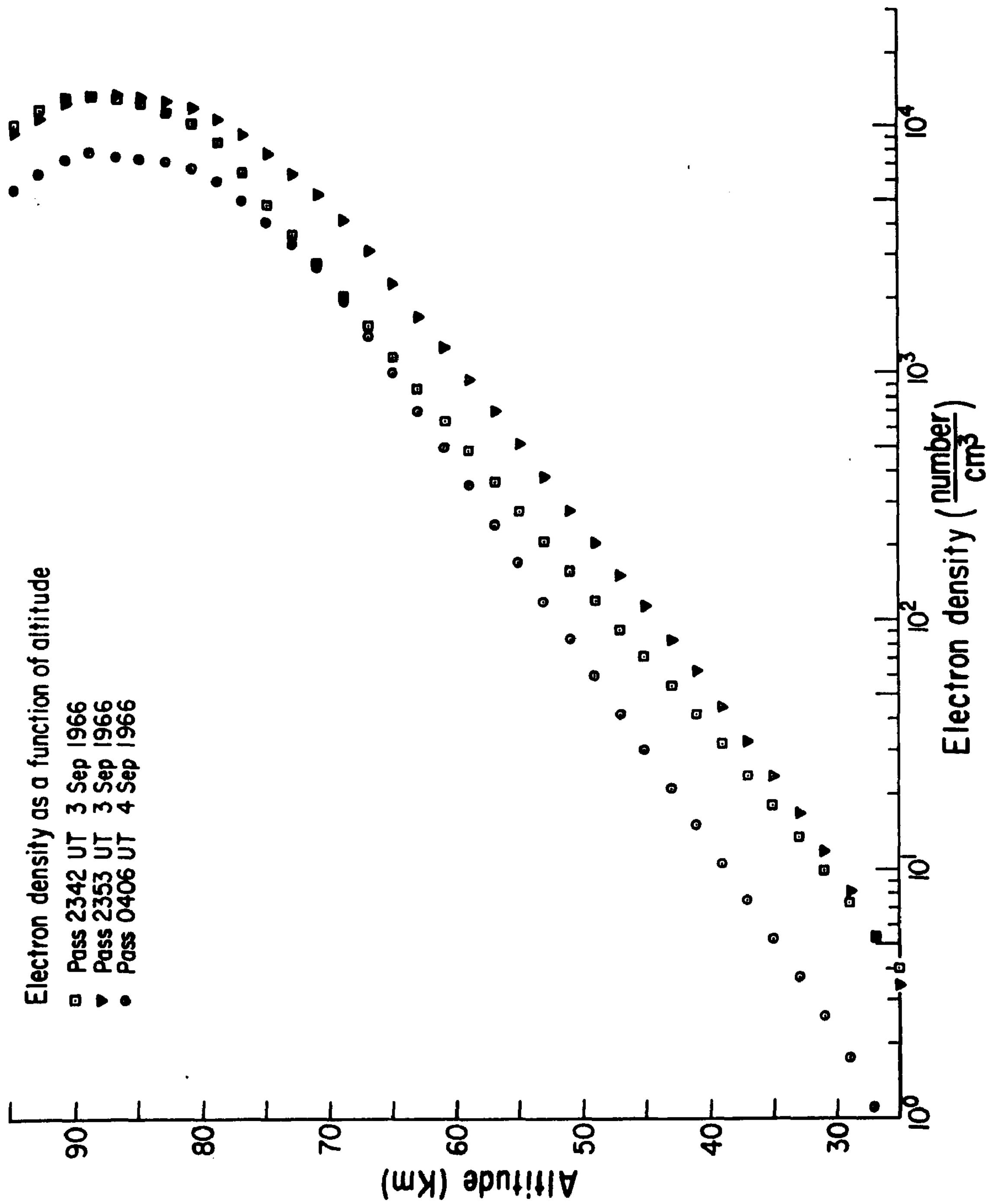
Electron density as a function of altitude
Pass 2342 UT 3 Sep 1966
Pass 2353 UT 3 Sep 1966
Pass 0406 UT 4 Sep 1966
Altitude (Km)
90
80
70
60
50
40
30
10^0
10^1
10^2
10^3
10^4
Electron density $\left(\frac{\text{number}}{\text{cm}^3}\right)$

Figure 48

the order of one Mev occurs at 90 km and above. A beam of one Mev protons shows a maximum in the production function at 90 km falling off by three orders of magnitude at 88 km and more slowly above 90 km [Adams, 1966]. Since the collision frequency at 90 km is 10^5 sec^{-1} compared to 5.0 x 10^7 sec^{-1} at 50 km there must be a tremendously large increase in electron density at 90 to 100 km to caluse any significant absorption. That such is not likely has been argued by Bailey [1959]. The upper limit in energy for this study is taken as 100 Mev.

Figure 49 shows a plot of cutoff invariant latitude versus time for the 2.2 to 8.2 Mev energy channel for the period of interest in September 1966. On the same figure a plot of D_{st} is shown to compare the change in the geomagnetic field to the cutoff of the protons. D_{st} is the average of the magnetic storm variation at low latitudes averaged over the longitude and is expressed in gammas ($1\gamma=10^{-5}$ gauss).

c. Riometer

Figures 50, 51, and 52 show the time history of the 22 MHz riometer absorption for the August-September period of interest. The absorption as plotted is corrected to vertical column absorption as previously discussed in this Chapter and also described in Appendix D. Table 2 shows the results of the calculations. All the theoretical absorption values were calculated using the effective recombination coefficients of Webber [1962] for nighttime conditions as

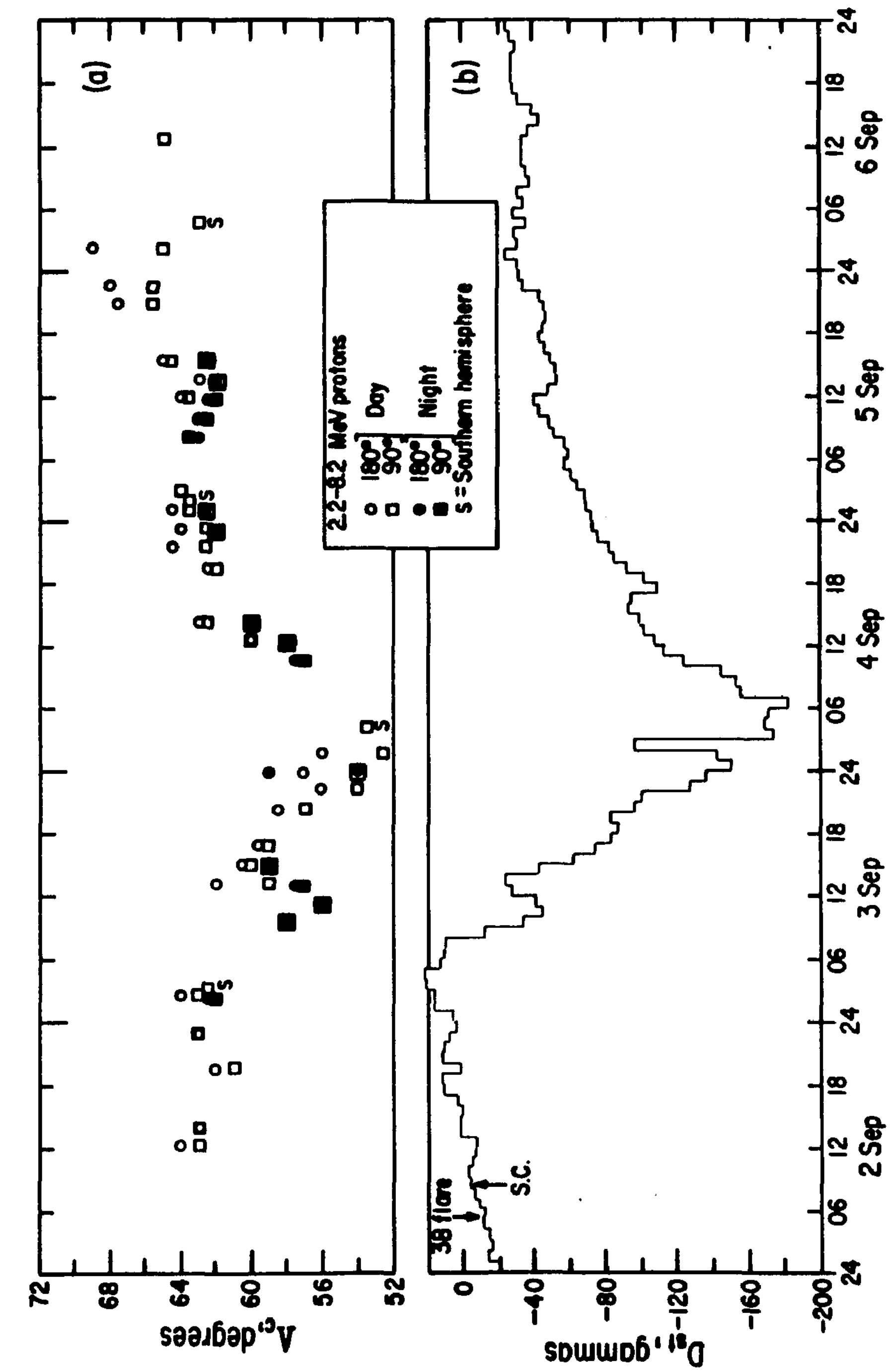
(a)
(b)
2.2–8.2 MeV protons
180° Day
90°
180° Night
90°
S = Southern hemisphere
Λc, degrees
72
68
64
60
56
52
Dst, gammas
0
−40
−80
−120
−160
−200
3B flare
S.C.
24 06 12 18 24 06 12 18 24 06 12 18 24 06 12 18 24 06 12 18 24
2 Sep
3 Sep
4 Sep
5 Sep
6 Sep
UT

Figure 49

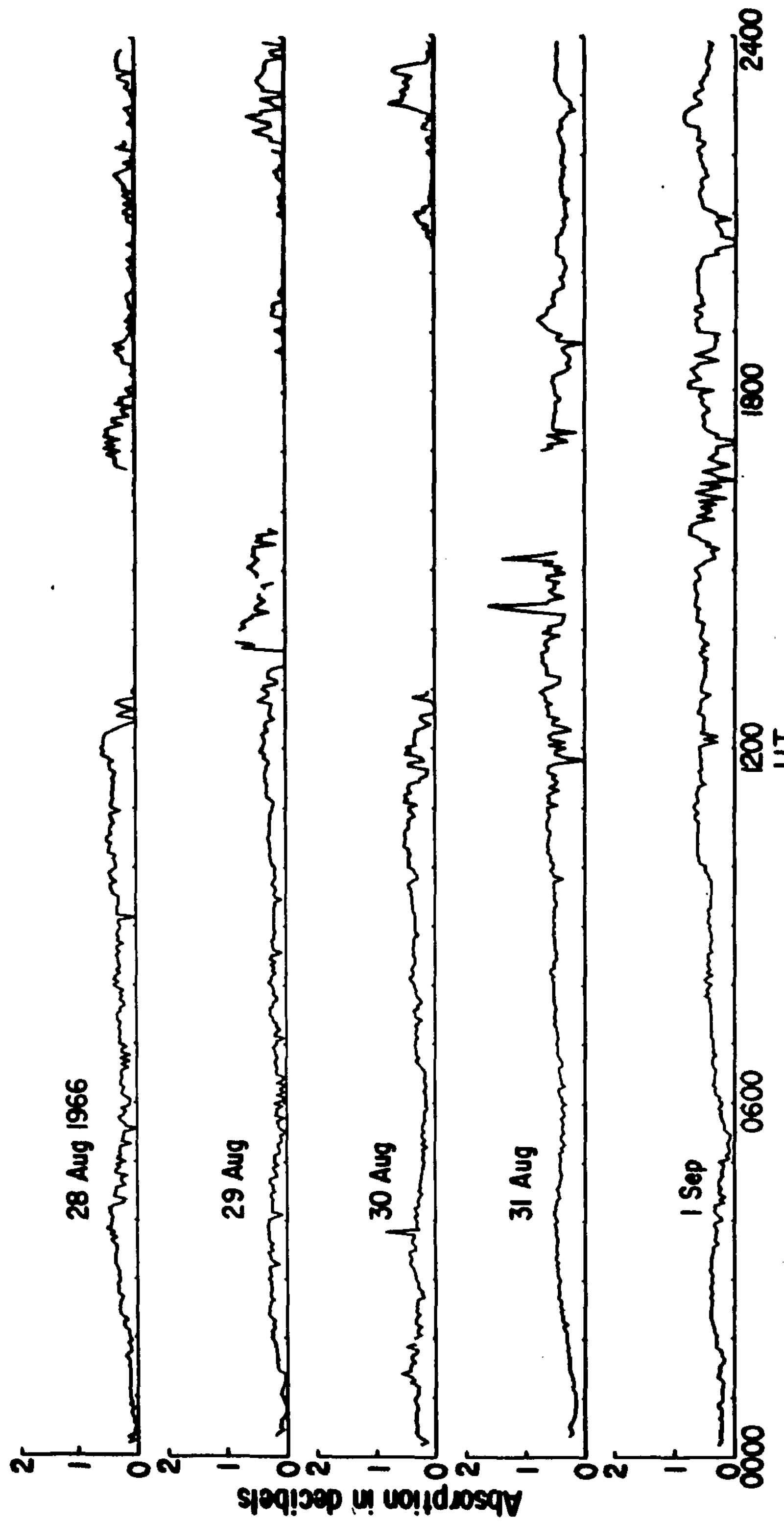
28 Aug 1966
29 Aug
30 Aug
31 Aug
1 Sep
Absorption in decibels
0
1
2
0000
0600
1200
1800
2400
UT

Figure 50

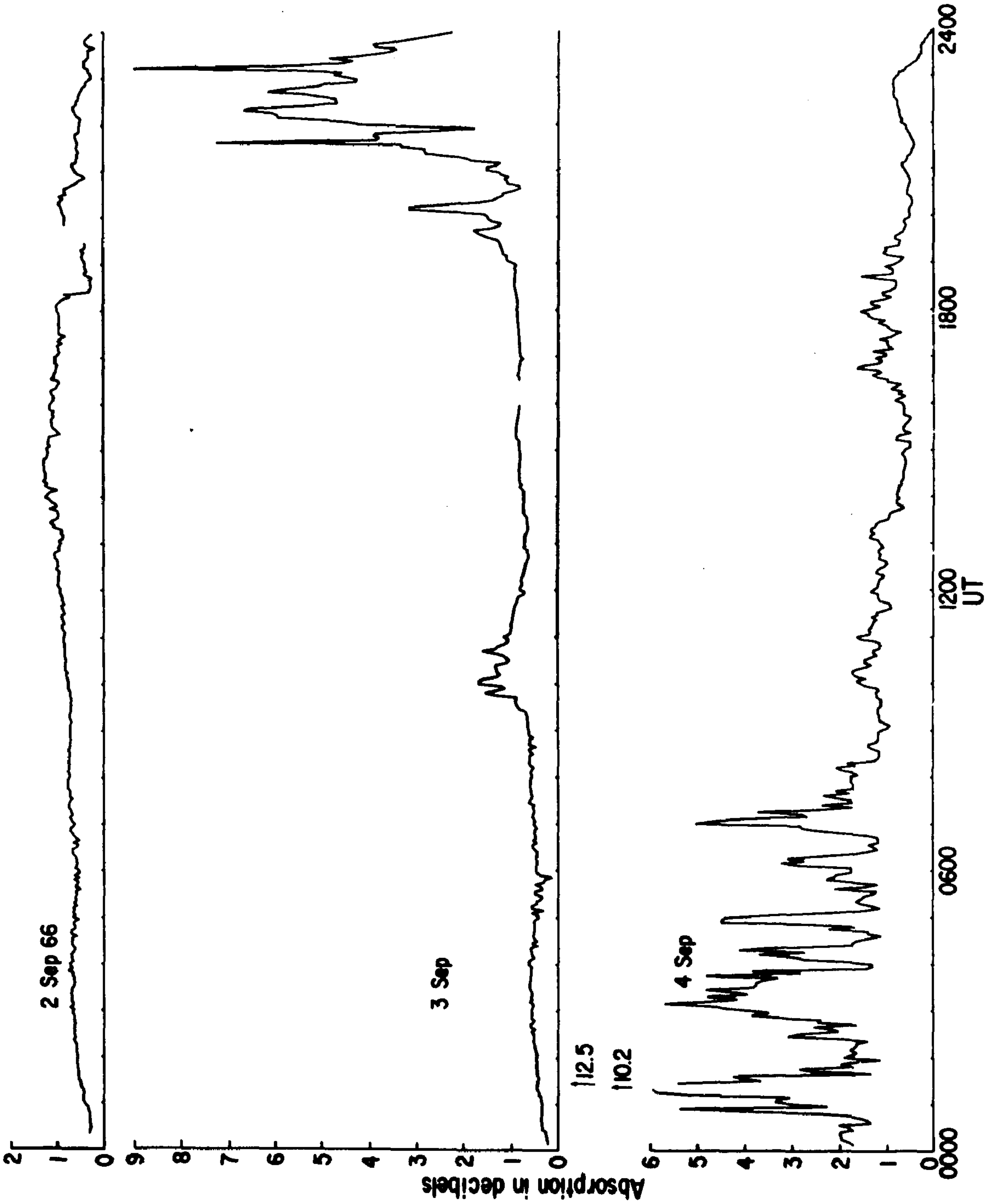
2 Sep 66
3 Sep
4 Sep
12.5
10.2
Absorption in decibels
0000
0600
1200
1800
2400
UT

Figure 51

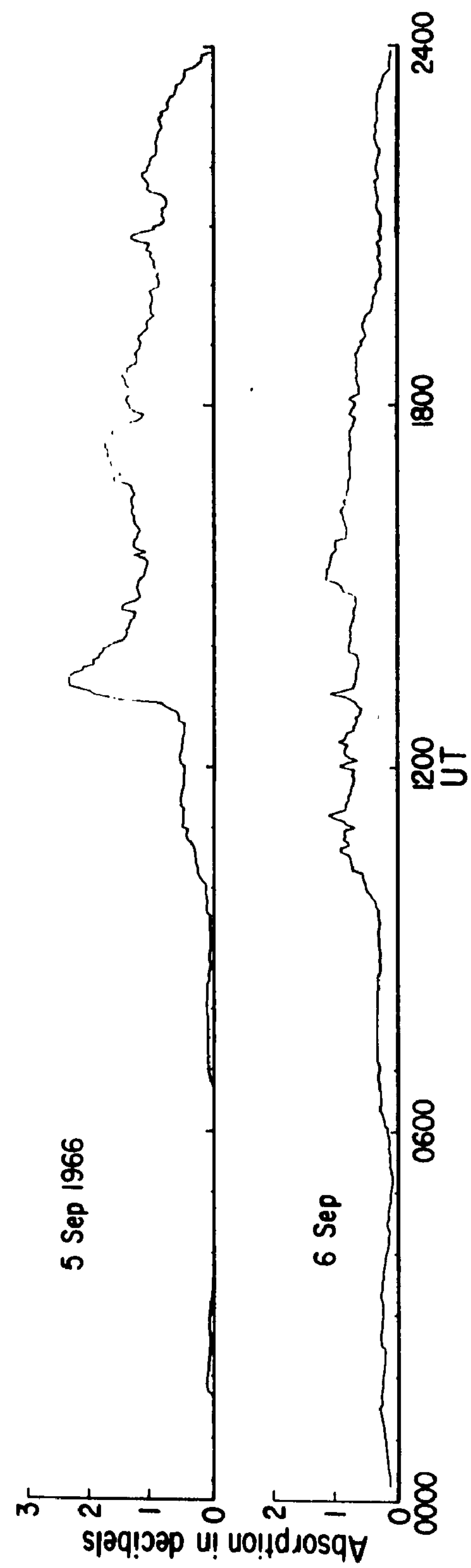

5 Sep 1966
6 Sep
Absorption in decibels
3
2
1
0
2
1
0
0000
0600
1200
1800
2400
UT

Figure 52

TABLE 2

DAY	PASS (UT)	VERTICAL COLUMN ABSORPTION MEASURED (dB)	VERTICAL COLUMN ABSORPTION CALCULATED (dB)
Sept. 3, 1966	2342	3.45	2.45
Sept. 3, 1966	2353	2.74	2.64
Sept. 4, 1966	0406	2.72	1.40

described in Chapter II. It should be pointed out that while pass 0406UT was clearly a nighttime pass, passes 2342UT and 2353UT correspond to the end of twilight conditions for the PCA. This is evident from scanning the period of time at approximately 2340UT on September 4 and 5 in Figures 51 and 52. The absorption at this time has decreased to almost full nighttime conditons. Therefore the nighttime effective recombination coefficients for these two passes should give absorption values that are smaller than the measured values, but not by very much.

The time history of the absorption preceding 2342UT on September 3 shows a sharp rise beginning at about 2100UT preceded by a smaller increase commencing at about 1900UT. The pass at 2342UT corresponds to a time of decrease in the primary peak of absorption with several small peaks of absorption on a steadily decreasing background. This pass corresponds to within five hours of the local time at Durham.

The experimental and theoretical values of absorption obtained at this time are 3.44 dB and 2.45 dB, respectively. The value of 245 dB agrees well with the steadily decreasing background of absorption occurring at this time seen in Figure 51. The absorption peaks rising above the background are likely electron precipitation although no data is presently available to confirm this assumption. At 2353UT the experimental and theoretical values of absorption are 2.74 dB and 2.64 dB, respectively.

The time history of the absorption preceding pass 0406UT is characterized by much irregular absorption. This is usually described as auroral absorption which is caused by precipitating electrons coming from the radiation belts. The experimental and theoretical values are 2.72 dB and 1.40 dB, respectively. The value, 1.40 dB, corresponds to the background from which the absorption peak rises as seen in Figure 51. This separation of auroral absorption (irregular peaks) from PCA (plateau value) has already been described by Leinbach et al. [1965] in Section 1 of this Chapter.

The three numerical calculations indicate that late on September 3 protons are causing a great percentage of the absorption recorded by the Durham 22 MHz riometer. Early on September 4 the absorption has decreased to a background completely accountable by protons and very irregular absorption peaks probably due to electron precipitation but not confirmed due to lack of electron data. These calculations indicate that for a period of several hours on September 3 and 4, the geomagnetic cutoffs are decreased allowing protons to enter the atmosphere over Durham.

Figure 53 shows the plot of D_{st} and K_p for this period of time. K_p is a mean standardized index of magnetic activity derived from three-hourly values obtained from twelve observatories between geomagnetic latitudes 47° and 63°. The scale is 0(very quiet) to 9(extremely disturbed). It is to be noted that the maximum values of D_{st} and K_p

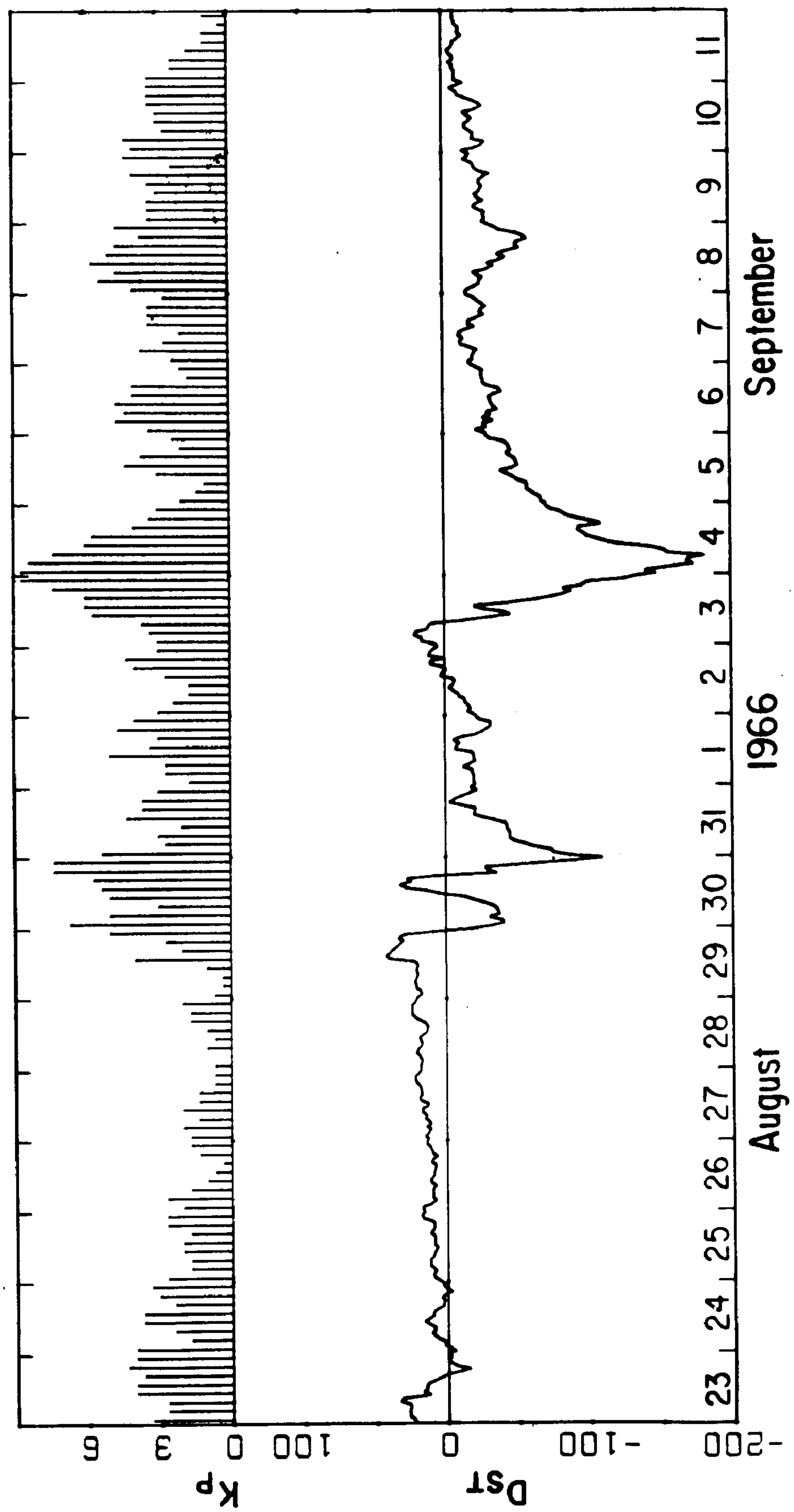
Kp
Dst
9
3
0
100
0
-100
-200
23
24
25
26
27
28
29
30
31
1
2
3
4
5
6
7
8
9
10
11
August
1966
September

Figure 53

occur for the period late on September 3 and early on September 4. This indicates that the geomagnetic field is very disturbed at the time of the intense riometer absorption.

A comparison of the cutoff changes previously shown in Figure 49 to the riometer absorption reveals an apparent interdependence. On September 3 at about 0925UT the riometer shows an increase in absorption that lasts until about 1300UT. Although there are no daytime cutoff measurements for the beginning of this time the daytime cutoff at about 1300UT is depressed to about 58°. The nighttime value of cutoff at 1100UT is 56°. These values indicate a decrease in the cutoffs to values that are similar to Durham's invariant latitude of 56.5°. Although this period of local time corresponds to sunrise it seems unlikely that the increase in absorption can be attributed to the atmospheric electron detachment effect since the absorption shows only a temporary increase. This change in absorption is then believed caused by a local change in cutoff allowing protons to reach the atmosphere over Durham between 0925 and 1300UT but not before or immediately after these times. At this time the magnetic field is not unusually disturbed ($D_{st} \sim 40\gamma$) indicating the cutoffs are anomalously low.

From about 1900UT on September 3 to about 1000UT on September 4, the cutoffs for 2.2 to 8.2 Mev protons are 56.5° or less. Simultaneously the riometer absorption is quite disturbed. It should be pointed out that during the times of extremely disturbed magnetic field the cutoffs for the 90° and 180° proton detectors of the same energy channel do not show the same cutoff. This indicates that at these times the particles allowed at a particular latitude depends both on pitch angle and energy. Although the departure from isotropy is not great, the effect is evident.

To contrast the disturbed conditions, a normal time pass at 1922UT on September 2 is compared from Figure 44. At this time the absorption is only a few tenths of a dB. The 90° 2.2 to 8.2 Mev proton detector shows no protons at 56.5° and actually no protons of 2.2 to 8.2 Mev reaching the satellite below 60°. This again strongly suggests that no particles means no absorption.

As a further indication that the riometer absorption at Durham is dependent on particles reaching the atmosphere and in turn the geomagnetic field condition, the solar proton event of August 29, 1966 is examined. The satellite 1963 38C sees no protons reaching the latitude of Durham on the days following the solar flare which occurs at 1531UT. Figure 53 shows two disturbed magnetic periods following the event. The one disturbance occurs on August 30 followed by a second and larger disturbance on August 31. The larger magnetic disturbance which occurs at 0000UT on August 31 reaches approximately - 115γ. At this same time the riometer is showing only a few tenths of a dB absorption as seen in Figure 50. There is no long duration, large magnitude, absorption seen at this time as occurs on September 3 and 4 when the magnetic field reaches a disturbed value of -185γ. The absence of any sharp irregular absorption peaks during the August 29 event indicates that no auroral absorption was occurring on the 22 MHz riometer caused by electrons precipitating from the trapped radiation belts.

One unusual period of absorption is not explainable. On September 2 the absorption shows a sudden decrease at 1820UT. There is no satellite data available at this time to check for a cutoff change. Consequently equipment malfunction must be considered a possibility.

In conclusion although the satellite data does not give continuous coverage the calculations and comparisons in this section are a strong indication that the absorption recorded at Durham under disturbed conditions is strongly dependent on the geomagnetic cutoff. The mechanism of how these protons get to the satellite cannot be explained by this study. It is to be noted that classical Störmer theory predicts a cutoff of roughly 840 Mev for protons under undisturbed conditions. The arrival of particles of energy 2.2 to 8.2 Mev is therefore not expected.

CHAPTER VI

CONCLUSIONS

For the years 1966 and 1967 the results of the total solar ionospheric absorption indicate: (1) a single maximum in absorption occurring very close to local noon; (2) a larger magnitude of absorption in the summer months than in the winter months; (3) an asymetry around local noon with the decay of absorption values to zero extending well into the nighttime; and (4) no solar ionospheric absorption at nighttime.

This study suggests a method for separating upper ionosphere solar absorption from lower ionosphere solar absorption using only riometer data. The results indicate that at local noon 35 to 50% of the solar ionospheric absorption is taking place in the upper ionosphere. The upper ionosphere solar absorption shows less solar control than the lower ionosphere. While the upper ionosphere shows more absorption in summer than in winter, the absorption is roughly constant for several hours on either side of local noon apparently not following the solar zenith angle. On the other hand the lower ionosphere absorption follows the solar zenith angle quite closely rising to a maximum value near local noon.

It should be pointed out that these results are based on two years in which the solar activity has been fairly low and may change during high sunspot years.

A further extension of this work should include two areas. The first would apply these techniques to years of high sunspot activity to determine if the physical processes are the same throughout the entire sunspot cycle. A second study should record data through the sunspot active years into the sunspot minimum years. Hence a reference curve free of solar absorption would be determined in a sunspot minimum year with the assumption that the ionizing radiation at this time is a minimum. By computing the solar ionospheric absorption for all the subsequent years in the solar cycle, an indication of the effect of the change in the x-ray flux over a solar cycle could be obtained. In addition to the assumption of minimum ionization during a sunspot minimum year, the assumption of little if any change in the ultraviolet flux is required. This seems reasonable from previous discussions.

The second portion of this study was concerned with making comparisons between experimentally measured riometer absorption during disturbed periods and theoretically calculated absorption.

The results for a disturbed period in September 1966 indicate that the irregularity of the absorption at Durham may be explained by changes in the geomagnetic cutoff alternately allowing and not allowing low energy protons to an invariant latitude of 56.5°. This result is an interesting addition to current interest in the anomalously low cutoffs which are sometimes seen with satellite measurements.

This study would suggest comparisons of measured disturbed periods of absorption with theoretical computed absorptions from available satellite data. The continued agreement between measured and calculated absorption values would definitely indicate cutoff changes at Durham under disturbed conditions.

A serious drawback for such an investigation is the lack of satellite data.

BIBLIOGRAPHY

Abdu, M. A., S. S. Degaonkar, and K. R. Ramanathan, Attenuation of Galactic Radio Noise at 25 MHz and 21.3 MHz in the Ionosphere over Ahmedabad during 1957-1964, J. Geophys. Res., 72, 1547-1554, 1967.

Abramowitz, M., and I. A. Stegun, Handbook of Mathematical Functions, Dover Publications, Inc., New York, 1965.

Adams, G. W., and A. J. Masley, Theoretical Study of Cosmic Noise Absorption due to Solar Cosmic Radiation, Planetary Space Sci., 14, 277-290, 1966.

Adams, G. W. and A. J. Masley, Determination of Solar Proton Energy Spectrums Below 100 Mev from Ground-Based Measurements, Douglas Report SM-51974, Douglas Aircraft Co., 1966.

Aikin, A. C., and S. J. Bauer, The Ionosphere, Introduction to Space Science, Ed. by W. N. Hess, 133-164, Gordon and Breach, New York, 1965.

Appleton, E., and W. R. Piggott, Ionospheric Absorption Measurements during a Sunspot Cycle, J. Atmospheric Terrest. Phys., 5, 141-172, 1954.

Bailey, D. K., Abnormal Ionization in the Lower Ionosphere Associated with Cosmic-Ray Flux Enhancements, Proc. Inst. Radio Engrs., 47, 255-266, 1959.

Bailey, D. K., and L. M. Branscomb, Bull. Amer. Phys. Soc. Series II, 5, 123, 1960.

Bailey, D. K., Polar-Cap Absorption, Planetary Space Sci., 12, 495-541, 1964.

Barth, C. A. Rocket Measurements of the Nitric Oxide Dayglow, J. Geophys. Res., 69, 3301-3303, 1964.

Barth, C. A., Nitric Oxide in the Upper Atmosphere, Ann. Geophys., 22, 198-207, 1966.

Basler, R. P., Radio Wave Absorption in the Auroral Ionosphere, J. Geophys. Res., 68, 4665-4681, 1963.

Beers, Y., Introduction to the Theory of Error, Addison-Wesley Publishing Co., Inc., Reading, Massachusetts, 1958.

Bethe, H. A., and J. Ashkin, Passage of Radiation Through Matter in Experimental Nuclear Physics, I, Ed. by E. Segre, John Wiley and Sons, Inc., 1953.

Bhonsle, R. V., and K. R. Ramanathan, Studies of Cosmic Radio Noise on 25 Mc/s at Ahmedabad, J. Ind. Sci. Ind. Res., 17A, 40-45, 1958.

Bolton, J. G., and G. J. Stanley, Variable Source of Radio Frequency Radiation in the Constellation of Cygnus, Nature, 161, 312-313, 1948.

Bostrom, C. O., J. W. Kohl, and D. J. Williams, The February 5, 1965, Solar Proton Event, J. Geophys. Res., 72, 4487-4495, 1967.

Bostrom, C. O., Private communication, 1968.

Bourdeau, R. E., A. C. Aikin, and J. L. Donley, Lower Ionosphere at Solar Minimum, J. Geophys. Res., 71, 727-740, 1966.

Brown, R. H., and C. Hazard, A. Model of the Radio-Frequency Radiation from the Galaxy, Phil. Mag., 44, 939-963, 1953.

Brown, R. R., and R. Parthasarthy, Observations of the September 2, 1966 PCA Event Midday Recovery in Absorption, Planetary Space Sci., 15, 1667-1675, 1967.

Chapman, S., The Absorption and Dissociation or Ionizing Effect of Monochromatic Radiation in an Atmosphere on a Rotating Earth, Proc. Phys. Soc., 43, 26-45, 1931.

Chapman, S., and T. G. Cowling, The Mathematical Theory of Non-Uniform Gases, Cambridge University Press, New York, 1960.

Davies, K., Ionospheric Radio Propagation, Chpt. 1, U. S. Government Printing Office, Washington, D. C., 1965.

Dingle, R. B., D. Arndt, and S. K. Roy, The Integrals

$C_p(x)=(p!)^{-1} \int_0 \varepsilon^p(\varepsilon^2+x^2)^{-1} e^{-\varepsilon} d\varepsilon$ and

$D_p(x)=(p!)^{-1} \int_0^\infty \varepsilon^p(\varepsilon^2+x^2)^{-2} e^{-\varepsilon} d\varepsilon$ and their Tabulation, Applied Sci. Res., 6B, 155-164, 1957.

Fredriksen, A., and R. B. Dyce, Ionospheric Absorption Investigations at Hawaii and Johnston Island, J. Geophys. Res., 65, 1177-1181, 1960.

Freir, P. S., and W. R. Webber, Exponential Rigidity Spectrums for Solar-Flare Cosmic Rays, J. Geophys. Res., 68, 1605-1629, 1963.

Hara, E. H., Approximations to the Semiconductor Integrals $C_p(x)$ and $D_p(x)$ for use with the Generalized Appleton-Hartree Magnetoionic Formulas, J. Geophys. Res., 68, 4388-4389, 1963.

Hofmann, D. J., and J. R. Winckler, Simultaneous Balloon Observations at Fort Churchill and Minneapolis during the Solar Cosmic Ray Events of July 1961, J. Geophys. Res., 68, 2067-2098, 1963.

Holt, O., B. Landmark, and F. Lied, A Study of Polar Radio Blackouts, Norweigian Defense Research Establishment Report 35, Parts I-II, 1961.

Houston, R. E., Jr., Private Communication, 1967.

Jackson, J. D., Classical Electrodynamics, 226-229, John Wiley and Sons, Inc., New York 1962.

Jansky, K. G., Atmospherics at High Frequencies, Proc. Inst. Radio Engrs., 20, 1920-1932, 1932.

Jansky, K. G., Minimum Noise Levels Obtained on Short-Wave Radio Receiving Systems, Proc. Inst. Radio Engrs., 25, 1517-1530, 1937.

Kane, J. A., Re-evaluation of Ionospheric Electron Densities and Collision Frequencies Derived from Rocket Measurements of Refractive Index and Attenuation, J. Atmospheric Terrest. Phys., 23, 338-347, 1961.

Kreplin, R. W., T. A. Chubb, and H. Friedman, X-ray and Lyman-Alpha Emission from the Sun as Measured from the N. R. L.S.R.-1 Satellite, J. Geophys. Res., 67, 2231-2253, 1962.

Kundu, M. R., and F. T. Haddock, A Relation Between Solar Radio Emission and Polar Cap Absorption of Cosmic Noise, Nature, 186, 610-613, 1960.

Larson, L. E., Electron Density Measurements in the Lower Ionosphere by a Rocket Borne Radio Propagation Method, Ph.D. Thesis, University of New Hampshire, 1967.

Leinbach, H., and G. C. Reid, Polar Cap Absorption During the Solar Cosmic Ray Outbursts of July 1959, July 1959 Events Symposium, Helsinki, 1960.

Leinbach, H., Interpretations of the Time Variations of Polar Cap Absorption Associated with Solar Cosmic Ray Bombardments, Sci. Rept. No. 3, NSF Grant No. G14133, Geophysical Institute, University of Alaska, 1962.

Leinbach, H., D. Venkatesan, and R. Parthasarathy, The Influence of Geomagnetic Activity on Polar Cap Absorption, Planetary Space Sci., 13, 1075-1095, 1965.

Leinbach, H., Midday Recoveries of Polar Cap Absorption, J. Geophys. Res., 72, 5473-5483, 1967.

Lerfald, G. M., C. G. Little, and R. Parthasarathy, D-Region Electron Density Profiles During Auroras, J. Geophys. Res., 69, 2857-2860, 1964.

Lerfald, G. M., Private communication, 1967.

Little, C. G., High-Latitude Ionospheric Observations Using Extra-Terrestrial Radio Waves, Proc. Inst. Radio Engrs., 42, 1700-1703, 1954.

Little, C. G., and H. Leinbach, Some Measurements of High-Latitude Ionospheric Absorption Using Extraterrestrial Waves, Proc. Inst. Radio Engrs., 46, 334-348, 1958.

Little, C. G., and H. Leinbach, The Riometer-A Device for the Continuous Measurement of Ionospheric Absorption, Proc. Inst. Radio Engrs., 47, 315-320, 1959.

Lusignan, B., Cosmic Noise Absorption Measurements at Stanford, California, and Pullman, Washington, J. Geophys. Res., 65, 3895-3902, 1960.

Maeda, K., Auroral Dissociation of Molecular Oxygen in the Polar Mesosphere, J. Geophys. Res., 68, 185-197, 1963.

McCracken, K. G., A Correlation Between The Emission of White Light and Cosmic Radiation by a Solar Flare, Nuovo Cimento, 13, 1081-1085, 1959.

McIlwain, C. E., Coordinates for Mapping the Distribution of Magnetically Trapped Particles, J. Geophys. Res., 66, 3681-3691, 1961.

Mitra, A. P., and C. A. Shain, The Measurement of Ionespheric Absorption Using Observations of 18.3 Mc/s Cosmic Radio Noise, J. Atmospheric Terrest. Phys., 4, 204-218, 1953.

Mitra, S. K., The Upper Atmosphere, The Asiatic Society, Calcutta, India, 1957.

Nicolet, M., and A. C. Aikin, The Formation of the D Region of the Ionosphere, J. Geophys. Res., 65, 1469-1483, 1960.

Nicolet, M., Theories on Electron Production and Recombination in the D and E Layers in Electron Density Profiles in the Ionosphere and Exosphere, Ed. by B. Maehlum, Pergamon Press and The Macmillan Co., New York, 1962.

Oort, J. H., Radio-Frequency Studies of Galactic Structure, Handbuch Der Physik, 53, 100-128, 1959.

Pawsey, J. L., and R. N. Bracewell, Radio Astronomy, Clarendon Press, Oxford, 1955.

Phelps, A. V., and J. L. Pack, Electron Collision Frequencies in Nitrogen and in the Lower Ionosphere, Phys. Rev. Letters, 3, 340-342, 1959.

Phelps, A. V., and J. L. Pack, Collisional Detachment in Molecular Oxygen, Phys. Rev. Letters, 6, 111-113, 1961.

Ramanathan, K. R., and R. V. Bhonsle, Cosmic Radio Noise Absorption on 25 Mc/s and F Scatter, J. Geophys. Res., 64, 1635-1637, 1959.

Ratcliffe, J. A., and K. Weeks, The Ionosphere, Physics of the Upper Atmosphere, Ed. by J. A. Ratcliffe, 377-470, Academic Press, New York, 1960.

Reid, G. C., and C. Collins, Observations of Abnormal V.H.F. Radio Wave Absorption at Medium and High Latitudes, J. Atmos. Terr. Phys., 14, 63-81, 1959.

Reid, G. C., A Study of the Enhanced Ionization Produced by Solar Protons During a Polar Cap Absorption Event, J. Geophys. Res., 66, 4071-4085, 1961.

Reid, G. C., Physical Processes in the D-Region of the Ionosphere, Rev. Geophys., 2, 311-333, 1964.

Roederer, J. G., W. N. Hess, and E. G. Stassinopoulos, Conjugate Intersects to Selected Geophysical Stations, NASA X-642-65-182, 1965.

Sen, H. K., and A. A. Wyller, On the Generalization of the Appleton-Hartree Magnetoionic Formulas, J. Geophys. Res., 65, 3931-3950, 1960.

Shain, C. A., Galactic Radiation at 18.3 Mc/s, Australian J. Sci. Res. A, 4, 258-267, 1951.

Shain, C. A., and C. S. Higgins, Observations of the General Background and Discrete Sources of 18.3 Mc/s Cosmic Noise, Australian J. Phys., 7, 130-149, 1954.

Skilling, W. T., and R. S. Richardson, Astronomy, Chpt. 4, Henery Holt and Co., New York, 1947.

Solar-Geophysical Data, CRPL-FB-267, Environmental Science Services Administration, Boulder, Colorado, November, 1966.

Spitzer, L., Physics of Fully Ionized Gases, Chpt. 1, Interscience Publishers, New York, 1962.

Steiger, W. R., and J. W. Warwick, Observations of Cosmic Radio Noise at 18 Mc/s in Hawaii, J. Geophys. Res., 66, 57-66, 1961.

Störmer, C., The Polar Aurora, Oxford University Press, London, 1955.

Tables of Sunrise, Sunset, and Twilight, Supplement to the American Ephemeris, United States Government Printing Office, Washington, D. C., 1946.

United States Standard Atmosphere, United States Government Printing Office, Washington, D. C., 1962.

Warwick, C. S., and M. W. Haurwitz, A Study of Solar Activity Associated with Polar-Cap Absorption, J. Geophys. Res., 67, 1317-1332, 1962.

Watanabe, K., and H. E. Hinteregger, Photoionization Rates in the E-and F-Regions, J. Geophys. Res., 67, 999-1006, 1962.

Webber, W. R., The Production of Free Electrons in the Ionospheric D Layer by Solar and Galactic Cosmic Rays and the Resultant Absorption of Radio Waves, J. Geophys. Res., 68, 6223-6228, 1963.

Weir, R. A., Jr., A Study of Ionospheric Absorption Produced by Solar Cosmic Rays, Doctoral Dissertation, University of California at Berkeley, 1962.

Whitten, R. C., and I. G. Poppoff, Physics of the Lower Ionosphere, Prentice-Hall, Inc., Englewood Cliffs, New Jersey, 1965.

Yonezawa, T., On the F-Region Theory, in Electron Density Profiles in the Ionosphere and Exosphere, Ed. by B. Maehlum, Pergamon Press and The Macmillan Co., New York, 1962.

APPENDIX A

SCATTER-PLOT PROGRAM

This program creates and stores on magnetic tape the data to be plotted on the IBM 1627 plotter. The plotter points are represented by + signs of size .05 inches. The x-coordinate of a point is the local sidereal hour angle at the time the observation was measured. The y-coordinate of the point is the normalized observed data value.

The normalization of a data value is done in the following manner. Let $S_i (i = 1, 2, \ldots, n)$ be the set of standard calibration values being used, i.e. the day to which all data is compared against, and let $C_i (i = 1, 2, \ldots, n)$ be the corresponding daily calibration values for the daily data set being plotted. Let d be an observed daily data value and let I_d be the corresponding normalized data value. The normalized value of I_d is then given by

$$I_d = \frac{(d-C_{j-1})S_j + (C_j - d)S_{j-1}}{C_j - C_{j-1}} \qquad \text{(A-1)}$$

when $C_{j-1} < d < C_j$

The program is written in Fortran IV with the time saving device of sorting all data into half hour intervals arranged in descending order to save the plotting pen unnecessary horizontal movement.

The program allows any two continuous sets of hourly (UT) data values to be plotted. In addition these two intervals may be changed at any time. Thus it is possible to plot data for 0000 - 0900 hours and 2200 hours for January and 0100 - 0800 for February on the same plot.

APPENDIX B

FOURIER ANALYSIS PROGRAM

This program takes the 24 hourly EA values, $f(X_i)$, read from the scatter plot and determines the Fourier coefficients. The coefficients are given as

$$a_o = \frac{1}{24}\sum_{i=1}^{24} f(X_i) \tag{B-1}$$

and

$$a_j = 2/L \sum_{i=1}^{24} f(X_i) \cos \left(\frac{2\Pi j\left(\frac{iL}{N} + X_o\right)}{L}\right) (L/N) \tag{B-2}$$

and

$$b_j = 2/L \sum_{i=1}^{24} f(X_i) \sin \left(\frac{2\Pi j\left(\frac{iL}{N} + X_o\right)}{L}\right) (L/N) \tag{B-3}$$

Here L is the length of one period, j is the number of harmonics to be considered, and X_o is the origin if not zero.

The output of the program consists of the coefficients a_o, a_1,--a_n and b_1, b_2,--b_n which will reproduce analytically the envelope curve. The program is written in Fortran IV.

APPENDIX C

ABSORPTION PROGRAM

The absorption program computes, lists, and stores absorption values. Riometer readings, after normalization, are compared to a periodic reference function in sidereal time. The absorption is computed, printed, and stored on magnetic tape.

At the universal time t a riometer reading d(t) is made. Converting t to sidereal time S(t) and normalizing d(t) to a particular value as defined by A-1 in Appendix A gives the normalized riometer value at time t,I_d. The program reads in the coefficients a_o, a_1--, a_n and b_o, b_1-- b_n as determined by B-1, B-2, and B-3 in Appendix B. The reference value r(t) is then determined from the equation

$$I_q = a_o + \sum_{i=1}^{n} a_i \cos \frac{(2\Pi i S(t)}{24} + b_i \sin \frac{2\Pi i S(t)}{24} \qquad \text{(C-1)}$$

The absorption at time t is then given as

$$A(dB) = 10 \log_{10} \frac{I_q}{I_d} \qquad \text{(C-2)}$$

The program tabulates t, I_d, I_q, and A for each time t that a riometer value is taken. In the event that data for a particular time, t_1, is missing, the value t_1 and the words "no data" are printed out. The absorption values may be stored on magnetic tape if desired. A listing of the data stored on the magnetic tape is printed at the end of the processing. The time interval between values for which absorption is to be computed may be an integral value in minutes.

It must be stressed that the program checks the input cards for chronological order and agreement of identification parameters. An error in either of these two categories could cause the magnetic tape to loose its information and require reprocessing. The program is written in Fortran IV.

APPENDIX D

ABSORPTION PLOT PROGRAM

The absorption plot program selects absorption values from a magnetic tape and plots these values as a function of universal time. The user requests the number of plots desired with a maximum number of 20. The input tape is searched for data matching the plots requested and a plotter tape is created for subsequent plotting on the IBM 1620/1627.

The user may specify the time abscissa scale and the following absorption ordinate scales: .05 dB/in., 0.1 dB/in., 0.2 dB/in., 0.5 dB/in., 1.0 dB/in., 2.0 dB/in., 5.0 dB/in., 10.0 dB/in., and 20 dB/in. The user is also allowed to choose the number of title lines and size of characters to be printed in the title. The input tape used here is the output from the absorption program. The program is written in Fortran IV.

APPENDIX E

ERROR ANALYSIS

The error indicated in the figures comes from two sources. One is the actual reading error of the EA values from the reference and disturbed curves while the other is the statistical error of the mean value of the monthly hourly averages.

The equation used to calculate the experimental absorption values is

$$A(\mathrm{dB}) = 10 \log \frac{I_q}{I_d} \tag{E-1}$$

As I_q changes A will change as

$$\frac{dA}{dI_q} = \frac{10}{I_q/I_d} \left(-\frac{1}{I_d}\right) \log_{10} e \tag{E-2}$$

or

$$\frac{dA}{dI_q} = -\frac{10}{I_q} \log_{10} e \tag{E-3}$$

Using the incremental form gives

$$\Delta A = -\frac{10}{I_q} \log_{10} e \, \Delta I_q \tag{E-4}$$

If the reading error is $\pm$ .2 EA units, then

$$\Delta A = \mp \frac{10}{I_q} (.43429)\ (.2) \tag{E-5}$$

or

$$\Delta A = \mp \frac{.86858}{I_q} \tag{E-6}$$

This equation shows that the error in absorption is dependent on the value of the EA reading of the reference curve. For instance, if I_q equals 30 EA units, then

$$A = \mp .029 \text{ decibels} \tag{E-7}$$

If equation E1 is differentiated with respect to I_d, one obtains

$$\frac{dA}{dI_d} = - \frac{10}{I_d} \log_{10} e \tag{E-8}$$

or

$$\Delta A = \mp \frac{.86858}{I_d} \tag{E-9}$$

The errors introduced through I_q and I_d are independent errors and using a conservative approach these errors will be added. Beers [1957] states that for independent errors the resultant error is the square root of the sum of the squares which is a less conservative approach than taken here.

The statistical error of the mean value of the monthly hourly averages is taken as the standard deviation of the mean. The standard deviation of the average is given by Beers [1957] as

$$S_{\bar{x}} = \left(\sum_{n=1}^{k} \frac{(X_n-\bar{X}_k)}{k(k-1)}\right)^{1/2} \qquad \text{(E-10)}$$

where $\bar{X}_k$ is the mean value of k measurements and X_n is the value of a particular measurement. The error bars are the sum of the reading error and the statistical error, again using the largest error.

The error introduced by the f_oF_2 proportional absorption is not included since as stated in Chapter IV it is very very small. The sampling method used the criteria of selecting all points falling within .10 dB of the quiet day curve. Hence there are points both positive and negative not utilized which in turn means this effect should tend to zero. By using conservative errors in the cases computed, it is felt that the error bars are sufficient to take into account all error present.

APPENDIX F

ELECTRON DENSITY DETERMINATION FROM EXPONENTIAL PROTON ENERGY SPECTRUM

The purpose of this program is to take the given power law in energy proton spectrum and calculate the electron density resulting from the proton bombardment. The program is written in two segments to cover the energy interval 1.2 to 100 Mev; namely, 1.2 to 8.2 Mev and 8.2 to 100 Mev. The spectrum values read in are given for an altitude of 100 km. The omnidirectional differential spectrum is corrected for atmospheric attenuation every km from 20 km to 99 km.

At a particular level this correction is executed by taking a particular energy and integrating the pitch angle distribution by Simpson's rule. The energy is then increased by .25 Mev and the process repeated. At each energy interval the production function is calculated for that interval. This continues until the upper limit of 100 Mev is reached summing all the q's calculated at each energy interval. This gives the q for the given altitude and is stored in the computer memory. The process is repeated at each succeeding altitude.

The effective recombination coefficients appropriate to day and night conditions are read in for each km from 20 to 99 km. The electron densities are then calculated and printed. Although the program does not take into account alpha particle production the only quantity needed to do this is the alpha particle energy loss in air. It should be noted that a single computer run over the altitude 20 to 99 km takes two hours of IBM 360 time. The program is written in Fortran IV.

APPENDIX G

IONOSPHERIC ABSORPTION FROM THE ELECTRON DENSITY DISTRIBUTION

The purpose of this program is to calculate the ionospheric absorption at a particular frequency for a given electron density distribution. The electron density distribution used as input here is the output from the program in Appendix F. The program calculates and prints the real and complex indices of refraction for the ordinary and extraordinary mode as determined by Sen-Wyller theory. The complex indices of refraction yield the absorption coefficients k from which the absorption is calculated and printed for the ordinary, extraordinary, and the average of the two modes.

The absorption is computed at one km increments from 20 through 99 km with the absorption at one k added to the absorption determined from the previous km steps. The absorption is computed for a single frequency initially specified taking into account only electron-neutral collisions. The angle between the vertical and the field line at Durham is taken as 16.9 along with a gyrofrequency of 9.66 MHz. The program is written in Fortran IV.

APPENDIX H

ABSORPTION CORRECTION PROGRAM

The principal purpose of the absorption correction program is to take the absorption values determined from the absorption program as stored on magnetic tape and correct them to the absorption expected for a pencil-beam antenna. The program is general enough to allow more than one set of corrections to be used. The corrected data is written on what is called the first storage tape.

In addition, the program will, at the user's option copy absorption values from the input magnetic tape onto the first storage tape. Also, the program copies all information copied on the first storage tape onto a second tape called a second storage tape. This tape is used as a safety storage in case the first storage tape is lost or has its data accidentally erased. The program is written in Fortran IV.